ERDC TR-13-11

US Army Corps
of Engineers®
Engineer Research and
Development Center

ERDC
INNOVATIVE SOLUTIONS
for a safer, better world

Flood and Coastal Systems

Laboratory Studies of Wave Attenuation through Artificial and Real Vegetation

Mary E. Anderson, Jane McKee Smith, Duncan B. Bryant,
and Robert G. W. McComas

September 2013

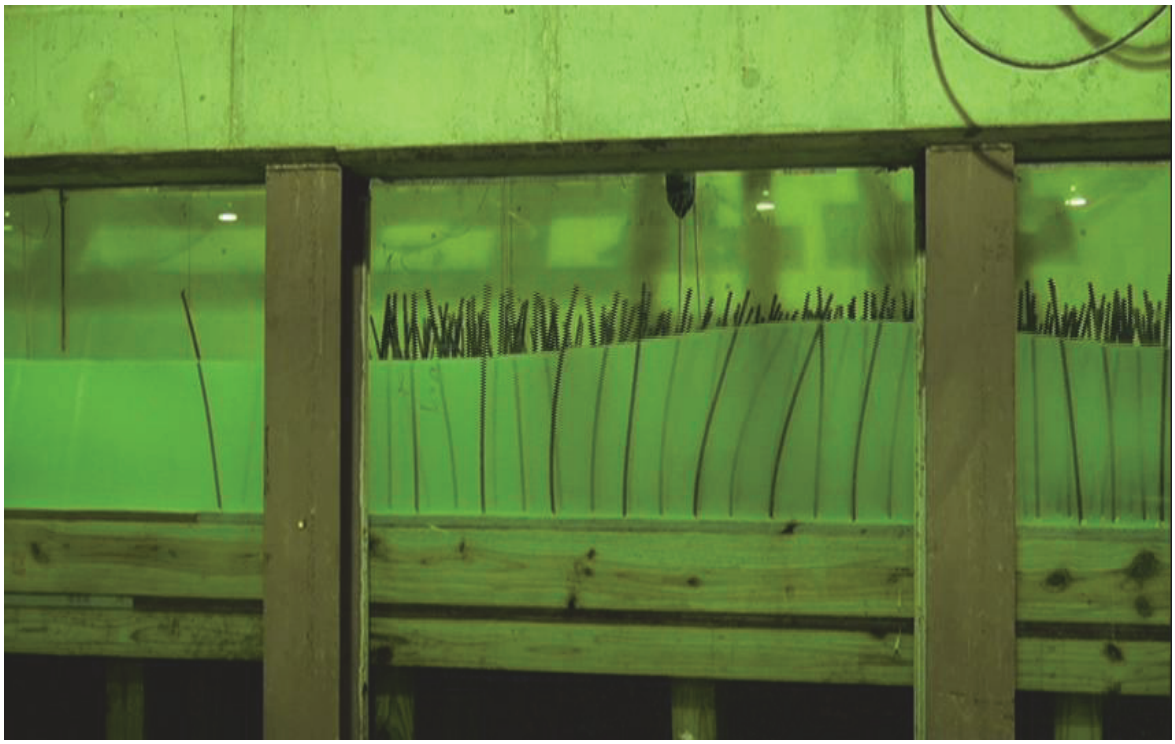

Engineer Research and Development Center

The US Army Engineer Research and Development Center (ERDC) solves the nation's toughest engineering and environmental challenges. ERDC develops innovative solutions in civil and military engineering, geospatial sciences, water resources, and environmental sciences for the Army, the Department of Defense, civilian agencies, and our nation's public good. Find out more at www.erdc.usace.army.mil.

To search for other technical reports published by ERDC, visit the ERDC online library at http://acwc.sdp.sirsi.net/client/default.

ERDC TR-13-11
September 2013

Laboratory Studies of Wave Attenuation through Artificial and Real Vegetation

Mary E. Anderson, Jane McKee Smith, and Duncan B. Bryant

Coastal and Hydraulics Laboratory
US Army Engineer Research and Development Center
3909 Halls Ferry Road
Vicksburg, MS 39180-6199

Robert G. W. McComas

Environmental Laboratory
US Army Engineer Research and Development Center
3909 Halls Ferry Road
Vicksburg, MS 39180-6199

Final report

Prepared for US Army Corps of Engineers
441 G Street, NW
Washington, DC 20314-1000

Monitored by Coastal and Hydraulics Laboratory
US Army Engineer Research and Development Center
3909 Halls Ferry Road, Vicksburg, MS 39180-6199

Abstract

A physical model study investigating the dissipation of wave energy by artificial and real *Spartina alterniflora* was performed in a large-scale two-dimensional flume. The purpose of the study was to isolate the influence of a single plant or wave property on wave dissipation through vegetation by varying the parameter of interest while holding other parameters constant. The varied parameters included vegetation submergence depth, incident zero-moment wave height, incident peak wave period, and stem density. Measurements of the free surface and instantaneous velocity were collected for single- and double-peaked irregular wave spectra. The experiment setup and data collection methodology are described in detail.

Results from the artificial and real vegetation tests indicate vegetation submergence depth and stem density strongly influence wave attenuation while the effects of incident wave height and peak period were small and unclear in comparison. An increase in stem density of the artificial vegetation resulted in a greater reduction in wave height for all modeled wave conditions. As water depth exceeded canopy height, the wave attenuation capacity of both the artificial and real vegetation decreased. Dissipation occurred at all frequencies of the spectra with the most evident loss of energy at the peak frequencies; however, separating the double-peaked spectra into two wave spectra revealed a preferential dissipation of higher frequency wave energy compared to lower frequency wave energy through the artificial array.

The real vegetation was found to dissipate wave energy more efficiently than the artificial vegetation which is likely due to the additional drag induced by the leaves.

Contents

Figures and Tables

Figures

Tables

Preface

This study was conducted under the Flood and Coastal Systems Program's Wave Dissipation by Vegetation for Coastal Protection Work Unit. The Program Manager was Dr. Cary Talbot.

This report was prepared by Mary E. Anderson, Dr. Jane McKee Smith, and Dr. Duncan B. Bryant, Coastal Processes Branch (CEERD-HF-C), of the Flood and Storm Protection Division (CEERD-HF), Coastal and Hydraulics Laboratory (CHL), US Army Engineer Research and Development Center (ERDC), and Robert G. W. McComas, Environmental Engineering Branch (CEERD-EP-E), of the Environmental Processes and Engineering Division (CEERD-EP), Environmental Laboratory (EL), US Army Engineer Research and Development Center. Work was performed under the general administrative supervision of Mark Gravens, Chief, CEERD-HF-C; Dr. Ty Wamsley, Chief, CEERD-HF; José E. Sánchez, Deputy Director (CHL); and Dr. William D. Martin, Director (CHL). William Curtis was the Technical Director for the Flood and Coastal Storm Damage Reduction. Experiments were conducted by Mary Anderson and William Henderson, Harbors, Entrances, and Structures Branch (CEERD-HN-H). Tim Nisley and David Daily, of the ERDC Information Technology Laboratory, provided instrumentation support. Lauren A. Coe and Zeki Demirbilek provided valuable review of the draft version of the report.

At the time of publication, COL Jeffrey R. Eckstein was Commander and Executive Director of ERDC, and Dr. Jeffery P. Holland was Director.

1 Introduction

1.1 Background

Coastal areas are vulnerable to devastating storm surge and waves, a vulnerability that will increase with the ever-increasing population and infrastructure near the coast. The threat will be exacerbated by sea level rise and a possible increase in frequency and severity of the hurricane hazard due to climate change. The storm surge and waves generated by powerful hurricanes can have devastating consequences for coastal areas, in terms of damage and loss of life. The severity of damage greatly influences the ability of communities to rebound from natural hurricane disasters. Methods that can reduce these severe consequences are needed. The analysis, design, and construction of coastal protection following Hurricane Katrina have neglected the beneficial effects of vegetation because there have been insufficient data and analysis to quantify those benefits. It is generally acknowledged that vegetated coastal features such as wetlands can reduce the effects of surge, waves, and tsunami propagation, but we lack data and quantitative methods to address the reduction in modeling and design.

Literature exists on steady flow through vegetation (Nepf 2012; Serra et al. 2004) and on wave height attenuation by vegetation (Koftis et al. 2013; Manca et al. 2012; Yoon et al. 2011; Augustin et al. 2009; Lima et al. 2006; Cooper 2005; Wallace and Cox 2000; Løvås and Tørum 2000; Méndez et al. 1999; Kobayashi et al. 1993; Fonseca and Cahalan 1992; Knutson et al. 1982; Markle 1979). A comprehensive review of vegetation-induced wave attenuation can be found in Anderson et al. (2011). There have also been some studies of the hydrodynamics and sediment transport through mixed emergent tidal marshes (Neumeier and Ciavola 2004; Leonard and Reed 2002). However, the influence of vegetation under hurricane conditions, including the influence on the magnitude of wave setup and runup, is not well understood. Numerical studies have demonstrated the potential for vegetation on a landscape scale to impact inundation (Wamsley et al. 2009, 2010; Loder et al. 2009), but the validation of model physics has been lacking due to the paucity of detailed measurements and validation. In the presence of waves, particularly during breaking, the steady flow velocity is changed by the addition of wave radiation stresses and enhanced wave bottom friction.

In this study, data documenting the interactions of plants and water levels and waves were collected in the laboratory. The laboratory provides a controlled environment to evaluate wave attenuation, including the parameters of water depth, wave height and period, and vegetation characteristics including stem density, height, and rigidity. Measurements include water surface elevations and instantaneous velocity time series.

1.2 Purpose of study

The primary objectives of this project are as follows:

- Demonstrate wave attenuation potential of vegetation for coastal protection.
- Quantify wave attenuation by vegetation, specifically *Spartina alterniflora*, from the lab experiments.
- Develop algorithms for vegetative dissipation that can be implemented in phase-averaged wave models to provide an improved tool for engineering application, disaster preparedness, planning, and risk management.

With the emphasis of the investigation on wave attenuation, it is assumed that natural and engineered vegetative buffers reduce wave energy and wave setup and runup, and the associated damage and potential for loss of life. The goal of this study is to quantify this effect in engineering design. The design, construction, and results from the artificial vegetation and the real *Spartina alterniflora* experiments are discussed in Chapters 2 and 3, respectively. A summary of the study is provided in Chapter 4. Appendix A contains figures of wave decay through the artificial vegetation bed. Figures of wave transformation through *S. alterniflora* are provided in Appendix B.

2 Artificial Vegetation Experiments

This chapter describes the design, construction, and execution of the artificial vegetation laboratory experiments. The purpose of these experiments was to obtain wave dissipation data under idealized conditions to quantify the impacts of vegetation on waves.

2.1 Description of experiments

2.1.1 Test facilities

The experiments were conducted in two on-site wave flumes, which were 1.5 m and 3.0 m wide, 63.4 m long, and 1.5 m deep. The flumes are equipped with computer-controlled electro-hydraulic piston wave generators capable of creating irregular waves with a maximum wave height of 0.46 m and wave periods of 0.75–10.0 sec.

Both flumes are approximately 0.45 m deeper at the wave generator than the testing section. The deep section housing the wave paddle is 5.4 m long and is followed by a 1:44 slope of 19.5 m. The 1:44 slope leads to a 38.5 m long, 1.5 m deep flat section. There is an 11.3 m long, 1:20 concrete slope within the 1.5 m flume. This structure was leftover from an earlier breakwater study and is constructed 12.2 m behind the transition to the 1.5 m deep flat testing section.

2.1.1.1 3.0 m flume

The artificial vegetation experiments started in the 3.0 m flume. A 1:22 marine plywood slope was installed 24.7 m from the wave paddle at rest (approximately 2.8 m after the beginning of the flat testing area). The slope measured 13.3 m long and connected flush with a 13.3 m long false floor. The floor was lowered to 0.45 m to create a ledge such that real vegetation could be placed level with the slope interface. In order to accommodate the artificial vegetation, 2 × 6 treated lumber edges were installed over the length of the setup, and 0.02 m thick plywood sheets secured on top, bringing the floor flush with the slope at 0.61 m high. These top plywood sheets could easily be removed and altered to test different stem arrays. A detailed diagram of the false floor is shown in Figure 1.

Figure 1. Details of 3.0 m flume false floor.

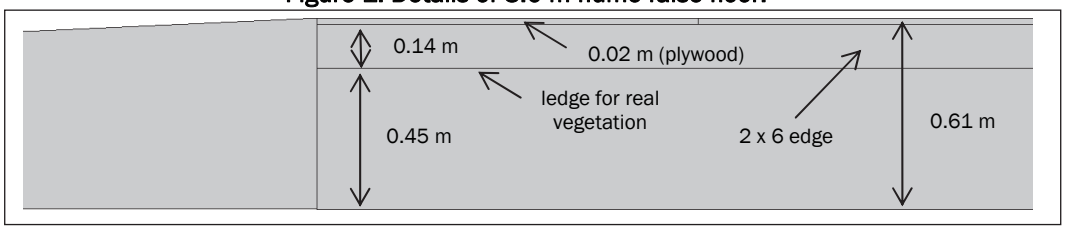

The setup was constructed the width of the flume and then divided in half by a plywood wall into two neighboring, individual channels of equal width. This division allowed for simultaneous sampling in an unvegetated, blank control channel and a vegetated channel. The existing rock beach behind the test section was reshaped and lined with new wave absorber. The vegetation field started 39.2 m from the wave paddle at rest and was 9.8 m long. The cross section of the 3.0 m wave flume and its setup is shown in Figure 2. The initial 1.2 m of the false bottom was left blank to allow for turbulence dissipation and reformation of the waves before the vegetation field. The final 2.3 m was left blank to remove discontinuity effects within the sampling area resulting from the setup.

Figure 2. Cross section of 3.0 m flume.

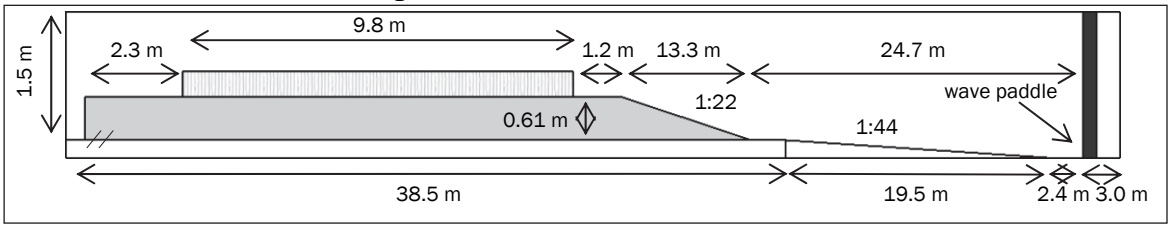

2.1.1.2 1.5 m flume

The artificial vegetation experiments were later moved to the 1.5 m flume following a malfunction with the 3.0 m flume wave generator. In order to account for the concrete slope in the 1.5 m flume and minimize water requirements, the 1.5 m flume setup was modified slightly from that of the 3.0 m flume. A 1:20 marine plywood slope measuring 6.1 m was installed 19.6 m from the wave paddle at rest. A 12.2 m long false floor was constructed flush with the plywood slope. The design of the false floor was similar to that in the 3.0 m flume, except the floor ledge was lowered to 0.09 m high (Figure 3). This base floor was again lined with 2 × 6 edges topped with removable 0.02 m thick plywood sheets, bringing the total floor height to 0.25 m.

Figure 3. Details of 1.5 m flume false floor.

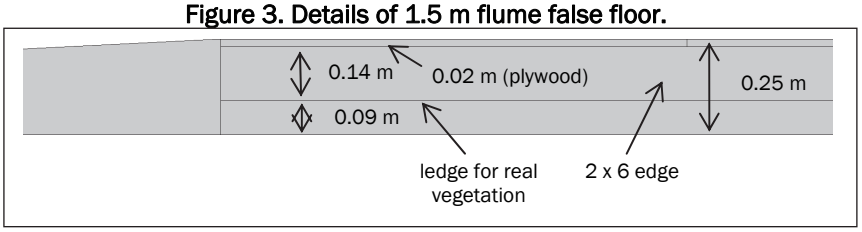

The 9.8 m long vegetation field started 26.9 m from the wave paddle at rest. The posterior 1:20 concrete slope was lined with wave absorber to reduce wave reflection. The experiment layout and dimensions of the 1.5 m flume are shown in Figure 4. The 1.2 m flat areas before and after the vegetation bed were designed as sub areas for promoting turbulence dissipation and wave reformation and avoiding sampling near the 1:20 sloping beach face.

Figure 4. Cross section of 1.5 m flume.

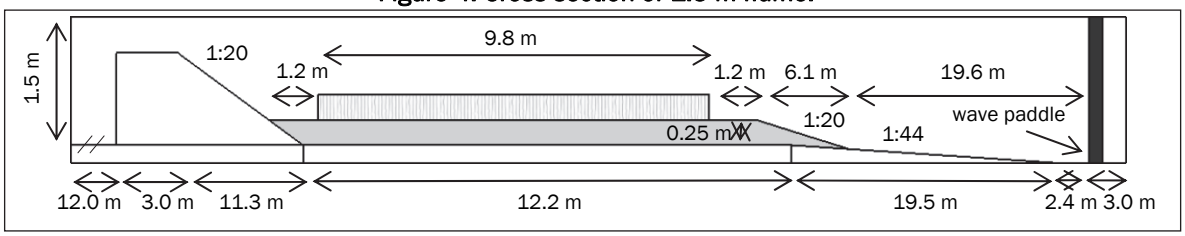

2.1.2 Instrumentation

2.1.2.1 Free surface measurements

Water surface elevations were collected by single wire capacitance-type wave gauges (WG) sampling at 25 Hz. The coordinates of the WGs in the 3.0 m flume and the 1.5 m flume are listed in Table 1, where the origin is at the wave generator at rest. Water surface oscillations were measured by 18 WGs in the 3.0 m flume. WGs 1–3 formed an offshore Goda array to calculate reflection and were located at x = 6.1, 6.4, and 7.0 m. WGs 4–18 were split between the vegetation and control channel, with 4–13 installed in the vegetation and 14–18 installed in the control channel. The distances between WGs 4–18 varied, allowing for changing spatial resolution within the channels (Figure 5 and Figure 6). WGs 4–13 were installed in the middle of the vegetation channel at x = 38.3, 39.2, 39.7, 40.2, 40.8, 41.8, 43.3, 45.0, 46.7, and 48.5 m from the generator. WGs 14–18 were installed along the center axis of the adjacent control channel, and were paired with WGs 4, 5, 7, 10, and 13, respectively, at x = 38.3, 39.2, 40.2, 43.3, and 48.5 m.

Fewer wave gauges were used in the 1.5 m flume as the flume was not divided; surface elevation was measured by 13 WGs. WGs 1–3 were located the same distance from the wave generator as those in the 3.0 m flume (at x = 6.1, 6.4, and 7.0 m). WGs 4–13 were installed at x = 26.0, 26.9, 27.4, 27.9, 28.5, 29.5, 31.0, 32.7, 34.4, and 36.2 m along the center of the flume (Figure 7 and Figure 8). While the gauges are closer to the wave generator in the 1.5 m flume than the 3.0 m flume, the locations of WGs 4–13 with respect to the vegetation field remained constant.

Table 1. Location of wave gauges from the wave generator.

Wave gauge no.	3.0 m flume (m)	1.5 m flume (m)
1	6.1	6.1
2	6.4	6.4
3	7.0	7.0
4	38.3	26.0
5	39.2	26.9
6	39.7	27.4
7	40.2	27.9
8	40.8	28.5
9	41.8	29.5
10	43.3	31.0
11	45.0	32.7
12	46.7	34.4
13	48.5	36.2
14	38.3	x
15	39.2	x
16	40.2	x
17	43.3	x
18	48.5	x

2.1.2.2 Velocity measurements

Water particle velocities were measured in addition to the free surface elevation. All three instantaneous velocity components were measured using fixed-stem high-resolution acoustic Doppler velocimeters (ADV; model Nortek AS Vectrino). The ADVs use the Doppler shift to measure the velocity of particles in a remote sampling volume. For this experiment,

the sampling volume was measured 0.05 m from the probe and its length was 7 mm. The length of the transmit pulse was 1.8 mm, and the velocity range was set to 1.0 m/s.

Six ADVs were paired with WGs 7, 10, 13, 16, 17, and 18 in the 3.0 m flume, and four ADVs were paired with WGs 5, 7, 10, and 13 in the 1.5 m flume. The ADVs were mounted on aluminum angle using adjustable worm gear hose clamps.

All ADVs were controlled from a single computer using Nortek's PolySync data collection software (Nortek AS). The WGs and ADVs were synchronized using a trigger from the data acquisition system to ensure both instrument types began sampling simultaneously. The ADV receiving the trigger from the control program was classified as the sync master, while the other ADVs were designated sync slaves. The sampling rate of the ADVs and WGs was the same (25 Hz).

In addition to ADVs, the 3D velocity profile was measured using a Nortek AS Aquadopp acoustic Doppler current profiler (ADCP). An ADCP works similarly to an ADV, but calculates the water velocities over a depth range by bin-averaging sampling layers or cells within the water column. The ADCP was installed 0.4 m shoreward of WG 10, and was run in high-resolution burst mode with three beams, a cell size of 20 mm, and a sampling rate of 4 Hz. The ADCP was started manually and not synched to other instruments.

A plan view of the 3.0 m flume and the 1.5 m flume instrumentation layout is shown in Figure 5 and Figure 7, respectively, with corresponding photographs provided in Figure 6 and Figure 8. The vegetation field is green in color. Circles signify WGs where yellow color indicates WGs paired with ADVs. The location of the ADCP is marked by a blue triangle.

2.2 Idealized vegetation

The element serving as artificial *S. alterniflora* was selected based on these three requirements:

1. Have similar geometry to a stem.
2. Reproduce the observed swaying motion of sea grass under wave action.
3. Remain upright to allow the modeling of emergent conditions.

Figure 5. Plan view of 3.0 m flume. White and yellow circles are unpaired wave gauges and those paired with ADVs, respectively. The blue triangle is the ADCP.

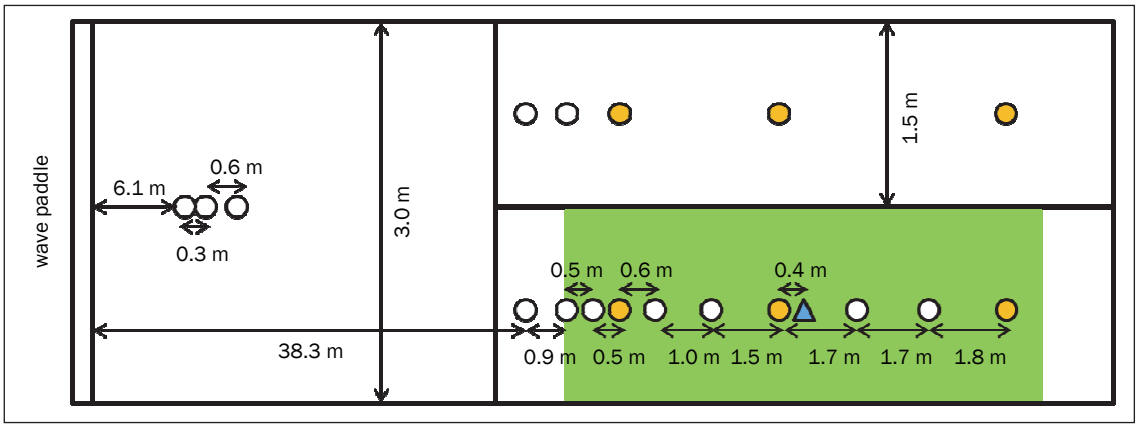

Figure 6. Photograph of 3.0 m flume channels.

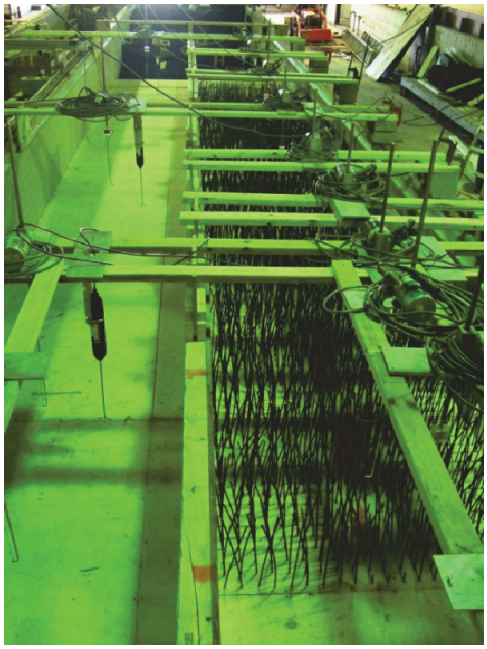

Figure 7. Plan view of 1.5 m flume. White and yellow circles are unpaired wave gauges and those paired with ADVs, respectively. The blue triangle is the ADCP.

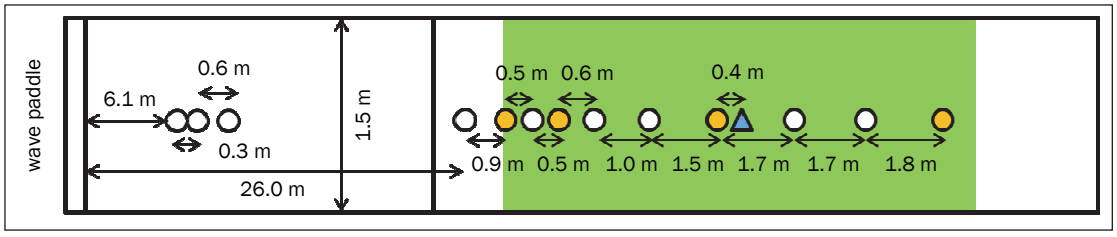

Figure 8. Photograph of 1.5 m flume channel.

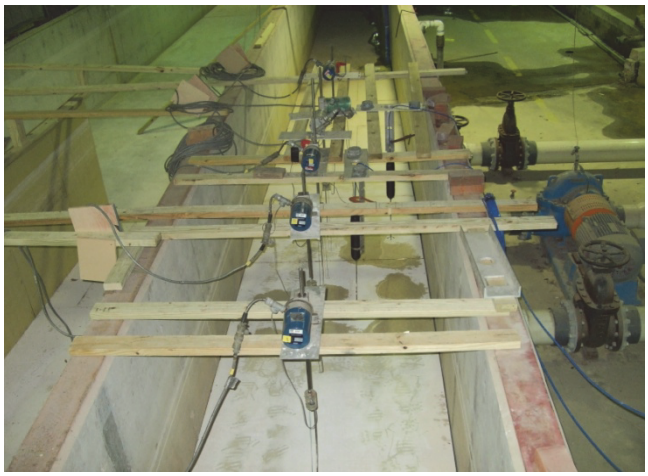

To simulate the basic geometry of *S. alterniflora*, 6.4 mm diameter tubing was selected based on reports of average stem diameters near this value, and the tubing was cut into equal lengths of 0.415 m (Chatagnier 2012; Feagin et al. 2011; Wu et al. 2011; Ysebaert et al. 2011). The rigidity of *S. alterniflora* was represented reasonably well by cross linked polyolefin tubing. The reported modulus of elasticity (E) for *S. alterniflora* by Chatagnier (2012) is E = 159.8 MPa and by Feagin et al. (2011) is E = 1410 ± 710 MPa. While both researchers used traditional beam theory to calculate E, the methodologies and location of samples were different. Non-uniformity of the plant stem, plant age and health, water content, and salinity are all naturally occurring factors that could affect E (Salpeter et al. 2012; Touchette et al. 2009a, 2009b; Pezechki et al. 1993). As polyolefin does not conform to Hooke's law for elastic materials, the 2 percent secant modulus is used for comparative evaluations to E and generally results in a lower value than that for E (ASTM Standard D5323). Cross linked polyolefin tubing has a density of 1350 kg/m^3 and a maximum secant modulus of 172 MPa, which is close to the value reported by Chatagnier (2012) for *S. alterniflora* (ASTM Standard D3149).

The stem density of natural *S. alterniflora* beds is highly variable, depending upon the depth, health, and age of the stand. Three spatial densities of 100, 200, and 400 stems/m^2 were tested, which correspond to an element grid spacing of 0.10, 0.071, and 0.05 m. These densities cover the range of values reported by Knutson et al. (1982). Each higher density array was constructed by adding additional elements to the previous lower density array (Figure 9). The polyolefin tubing was secured to 0.02 m thick plywood sheets using 0.08 m wood screws and construction adhesive. Completed density arrays are shown in Figure 10, and the installation in the 1.5 m flume shown in Figure 11.

Figure 9. Stem spacing of artificial vegetation.

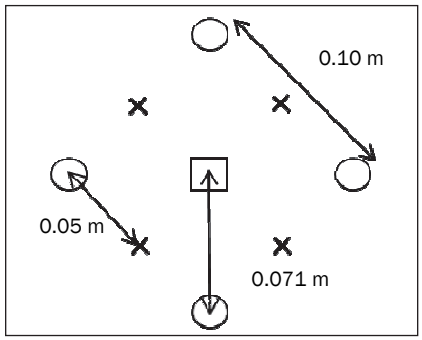

Figure 10. Photograph of stem densities: 100 stems/m² (top left), 200 stems/m² (top right), 400 stems/m² (bottom center).

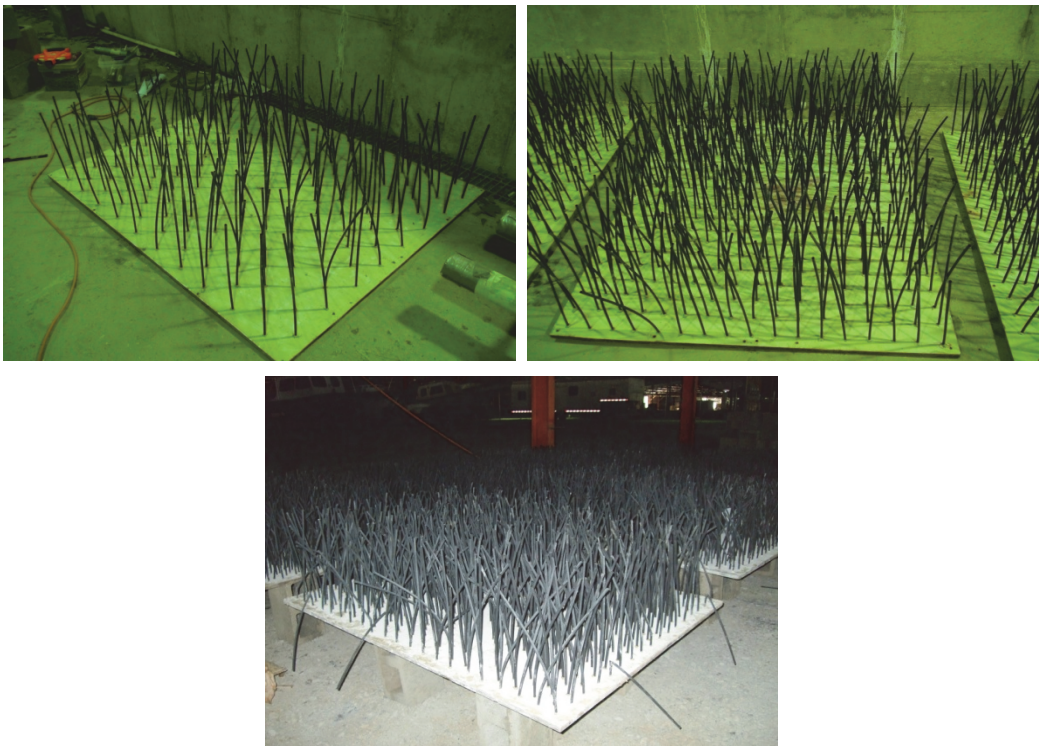

2.3 Wave and water level conditions

A total of 21 wave and water level conditions were generated for this study and are given in Table 2 where water depth (h), incident zero-moment wave height (H_o), and peak wave period (T_p) were measured at the leading edge of the vegetation field (WG 5). Because wave signals were repeated for different configurations (e.g., control tests, varying stem densities, artificial and real vegetation), the average incident wave height and its standard deviation are provided for each test. The maximum standard deviation was less than 3 mm, indicating nearly the same wave conditions were used for each phase of the experiment.

Figure 11. Photograph of artificial vegetation meadow installed in 1.5 m flume (N = 400 stems/m^2).

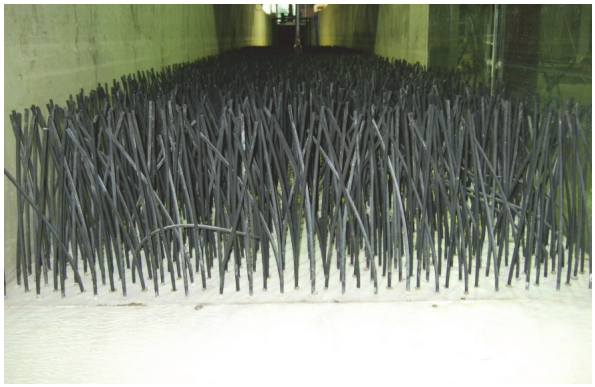

Table 2. Tested single- and double-peaked irregular wave conditions (WG5).

Test No.	h (m)	H_0 (m)	T_p (sec)
1	0.533	0.111 ± 0.0012	1.5
2	0.533	0.111± 0.0016	1.75
3	0.533	0.111 ± 0.0017	2.0
4	0.533	0.137 ± 0.0018	1.25/2.0
5	0.533	0.109 ± 0.0016	1.25/2.0
6	0.457	0.081 ± 0.0004	1.5
7	0.457	0.109 ± 0.0011	1.5
8	0.457	0.139 ± 0.0012	1.5
9	0.457	0.050 ± 0.0008	2.0
10	0.457	0.107 ± 0.0010	2.0
11	0.457	0.153 ± 0.0014	2.0
12	0.457	0.192 ± 0.0015	2.0
13	0.457	0.136 ± 0.0019	1.25/2.0
14	0.457	0.107 ± 0.0007	1.25/2.0
15	0.305	0.111 ± 0.0028	1.25
16	0.305	0.109 ± 0.0027	1.5
17	0.305	0.112 ± 0.0020	1.75
18	0.305	0.110 ± 0.0015	2.0
19	0.305	0.111 ± 0.0018	2.25
20	0.305	0.129 ± 0.0018	1.25/2.0
21	0.305	0.106 ± 0.0015	1.25/2.0

Fifteen single-peaked wave conditions were generated using a Texel Marsen Arsole (TMA) shallow-water wave spectrum with γ = 3.3. Peak periods ranged from 1.25 to 2.25 sec, and average zero-moment wave

heights varied from 0.05 to 0.192 m. Double-peaked spectra with peaks at 1.25 and 2.0 sec were also investigated. The double-peaked spectra were generated externally by linearly superimposing two independent wave spectra with γ = 10.0. The larger γ value produces narrower spectral peaks with greater separation in frequency. Target incident wave conditions were the same for the 3.0 m flume and the 1.5 m flume experiments.

The capacity of vegetation to attenuate surge and waves during storm events, and thus during elevated water levels, is largely undocumented due to the unpredictable nature of storm development and the difficulty in deploying, maintaining, and retrieving instrumentation during and following these high-energy events. Thus, waves were generated at three water depths, representing an emergent and two submergent conditions. The three water depths measured at the vegetation were the following: 0.305, 0.457, and 0.533 m. A convenient way to report the relative depth of submergence of the vegetation is to define the vegetation submergence ratio. The vegetation submergence ratio is defined as the ratio of average plant height (l_s) to water depth (h). The tested water depths correspond to vegetation submergence ratios of 1.36, 0.91, and 0.78, respectively, where 1.0 and greater indicates emergence.

2.4 Test procedures

The effects of stem density, submergence ratio, peak period, and incident wave height on irregular wave dissipation were assessed by varying the parameter of interest while holding other wave and plant parameters constant. Data were collected for a total of 76 runs which were performed in four test groups: (1) without artificial vegetation, (2) with N = 100 stems/m^2, (3) with N = 200 stems/m^2, and (4) with N = 400 stems/m^2. The lowest stem density runs were completed in the 3.0 m flume while the other runs were done in the 1.5 m flume. Control tests with blank plywood served to measure the background attenuation losses due to the installed plywood setup and the concrete/glass flume walls. Note that the background losses within the 3.0 m flume were recorded in the blank channel (without vegetation) adjacent to the vegetation channel. Three tests for N = 100 stems/m^2 were not completed, including runs at the 0.305 m water level for 0.111 m wave height and 1.25 sec period, the 0.457 m water level for 0.081 m wave height and 1.5 sec period, and the double-peaked spectra.

Wave gauges were calibrated daily to minimize calibration errors where the maximum accepted error was 1.5 mm. The calibration process consists of raising and lowering the gauges a known distance relative to the still water level and acquiring a sample at each position. This output is used to obtain a mathematical curve-fit, ideally linear, between the gauge output and surface elevation change (Hughes 1993). Displacements were selected to ensure wave heights were bounded by the calibrated range.

The ADVs were displaced within the water column depending on water depth to avoid submerging the bulkhead housing unit. The ADVs were installed approximately 0.23 m from the false bottom for h = 0.305 m and approximately 0.36 m from the bottom for h = 0.457 and 0.533 m. Often tap water is too clean to provide adequate signal strength as indicated by the correlation and signal to noise ratio (SNR). Non-soluble seeding particles were added periodically to the wave flume to ensure a correlation > 80 and an SNR > 20. Artificial vegetation around the ADVs was shortened to eliminate potential disturbances of the measurements.

The ADCP was installed upward-looking in the 3.0 m flume by mounting the instrument underneath the top plywood layer and cutting a hole for the transducers. The pulse distance was calculated by adding the width of the plywood sheet to the water depth and rounding to the nearest centimeter. The pulse distances were set as 0.33, 0.48, and 0.56 m for h = 0.305, 0.457, and 0.533 m, respectively. Samples close to the transducers were neglected by setting the blanking distance to 0.05 m.

The deployment of the ADCP was changed to downward-looking in the 1.5 m flume. The ADCP was anchored from a bridge using an adjustable steel angle mount. The height and pulse distance of the ADCP was adjusted based on water depth. The height of the ADCP was 0.23, 0.36, and 0.43 m above the false bottom for h = 0.305, 0.457, and 0.533 m, and the corresponding pulse distances were 0.27, 0.40, and 0.47 m, respectively. The blanking distance was set to 0.03 m. Artificial vegetation swaying in front of the ADCP transducers was removed to avoid interference with the profiler.

Prior to each run of a test case, the water level of the flume was checked using a point gauge and adjusted as needed. All wave gauges were zeroed, and the desired wave condition file was selected on the control computer. The data acquisition system (which also triggered the ADVs) was started

2 minutes prior to wave generation to sample the mean water level to identify wave setup or setdown generated within the vegetation field. The ADCP was also started manually at this time. Wave time series records were generated for 8 minutes to sample a minimum of 200 waves, and each record was repeated three times to obtain a more stable signal for spectral analysis. Sampling continued for 1 minute after wave generation to allow wave propagation down the flume. All instrumentation sampled for a total of 11 minutes. Output from the data acquisition system, including time series and wave height, were visually inspected, and water in the flume was allowed to calm before the next test.

A video camera mounted on a tripod was used to document each experiment through a viewing window. Video of the experiment was started immediately following the initiation of the waves and ended following the wave action. The experiments were also documented through photos and notes.

2.5 Data analysis

Data analyses were performed on time series from individual gauges which included (1) reflection analysis using the offshore three-gauge array, (2) spectral analysis to calculate zero-moment height (H) and peak period (T_p), and (3) up-crossing analysis to obtain root-mean-square wave height (H_{rms}).

Data acquisition was started approximately 2 minutes prior to wave generation with the initial portion of the time series including still water. This data segment was eliminated from the wave height analyses by defining the start of the waves as the time when the water surface exceeded 5 mm. Sometimes this threshold was met prematurely due to noise in the signal. Consequently, a routine was implemented to check that the chosen time had to be later in the time series than the one selected for the previous gauge. The length of the wave signal was taken as 8 minutes from that identified start time. An example of the wave signal identification scheme is shown in Figure 12 where red indicates the portion of the time series used for wave height analysis.

Figure 12. Identified wave portion of measured time series (red) and full time series (black).

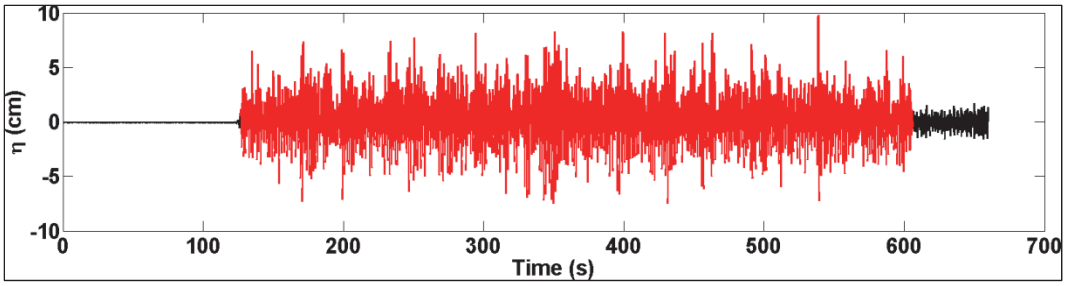

2.5.1 Reflection analysis

The amount of energy reflected is expressed by the reflection coefficient (K_r) defined as the ratio of the reflected wave height to the incident wave height. If 100% of the incident wave energy is reflected, $K_r = 1$. Reflection coefficients were calculated using a three-gauge separation technique based on the method by Goda and Suzuki (1976) and Seelig (1981). Goda and Suzuki (1976) developed a separation technique using two gauges separated by a known distance where incident and reflected wave components are separated using a Fast Fourier Transformation (FFT). This method was modified for a three-gauge array and performed using WGs 1–3.

Reflection coefficients ranged from 0.05 to 0.22 with all but seven runs having $K_r < 0.15$. These higher K_r values were all associated with $N = 100$ stems/m^2, and upon further inspection it was found that a problem with the wave generator resulted in noisy wave spectra in these early wave runs. This issue was resolved by moving the experiment to the 1.5 m flume. Consequently, wave reflection was neglected as K_r was small for the majority of the tests.

2.5.2 Wave height analysis

The wave spectral energy density ($S(f)$) at each gauge was estimated from the surface elevation time series using a FFT. The mean was removed from the data, and the data were broken into segments of 2048 points. The spectra were smoothed by averaging five neighboring frequency bands. The resulting resolution bandwidth was 0.061 Hz, and spectral estimates had 60 degrees of freedom. A filter was applied to remove all energy at frequencies greater than 2 Hz to eliminate high-frequency oscillations from the data. The zero-moment wave height (H) is estimated from the wave spectra using the following relationship:

$$H = 4\sqrt{\sum_{j=1}^{n} S(f)_j \Delta f} \quad (1)$$

where:

n = number of frequency components
Δf = frequency resolution (Hz).

The root-mean-square wave height (H_{rms}) was obtained from the zero up-crossing wave heights from the demeaned time series:

$$H_{rms} = \sqrt{\frac{1}{M}\sum_{j=1}^{M} H_j^2} \quad (2)$$

where:

H_j = individual wave height (m)
M = total number of waves.

The precision of the data was assured by repeating each test run a minimum of three times. Repeatability was high as the maximum standard deviation for a series of nine repeats of the 0.457 m water level for 0.081 m wave height at 1.5 sec was 1.0 mm. Final wave heights were obtained by averaging wave heights from repeated runs where the standard deviation was less than three times the maximum standard deviation for the nine repeats (i.e., standard deviations greater than 3.0 mm were flagged and the outlying wave heights(s) neglected). This criterion was rarely exceeded – in total, 13 wave measurements were neglected, 11 for N = 100 stems/m² and 2 for N = 400 stems/m². No wave heights were omitted for the control or N = 200 stems/m².

2.5.3 ADV analysis

The ADVs were closely monitored during the experiments to guarantee an SNR > 20. The processed ADV signal neglected the still water measurements and consisted of only the 8 minutes (12000 data points) when waves were present in the signal (Figure 13). The velocities were

filtered by setting a threshold value of 70 for the correlation and 10 for SNR. Typically, less than 4% of the ADV velocity data was filtered using this method. After the ADV data were filtered, the velocity spectrum and statistics were calculated.

Figure 13. Wave portion of measured velocity time series.

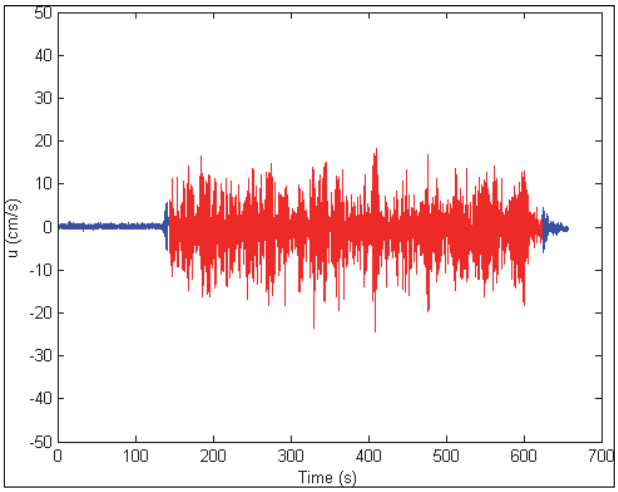

2.6 Results

2.6.1 Wave height attenuation

Control tests showed a maximum dissipation close to 15% over the measured length of the unvegetated bed (WG 13 at x = 9.3 m). This background dissipation is small compared to that induced by the idealized vegetation; thus, the measured wave attenuation is assumed to be caused mostly by the idealized vegetation.

The spectral energy loss for waves propagating through vegetation is presented in Figure 14, where wave energy spectra are presented for two wave conditions, one single- and one double-peaked. Spectra are shown at WGs 5, 7, 10, and 13, which are at x = 0.0, 1.0, 4.1, and 9.3 m where x is the distance from the beginning of the vegetation field. A continuing loss of wave energy is observed at all frequencies for both single- and double-peaked spectra as waves propagate through the artificial vegetation. The most evident loss of wave energy occurs at the peak frequencies. High-frequency variations, such as harmonics clearly seen at f = 0.88 Hz in the single-peaked spectra and f = 1.0 Hz in the double-peaked spectra, disappear by the end of the vegetation field.

Figure 14. Wave spectral transformation through artificial vegetation. [l_s/h = 1.36, H_0 = 0.113 m, T_p = 2.25 sec, N = 400 stems/m² (left), l_s/h = 1.36, H_0 = 0.131 m, T_p = 1.25/2.0 sec, N = 400 stems/m² (right)].

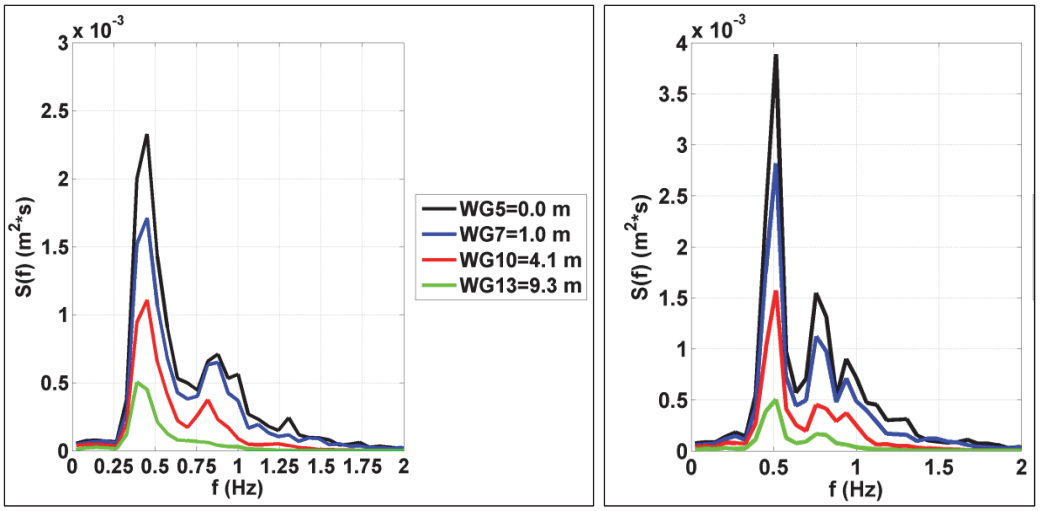

The effects of stem density (N), vegetation submergence ratio (l_s/h), peak period (T_p), and incident wave height (H_o) on wave attenuation were evaluated based on wave height. Wave attenuation due to the idealized vegetation was quantified by fitting the normalized zero-moment wave height (H/H_o)to the following exponential decay function (Kobayashi et al. 1993):

$$\frac{H}{H_o} = e^{-k_i \Delta x} \tag{3}$$

where:

H = local wave height (m)
H_o = incident wave height (m)
k_i = decay coefficient (m^{-1})
Δx = horizontal distance between gauges (m).

How well the above equation predicts the wave evolution is indicated by the squared correlation coefficient (R^2) where R^2 = 1.0 indicates a perfect fit. Figures of wave transformation though artificial vegetation are given in Appendix A.

The exponential function predicted the wave decay of single- and double-peaked wave spectra through the artificial bed very well. R^2 exceeded 0.95 for N = 200 stems/m² and exceeded 0.98 for N = 400 stems/m² for all

single-peaked tests. The lowest density N = 100 stems/m² had only two single-peaked wave conditions with $R^2 < 0.90$ (R^2 = 0.82 and 0.85). For the double-peaked spectra, R^2 exceeded 0.98 for N = 200 and 400 stems/m². Decay coefficient (k_i)ranged from 0.011 to 0.121 m^{-1}. Figure 15 shows the comparison between the exponential decay function and the measured data for one characteristic wave condition.

Figure 15. Exponential decay model fitted to measured wave heights [l_s/h = 1.36, H_0 = 0.113 *m*, T_p = 2.25 sec, N = 400 stems/m²].

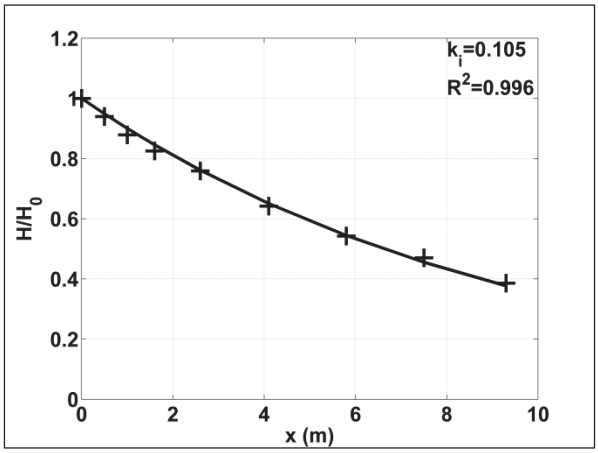

2.6.2 Single-peaked spectra

2.6.2.1 Stem density

The effect of stem density on wave height decay is shown in Figure 16 for l_s/h = 1.36. Wave attenuation was found to increase with denser arrays for all modeled wave conditions. The maximum attenuation in the unvegetated control channel was about 15%. The amount of attenuation along the idealized bed increases to 25% for N = 100 stems/m² and then to 45% for N = 200 stems/m² at x = 9.3 m. Waves propagating through the densest array experienced the greatest energy loss with a 60% decrease in wave height.

This trend is reflected in the decay coefficient as k_i was found to increase with stem density for all wave conditions (Figure 17). This behavior is expected given that the degree of wave energy loss is directly related to the drag force induced by the plants which is greater when more plants are encountered.

Figure 16. Effect of stem density on wave decay [artificial vegetation].

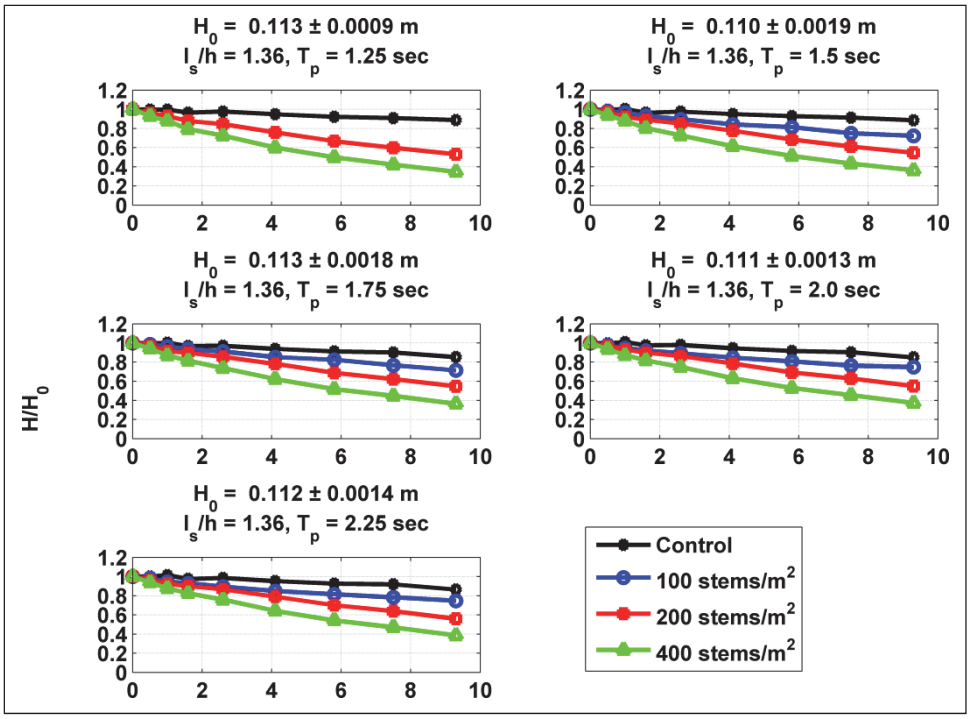

Figure 17. Decay coefficient (k_i) versus stem density (control tests correspond to N = 0 stems/m²) [artificial vegetation].

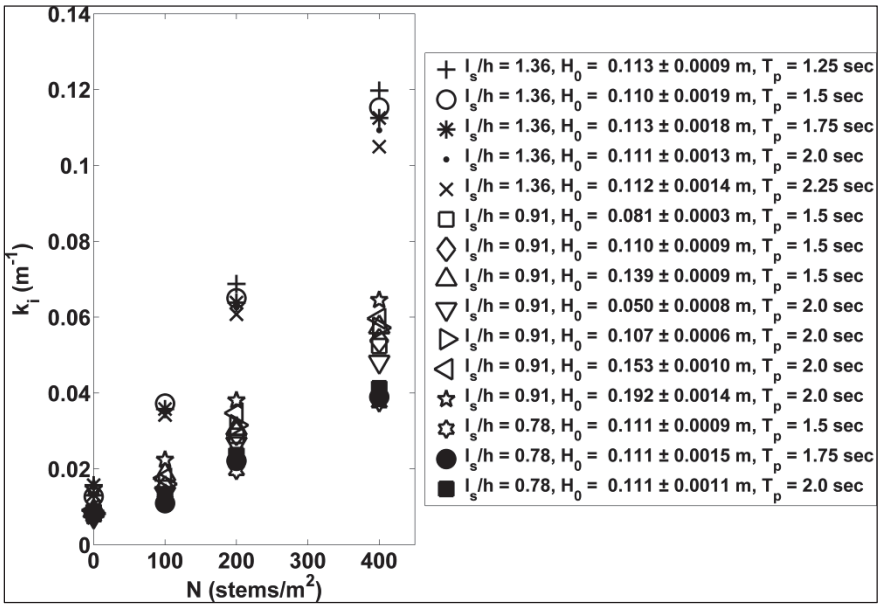

2.6.2.2 Vegetation submergence ratio

A convenient way to approach the effect of water depth on vegetation-induced wave attenuation is to define the vegetation submergence ratio. The vegetation submergence ratio represents the percentage of the water

column occupied by the plant and is the ratio of average plant height to water depth (l_s/h).

The effect of submergence depth on wave height transmission is shown in Figure 18 where the normalized zero-moment wave height is plotted for the same incident wave condition. Wave attenuation increases with submergence ratio for all stem densities. For N = 400 stems/m², the incident wave height is reduced by 30%, 40%, and 64% for l_s/h = 0.78, 0.91, and 1.36, respectively, at x = 9.3 m.

Figure 18. Effect of vegetation submergence ratio on wave decay [artificial vegetation].

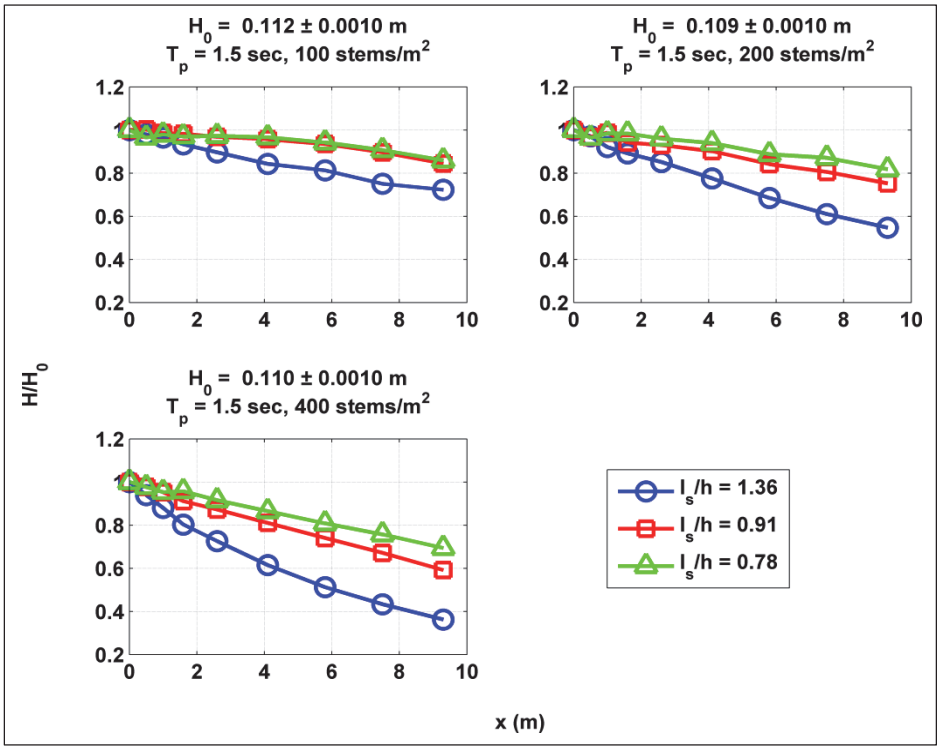

The decay coefficient (k_i) has a similar trend (Figure 19). The capacity of vegetation to attenuate wave energy diminishes as water depth increases due to the decreasing wave particle velocities with depth and smaller percentage of the water column impeded by the vegetation. Emergent conditions are expected to result in the greatest amount of wave attenuation because plants occupy the entire water column. However, as water depth exceeds canopy height, the greatest orbital velocities found in the top portion of the water column are not affected by the vegetation.

In general, the variation in wave attenuation caused by stem density is coupled to vegetation submergence ratio as evidenced by the range in k_i

considering the same relative submergence of the canopy (Figure 19). The widest range in k_i occurs for the emergent condition where differences in wave attenuation due to stem density are most evident. For example, the difference in k_i between N = 100 and 400 stems/m² is 0.078 m⁻¹ for l_s/h = 1.36 versus 0.023 m⁻¹ for l_s/h = 0.78. This dramatic drop (e.g., collapse) in the range of k_i suggests stem density becomes less influential on wave decay as the submergence ratio decreases (i.e., water depth increases).

Figure 19. Decay coefficient (k_i) versus vegetation submergence ratio [artificial vegetation].

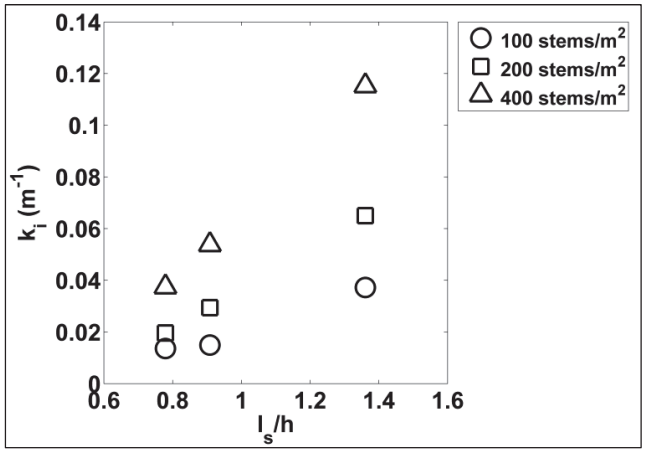

2.6.2.3 Incident peak wave period

The effect of peak wave period on the attenuation of wave energy is investigated using h/L_p where L_p is the wavelength at the spectral peak. This representation is useful as it defines wave period as a function of water depth, which determines the wave regime. Waves are classified as deepwater waves when $h/L > 0.5$ and shallow-water waves when $h/L < 0.05$. Figure 20 presents the wave decay for wave runs at l_s/h = 1.36. Wave period has little effect on total wave attenuation with x as the difference in attenuation between the shortest wave, T_p = 1.25 sec (h/L_p = 0.13), and the longest wave, T_p = 2.25 sec (h/L_p = 0.08), is 4% for N = 400 stems/m².

Plotting k_i versus relative depth did not show a clear trend (Figure 21). The decay coefficient (k_i) slightly increases with larger h/L_p at l_s/h = 1.36 but generally decreases with larger h/L_p at l_s/h = 0.78. The difference in k_i between wave periods is very small (e.g., 0.015 m⁻¹ between T_p = 1.25 and 2.25 sec at l_s/h = 1.36 and N = 400 stems/m²), but the range of periods tested is also small.

Figure 20. Effect of peak period on wave decay [artificial vegetation].

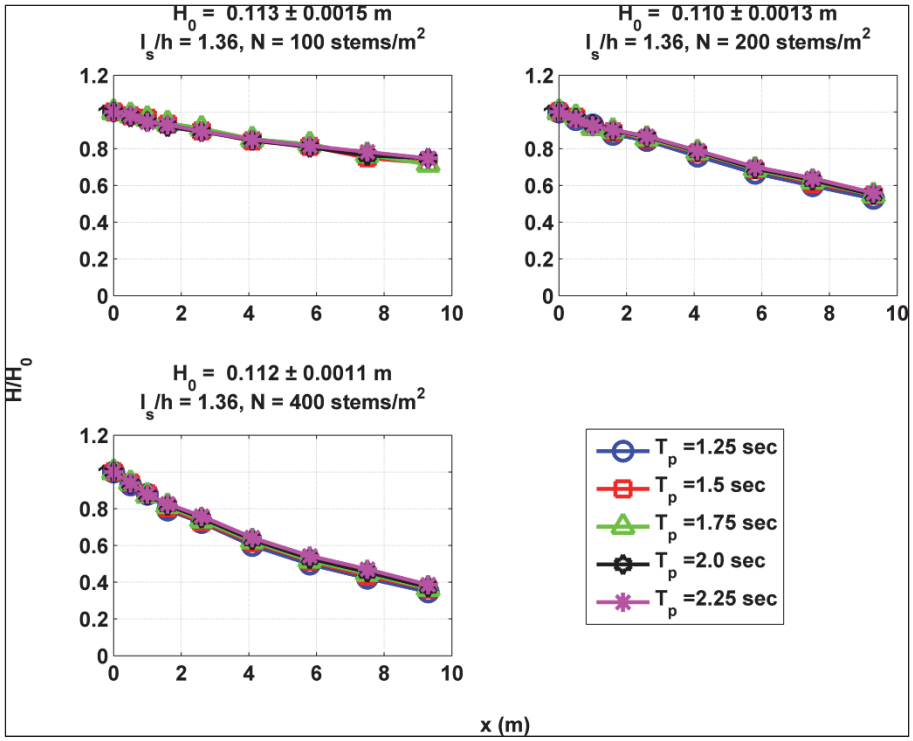

Figure 21. Decay coefficient (k_i) versus relative depth (open symbols are emergent conditions and closed symbols are submerged) [artificial vegetation].

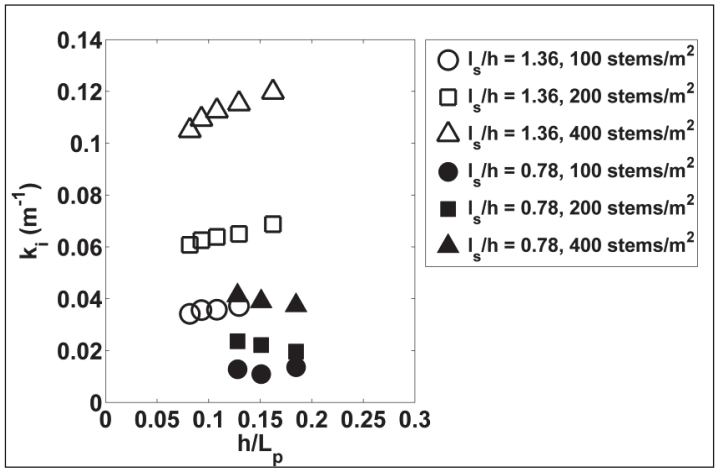

It was anticipated wave period would have a more noticeable impact on wave attenuation as waves interact with the bottom based on relative depth. A deepwater wave particle trajectory is a radius that decays exponentially with nearly negligible particle motion at the bottom. Shallow-water waves experience elliptical orbits with the same horizontal excursion but a decreasing vertical excursion until the bottom where the particles follow a reversing horizontal path (Sorensen 2006). Considering

these trajectories, shallow-water waves are more strongly affected by bottom features, and wave attenuation through vegetation was expected to increase as waves approach shallow-water classification (Cavallaro et al. 2010; Koch et al. 2006; Fonseca and Cahalan 1992). Note that all waves tested were in the intermediate depth range, so more variation may have been seen if a broader range of periods was tested.

2.6.2.4 Incident wave height

Figure 22 presents the effect of incident wave height on wave attenuation through vegetation for l_s/h = 0.91 and T_p = 2.0 sec. The measured attenuation for N = 400 stems/m² at x = 9.3 m for H_o = 0.050, 0.106, 0.152, and 0.192 m are 38%, 43%, 44%, and 45%, respectively.

Figure 22. Effect of incident wave height on wave decay [artificial vegetation].

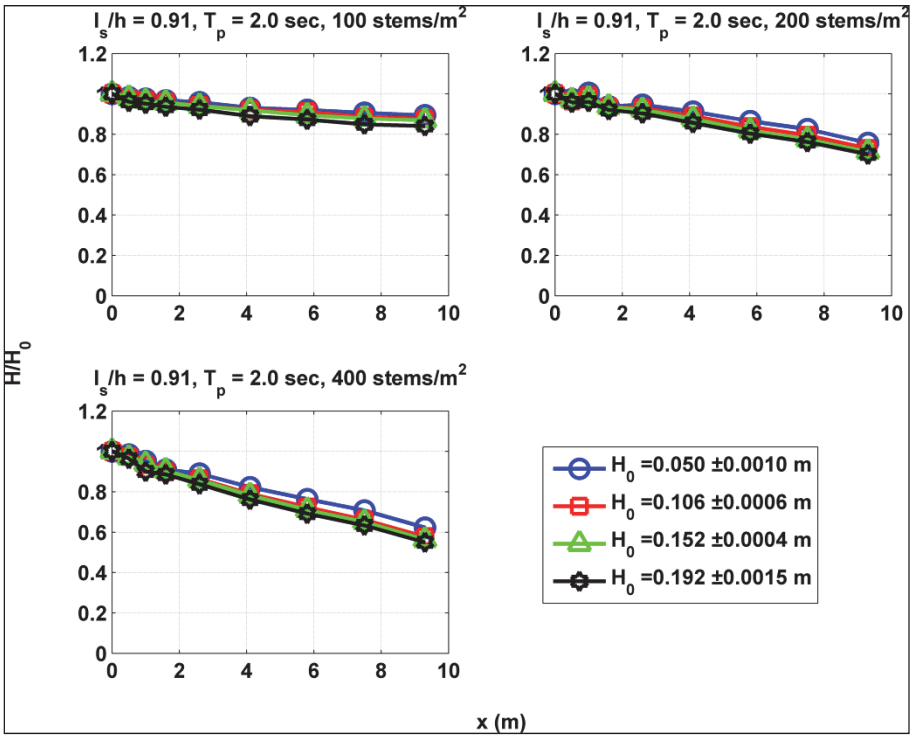

Wave attenuation, as represented by k_i in Figure 23, slightly increased with larger waves for both wave periods (T_p = 1.5 and 2.0 sec) considering the same stem density. Intuitively, larger wave heights contain more energy. The increased energy should result in a larger drag force induced by the plants and, thus, greater attenuation. However, previous studies have reported increases in wave attenuation with larger wave heights (Cavallero et al. 2010; Tschirky et al. 2000) as well as decreases (Manca et

al. 2012; Bradley and Houser 2009). One of the reasons for these conflicting results may be plant morphological differences, in particular, plant rigidity. Bradley and Houser (2009) reported decreases in wave attention with larger waves as the sea grass studied (primarily *Thalassia testudinim*) tended to extend in the direction of the flow for a longer part of the wave cycle and became streamlined, leading to reduced drag. Additional testing is necessary to further develop the relationship between wave height and vegetation-induced wave attenuation since the types of waves generated were limited by laboratory constraints (e.g., narrow period range and small wave heights).

Figure 23. Decay coefficient (k_I) versus incident wave height (open symbols are T_p = 1.5 sec and closed symbols are T_p = 2.0 sec) [artificial vegetation].

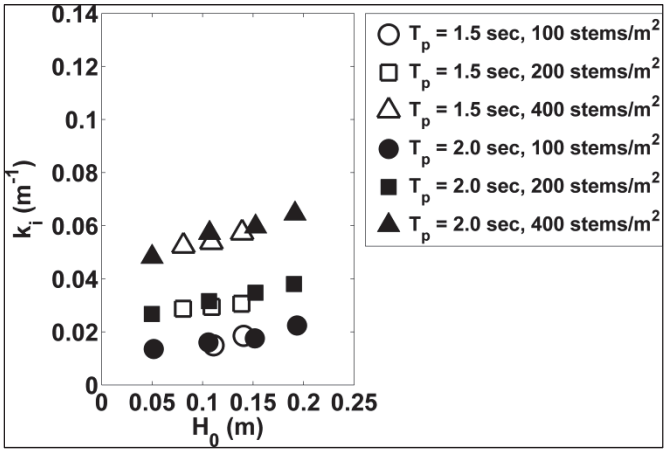

2.6.3 Double-peaked spectra

Previous studies on wave propagation through vegetation focused on field studies and single-peaked spectra. In this study, double-peaked spectra were generated to investigate the dissipation of superimposed wave spectra. Treating a double-peaked spectrum as the linear superposition of two wave systems (Figure 24), each spectrum was separated into two frequency ranges (T = 1.25 and 2.0 sec) and a decay coefficient (k_i) fitted to each (Figure 25). Decay coefficients calibrated for the entire spectrum and the separated wave systems increased with stem density for all wave conditions, mimicking the trend of the single-peaked spectra.

Figure 24. Identifying wave spectra of double-peaked spectrum [l_s/h = 1.36, H_0 = 0.108 m, N = 400 stems/m²]. The T = 1.25 and 2.0 sec frequency ranges are identified by the green and blue line, respectively.

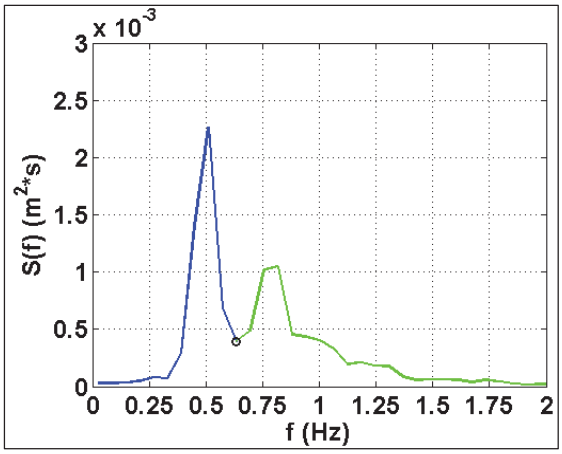

The attenuation of the two frequency ranges was not uniform and depended on vegetation submergence ratio and stem density. The decay coefficients (k_i) are nearly identical for the separated spectra under submergent conditions, but under emergent conditions a larger k_i value was calibrated for the higher-frequency system than the low-frequency system (Figure 26). Moreover, the degree of attenuation between the systems increased with stem density for emergent conditions. The difference in k_i between the two spectra for H_o = 0.108 m is 0.017, 0.035, and 0.044 m^{-1} for the control, N = 200 and 400 stems/m², respectively. A similar trend in k_i was found for H_o = 0.134 m.

Figure 25. Exponential decay model fitted for two superimposed wave spectra [l_s/h = 1.36, H_0 = 0.108 m, N = 400 stems/m²].

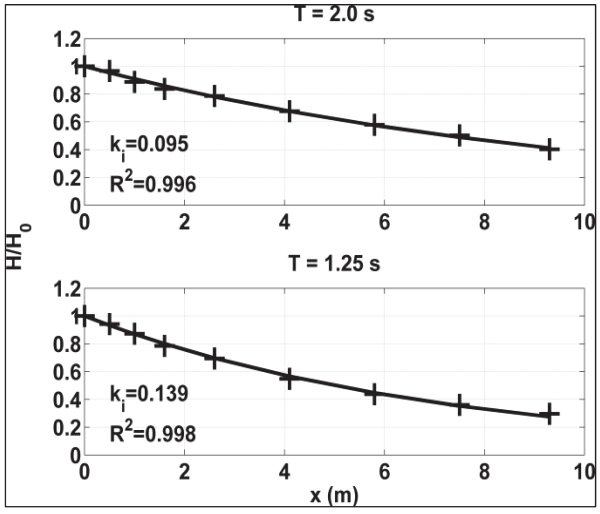

A larger k_i suggests wave energy is dissipated more efficiently among the higher frequency components of the wave spectra particularly during emergent conditions. Furthermore, preferential dissipation of the higher frequencies is enhanced for denser stem arrays. The more efficient dissipation of shorter-period wave components are supported by field observations over sea grasses under low energy conditions (Bradley and Houser 2009) and studies of in-canopy flow structure within submerged rigid canopies (Lowe et al. 2007).

Figure 26. Decay coefficient (k_i) for separated wave spectra of double-peaked spectrum versus vegetation submergence ratio [artificial vegetation].

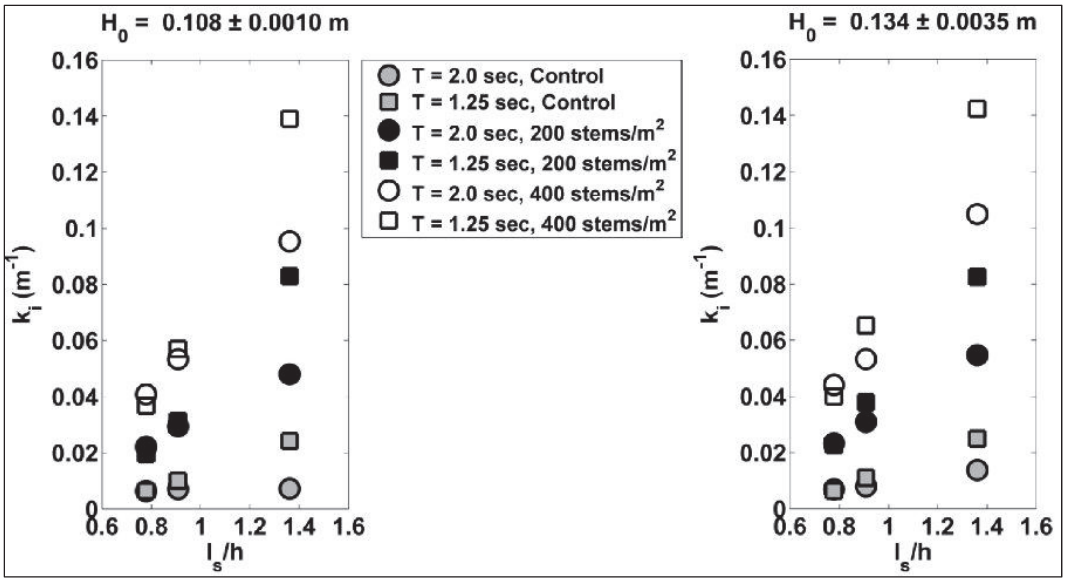

2.6.4 ADV results

2.6.4.1 Velocity reduction

The velocity measurements give further insight into the dynamics of waves propagating through vegetated environments. The dissipation of wave energy is observable in the reduction of wave height but also in the reduction of velocities. Typically, the time-averaged velocity gives insight into the flow magnitude. However, the time-averaged velocities for waves are nearly zero. In this study, the wave energy magnitude is represented using the mean of the velocity squared, $<U^2>$. This value contains both the wave and turbulent component of the velocity and can be viewed as representation of the kinetic energy.

Figure 27 shows the reduction of the horizontal velocity magnitude through the artificial vegetation field for the control, N = 200 and 400

stems/m² for T_p = 2.0 sec under different submergence ratios. For the emergent case, l_s/h = 1.36, the control has a total reduction of 15% over the entire test section (x = 9.3 m). The N = 200 and 400 stems/m² stem densities resulted in total reductions of 66% and 83%, respectively.

As with the wave height analyses, the denser artificial vegetation increased the reduction of wave velocity. This reduction supports the potential of vegetation to act as mitigating factor against sediment erosion. As the water depth increases over the vegetation, the velocity reduction decreases. For l_s/h = 0.91 and 0.78, the reduction in velocities for N = 400 stems/m² is 71% and 59%, respectively. As water depth and plant submergence increases, the effective blocking of the vegetation decreases, resulting in smaller velocities around the plant stems which lead to less turbulence production and energy dissipation.

Figure 27. Reduction in horizontal velocity with submergence ratio for T_p = 2.0 sec [artificial vegetation].

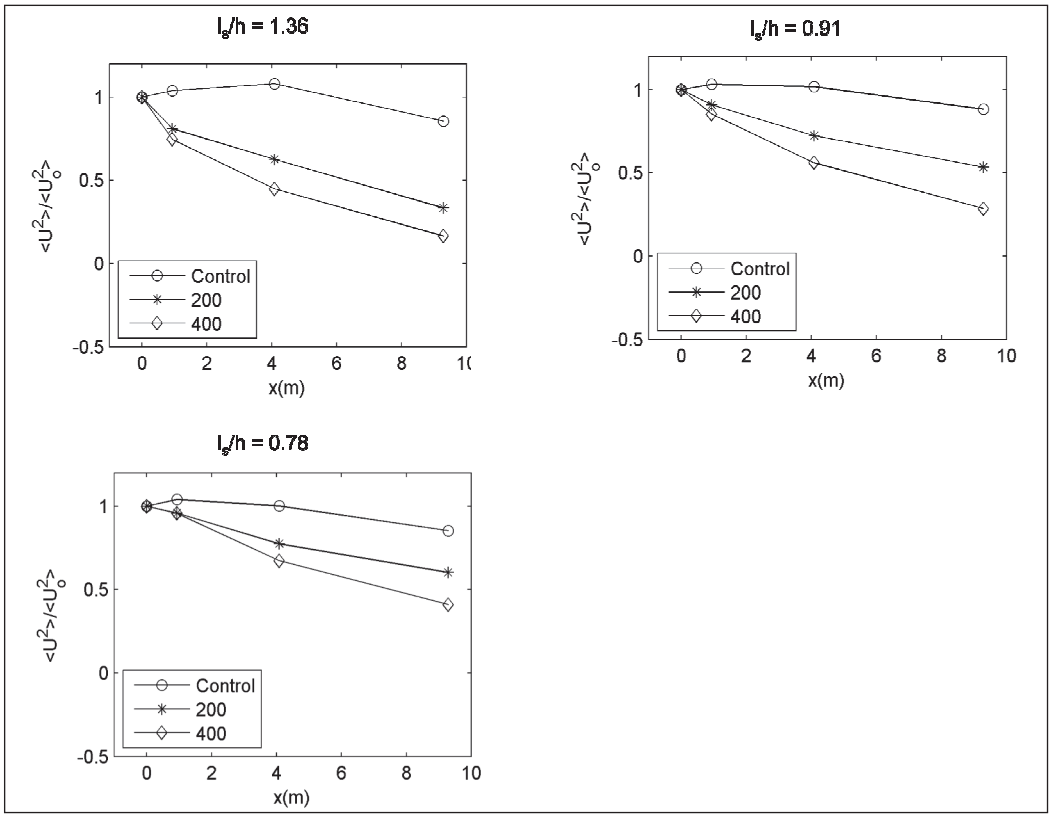

The reduction in velocity was similar for waves with different peak period. A wave spectrum with a peak period T_p = 1.25 sec had a total reduction in velocities of 72% versus 65% for a wave spectrum with a peak period T_p =

2.25 sec with identical H_o. Figure 28 presents the velocity reduction versus peak period for an artificial vegetation density of N = 200 and 400 stems/m² and a submergence ratio of l_s/h = 1.36. Both plots show that with increasing peak period there is a decrease in the total horizontal velocity reduction. However, a longer peak period slightly increased the horizontal velocity reduction for l_s/h = 0.78 (Figure 29). A wave spectrum with T_p = 1.5 sec had reduction of 38% whereas a horizontal velocity reduction of 40% was found for T_p = 2.0 sec. These results are in agreement with the observed trends in the wave gauge data.

Figure 28. Reduction in velocity with varying peak period for l_s/h = 1.36 [artificial vegetation].

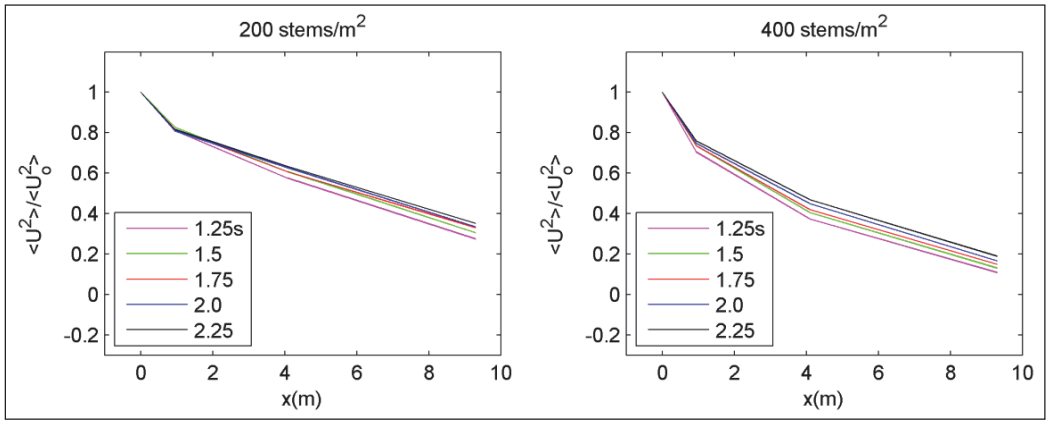

Figure 29. Reduction in velocity with varying peak period for l_s/h = 0.78 [artificial vegetation].

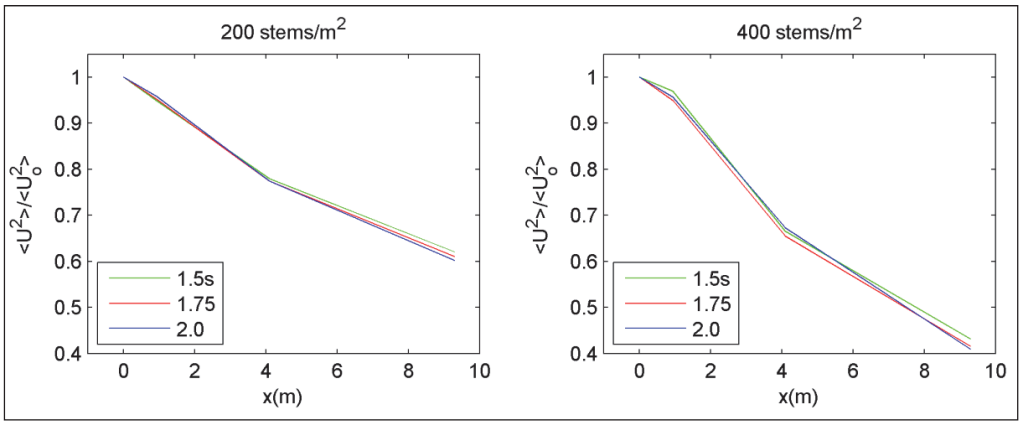

Figure 30 presents the changes in horizontal velocity magnitude reduction for a range of incident wave height H_o for l_s/h = 0.91 and T_p = 2.0 sec. In general, more velocity reduction was seen for larger incident wave heights. Velocity reductions of 44% and 46% were found for H_o = 0.05 and 0.19 m, respectively, for N = 200 stems/m². However, the greatest velocity reduction, 71%, was found for H_o = 0.15 m for N = 400 stems/m², which is

greater than the velocity reduction of 62% and 68% for H_o = 0.05 and 0.19 m, respectively. This finding deviates from that of the wave height analysis, where wave attenuation increased with incident wave height for both periods tested. It is recommended a wider span of incident wave heights be tested to clarify this discrepancy in future work.

Figure 30. Reduction in velocity with varying wave heights for l_s/h = 0.91 [artificial vegetation].

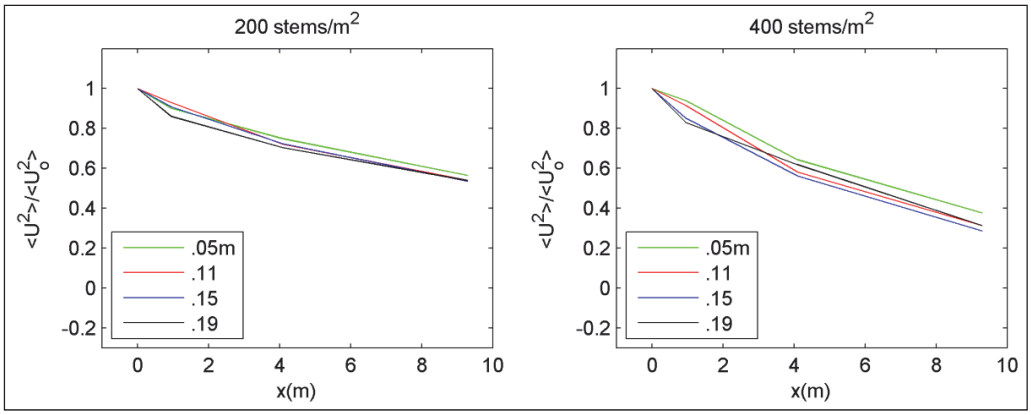

2.6.4.2 Turbulence generation

As the flow oscillates around the artificial vegetation, wave energy is dissipated through the generation of turbulence. The magnitude of turbulence generation is dependent on the velocity of the waves. The generation of turbulence around simple cylinders has been studied extensively; however, arrays of cylinders (rigid or flexible) remain an area of active research (Stoesser et al. 2010; Wilson et al. 2003; Evangelinos and Karniadakis 1999).

The strength of turbulence in a flow can be estimated using the spectral energy density of the velocities. For steady flow, the mean is removed from the velocity measurements before calculating the turbulent energy spectrum. However, the mean flow for waves is nearly zero, and the separation of the wave and turbulence velocity is difficult. One alternative method to examine the energy spectra is to use a simple band pass filter (Chakrabarti et al. 2011). Based on the surface wave spectrum, there is very little wave energy above frequencies of 2 Hz. Thus, when interpreting the velocity spectrum, frequencies below 2 Hz can be seen as being driven by the waves; whereas, energy at frequencies above 2 Hz is considered turbulence.

All velocity spectra have the corresponding background noise spectra subtracted. The noise spectra were found by measuring the velocity for 8 minutes in the flume when there was no flow. The background noise spectra were orders of magnitude smaller than the velocity spectra.

Figure 31 presents the velocity energy spectra at different locations in flume for l_s/h =1.36, H_o = 0.11 m, T_p = 2.0 sec for the control, N = 200 and 400 stems/m². The velocity spectra at the leading edge of the vegetation (x = 0.0 at WG 5) are nearly identical for all stem densities, including the unvegetated control, demonstrating the repeatability of the wave conditions. The portion of the spectrum with a frequency above 2 Hz is greater in the presence of artificial vegetation than the control at x = 1.0 m due to the generation of turbulence as the waves move through the artificial vegetation. However, the turbulence component is nearly the same magnitude as the control at x = 9.3 m. The magnitude of the turbulence generated is directly proportional to the available energy which is a function of wave height. Despite a reduced wave component (evident at x = 4.1 and 9.3 m), the turbulence energy is similar for all stem densities at x = 9.3 m, showing the artificial vegetation continued to dissipate energy throughout the entire test section.

Figure 31. Changes in velocity spectra (l_s/h = 1.36, H_o = 0.110 m, T_p = 2.0 sec) [artificial vegetation].

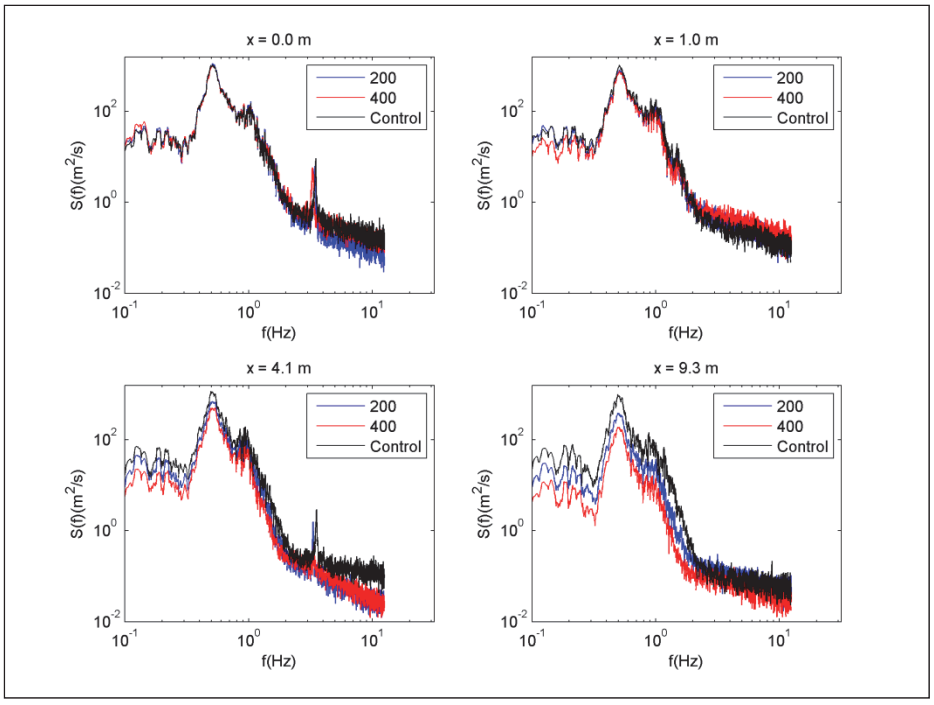

The velocity spectra for l_s/h = 0.91 and 0.78 are shown in Figure 32 and Figure 33, respectively. The trends are similar for the emergent and submerged cases for the artificial vegetation. The incident velocity spectra are nearly identical at x = 0.0 m, with an increase in the turbulence (f > 2.0 Hz) at x = 1.0, 4.1, and 9.3 m with respect to the wave component. Although the reduction in the wave dominant portion of the spectra is smaller for the submerged cases, the wave dissipation seems to be similar for all frequencies below 2 Hz. This is best observed in Figure 31 where the final velocity spectra (x = 9.3 m) for N = 400 stems/m² follows the same trend as the control spectrum but is simply shifted down in magnitude for frequencies less than 2 Hz.

Figure 32. Changes in velocity spectra (l_s/h = 0.91, H_0 = 0.153 m, T_p = 2.0 sec) [artificial vegetation].

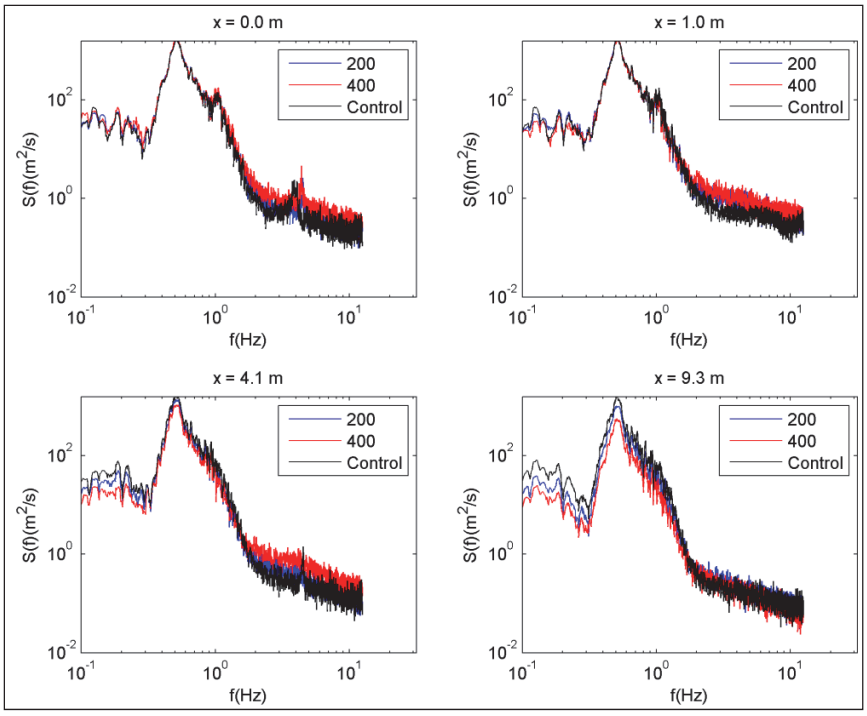

The double-peaked spectra were found to have similar results to the single-peaked spectra. The velocity spectra for one characteristic emergent, double-peaked wave condition is given in Figure 34. As with the single-peaked spectra, the wave component decreases as the waves propagate through the vegetation, but turbulent energy increases at frequencies above 2 Hz. The velocity data does not show any clear transfer of energy to other frequencies in the wave portion of the spectra.

Figure 33. Changes in velocity spectra (l_s/h = 0.78, H_0 = 0.111 m, T_p = 2.0 sec) [artificial vegetation].

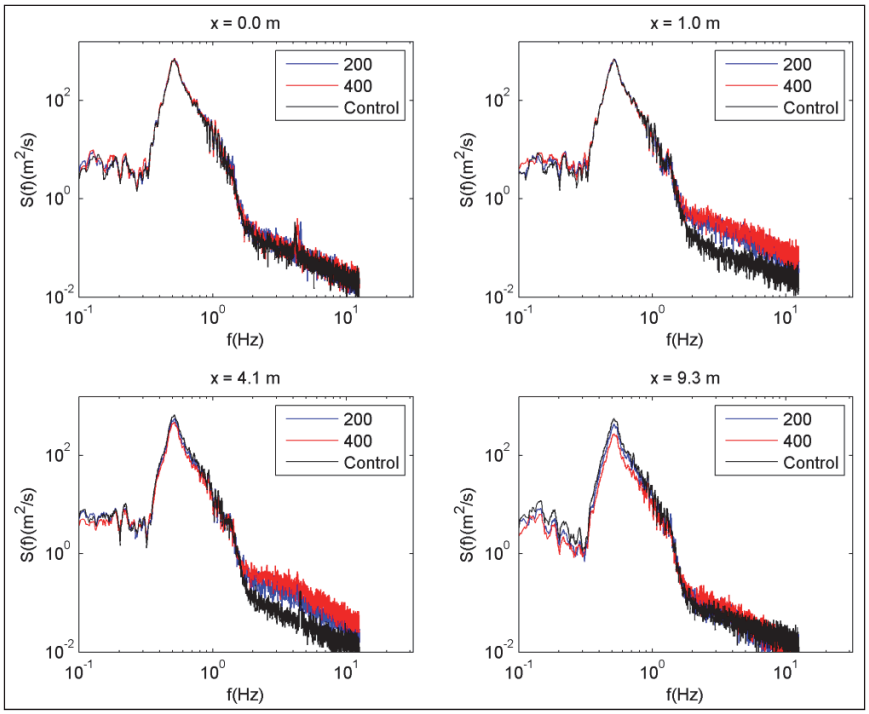

Figure 34. Changes in velocity spectra (l_s/h = 1.36, H_0 = 0.129 m, T = 1.25/2.0 sec) [artificial vegetation].

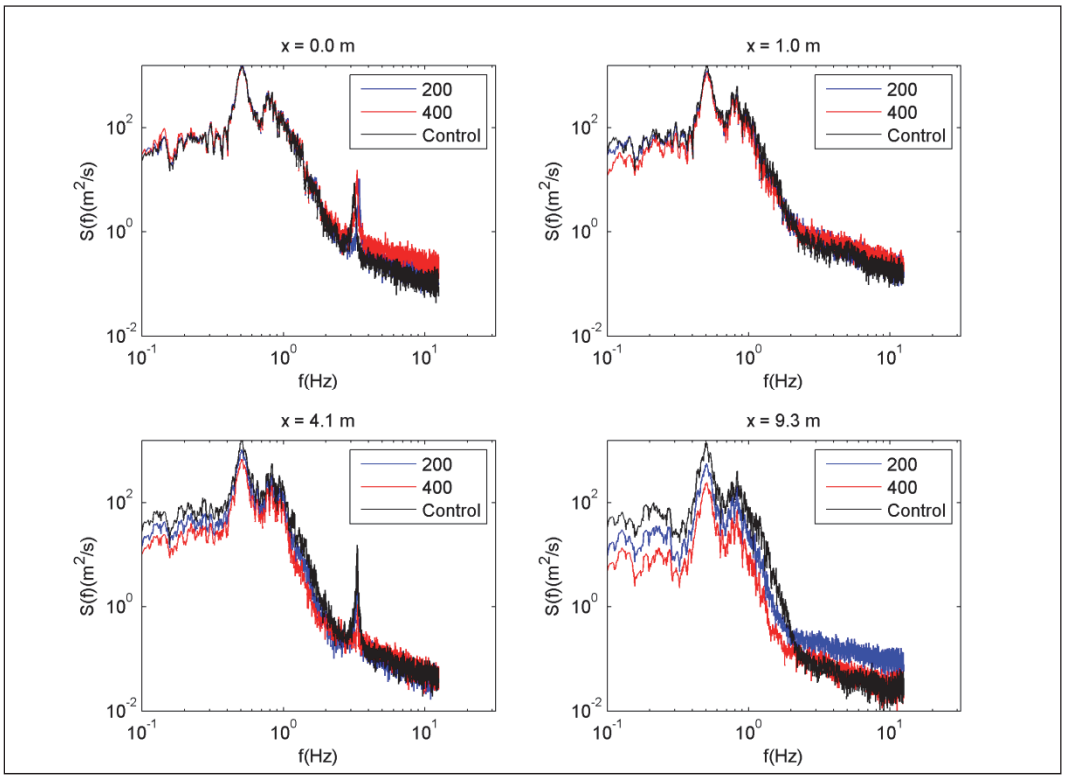

3 Real Vegetation Experiments with *Spartina alterniflora*

Spartina alterniflora is the dominant emergent sea grass growing along the Atlantic Ocean and Gulf of Mexico tidal marshes. It is commonly found between low and high tide, tolerates regular inundation, and grows from 0.6 to 2.1 m tall. Its lateral spread by rhizomes of 0.6 to 3.0 m annually makes it an effective soil stabilizer for marsh restoration while providing food and coverage to marsh birds and mammals and serving as a forage species for livestock (USDA, NRCS 2012a).

This chapter describes the design, construction, and execution of the *S. alterniflora* experiments. Conducted using the same wave records as the artificial vegetation tests, the purpose of these experiments was to obtain wave dissipation data using real vegetation to quantify the impacts of vegetation on waves.

3.1 Real vegetation

3.1.1 Establishing specimens

Preparation for growing *S. alterniflora* on-site began in April 2012. To eliminate the possibility of plant washout due to soil erosion, plants were grown hydroponically in coir mats. The coir mats from RoLanka International Inc. (http://www.rolanka.com/GN/WR-pillow.html) measured 0.91 m wide, 1.52 m long, and 0.05 m thick.

Prior to ordering the plants, ten rectangular box-frames (1.42 m wide, 1.83 m long, and 0.14 m deep) were constructed using untreated 2 × 6 lumber. The width and depth of the box frames allowed for the planted mats to easily fit within the existing flume setup (described in Section 2.1.1.2). Thick plastic sheeting wrapped around the frames and secured on top served as the impermeable bottom. All the trays were lined with a single layer of 0.05 m thick wave absorber. These absorbers supported the weight of the planted mats and were also fibrous, serving as an additional substrate in which the plants could anchor.

Nine thousand *S. alterniflora* cv. Vermilion bare-root plugs were ordered from Sustainable Native Plants, LLC (http://nativeplantsllc.com/). The

plugs varied in height from 0.15 m to 0.20 m. Smaller plugs were advised by the grower as younger plants have a lower susceptibility to shock, and *S. alterniflora* cv. Vermillion is robust, easily capable of reaching 0.61 m tall in 2–3 months (USDA, NRCS 2012b). A 50% plant material contingency was achieved assuming a target density of 400 stems/m^2. Plugs were secured in the coir on a rough 0.05 m staggered grid, and the coir was placed into the box-frames (Figure 35). A substantial amount of plugs remained after filling the box frames, and a 3.05 m wide × 2.74 m long container was quickly constructed using concrete blocks and plastic sheeting. This backup container was capable of holding six planted coir mats.

Figure 35. Securing *S. alterniflora* in coir mats (left) and newly planted mat (right).

The plants were grown in a 100 ppm nutrient solution of Peter's Professional® 20-20-20 water soluble fertilizer as is recommended for the continuous liquid feeding of plugs and by the Golden Meadow Plant Materials Center[1]. The trays were filled with the nutrient solution until the water level was slightly above the coir mats, and the solution was flushed and changed at least twice a week to minimize the growth of algae and cool the water. The plants grew in a greenhouse under natural light conditions from May – August. A photograph of *S. alterniflora* in the greenhouse is shown in Figure 36.

3.1.2 Measurements of real vegetation

Six box frames were selected for installation in the flume using color and fullness as an indication of plant health. Average plant parameters including stem density, total height, stem length, and stem diameter were collected prior to installation.

[1] Golden Meadow Plant Materials Center, 438 Airport Road, Galliano, LA 70354

Figure 36. Preparation of *S. alterniflora*.

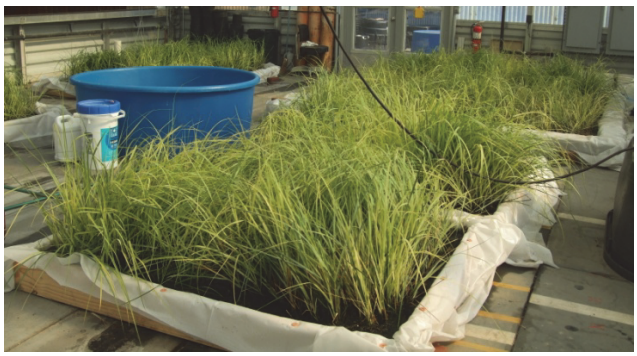

To select the sampled population, a 1 m² plot with 25 gridded quadrants (0.2 m × 0.2 m) was tossed over the plants so the plot boundaries remained within the confines of the tray. Plant stems, defined as the number of main stalks emerging from the root mass, within the 1 m² area were counted. Plant geometry was measured for a smaller population. In order to eliminate bias, 4 of the 25 square quadrants were selected by randomly drawing a letter-number combination. The total height, stem length, and stem diameter were recorded for each stem within the quadrants. The total height was taken as the distance from the root mass to the tip of the tallest leaf. The stem length was defined as the base of the plant to the meristem (i.e., beginning of the youngest juvenile leaf), and the stem diameter was measured at half the stem length using digital calipers. The average number of stems per m², the average total height, the average stem length, and the average stem diameter are presented in Table 3. A schematic of measured dimensions is shown in Figure 37.

Table 3. Average *S. alterniflora* characteristics.

Stem density (stems/m²)	Total height (m)	Stem length (m)	Stem diameter (mm)
162	0.93	0.19	5.2

Although the plugs were installed on a grid, the spatial distribution of the grown *S. alterniflora* was not uniform (Figure 38). It was common to see plant clumps where a unified stem or multiple stems emerged from the mats. This clumping resulted in pockets of very dense vegetation adjacent to areas of bare mat which is indicative of natural *S. alterniflora* marsh platforms (Feagin et al. 2011). As *S. alterniflora* spreads primarily by vegetative stem division, producing new shoots from an underground system of rhizomes, it is likely the plant spacing in the coir was too close and led to competition between the plants. Additionally, after the planted mats were moved into the box frames, several plugs fell into the water.

Attempts to right and straighten the plugs were undertaken, but many drowned. The combination of these issues, as well as general inexperience in hydroponics, resulted in the low stem density. It is recommended for future experiments to design a more appropriate hydroponic system (one capable of supporting the long-term growth of plants such as a continuous flow system), to plant the plugs further apart and have them fill in naturally, and to avoid moving newly planted mats to ensure plants remain upright.

Figure 37. Schematic of plant measurements.

Figure 38. Spatial distribution of *S. alterniflora*.

3.1.3 Installation of real vegetation

The top plywood sheet of the 1.5 m flume setup (described in Section 2.1.1.2) was removed, revealing the ledge seen in Figure 39. The ledge allowed for the real vegetation to be placed level with the slope interface.

Figure 39. Preparing 1.5 m flume setup for real plants.

A series of layers was used to raise the real vegetation flush with the slope. A 0.02 m thick plywood sheet cut the same dimension as the box frames served as the foundation. One layer of 0.05 m thick wave absorber was laid on top of the plywood. The plants were then lifted from the box frames and placed on top of the wave absorber. Note that the plants were grown in two substrates: a coir mat and a layer of wave absorber. These four layers were held together using metal banding, tightened and secured to the bottom of the plywood using screws. A photograph and schematic of the layers is shown in Figure 40.

Figure 40. Photograph (left) and schematic (right) of vegetation sections.

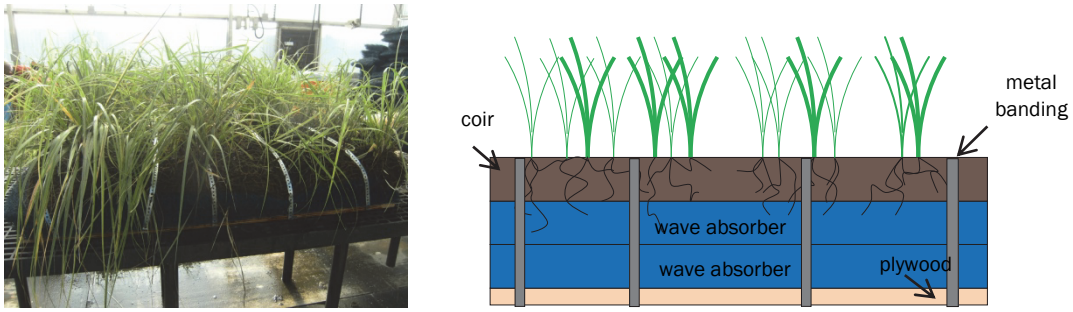

These sections were transported to the flume and installed between the 2 × 6 lumber edges by screwing the foundation plywood to the lowered floor. The layers were then secured in the four corners by screwing the

outermost banding to the floor, compressing the layers and preventing slipping beneath the metal banding. The sections were installed in succession flush to one another to avoid gaps. The real *S. alterniflora* installed in the 1.5 m flume is shown in Figure 41.

Figure 41. Installing *S. alterniflora* sections in the flume (left) with completed bed (right).

3.2 Description of experiments

3.2.1 Test facilities

The experiments with real vegetation were conducted in the 1.5 m flume using the setup and installation described in Section 2.1.1.2 and 3.1.3, respectively.

3.2.2 Instrumentation

The free surface was measured by 13 single wire capacitance wave gauges (WG), with the location of the gauges provided in Table 1. Four acoustic Doppler velocimeters (ADV) measured flow velocity and are described in greater detail in Section 2.1.2.2. The acoustic Doppler current profiler (ADCP) was removed for the real *S. alterniflora* tests as the leaves were too dense for the ADCP to adequately sample the water column.

3.3 Wave and water level conditions

The wave and water level conditions are the same as those for the artificial vegetation tests and are provided in Table 2. Defining the relative submergence of the plants immediately becomes challenging. The vegetation submergence ratio can be defined two ways: using either the average stem length or the average total height of the plant. Using the average stem length, the calculated vegetation submergence ratios for all modeled water depths are less than 1.0 and represent submergent

conditions. However, classifying the vegetation as *submerged* would be incorrect. While these ratios represent the percent of the water column occupied by the plant stem, the average total height of the plants is nearly five times greater. Thus, the vegetation is considered emergent at all modeled water depths if leaves are accounted for.

To address this issue, studies of wave attenuation over vegetation were reviewed. Unfortunately, a common definition of *average plant height* proved difficult as the standard for quantifying plant parameters varied with little to no explanation of how plant geometry was defined. It is recommended future studies clarify the methodologies for quantifying plant biophysical parameters. For this real vegetation study, the vegetation submergence ratio is calculated using the average total height of the plant l_{st} where l_{st}/h = 3.05, 2.04, and 1.74 for h = 0.305, 0.457, and 0.533 m, respectively.

3.4 Test procedures

The test procedures for the real vegetation experiments are similar to those outlined in Section 2.4. Data were collected for a total of 42 runs, and the experiment was performed in two test groups: (1) with unplanted coir mats and (2) with real *S. alterniflora*. The unplanted coir mats were installed using the same methodology as the real vegetation and served to measure the background attenuation of the mats (which are porous and rough). All wave conditions in Table 2 were completed with the order of tests selected to minimize plant uprooting and fatigue. Starting at the lowest water level, wave signals were tested from the smallest to the largest wave height. Once all the wave conditions were tested at the lowest depth, the tests moved on to the smallest wave height at the next water depth and so on.

Wave signals were repeated a minimum of two times to verify repeatability. If the output from the data acquisition system showed an anomaly in the time series or wave height, the test was repeated a third time to verify the trend. A minimum of three repeats was conducted for control tests. Leaves around the wave gauges and ADVs were cut down to prevent interference with the instruments. Videos, pictures, and notes were used to document the experiments.

3.5 Data analysis

Data analysis for the real vegetation tests included (1) reflection analysis, (2) spectral analysis, and (3) up-crossing analysis with details provided in Section 2.5. The 5 mm threshold used to identify the wave signal in the artificial experiments was often triggered too late or not at all in the real vegetation tests. The threshold was lowered to 2 mm. The difference in incipient zero-moment wave height using a threshold of 2 mm versus 5 mm was less than 0.5% for an artificial control test (h = 0.457 m, H_o = 0.081 m, and T_p = 1.5 sec). Thus, the potential implications of changing this threshold were considered negligible.

3.5.1 Reflection analysis

Reflection coefficient (K_r) was calculated for the real vegetation using the three-gauge separation method described in Section 2.5.1. Reflection coefficient (K_r) varied from 0.06 to 0.14, with 13 runs having K_r > 0.10. This range is similar to the K_r values of the 1.5 m flume artificial vegetation experiments. As real *S. alterniflora* did not noticeably increase the reflection of the incident wave, wave reflection was neglected.

3.5.2 Wave height analysis

Following the methodology used for the artificial vegetation in Section 2.5.2, zero-moment wave heights (H) were calculated from the spectral energy densities according to Equation 1, and the root-mean-square wave heights (H_{rms}) were calculated from the time series using Equation 2.

Final wave heights were calculated by averaging over repeated wave runs. Wave conditions with three or more repeats were subjected to the standard deviation check described in Section 2.5.2 where wave heights with a standard deviation greater than 3.0 mm were eliminated from the average. No wave measurements were neglected for the coir, and a total of five measurements were omitted for the real vegetation.

3.6 Results

3.6.1 Wave height attenuation

The amount of wave dissipation over the coir mats without vegetation was substantial for all wave conditions, unlike the control for the artificial

vegetation tests. The minimum dissipation over the 9.3 m sampled distance was 40% and the maximum reached 75%.

Figure 42 shows the spectral energy loss for a wave system propagating through the unplanted control and real *S. alterniflora*. Spectra are shown at WGs 5, 7, 10, and 13 at x = 0.0, 1.0, 4.1, and 9.3 m, respectively, where x is the distance from the beginning of the vegetation field. Energy losses occur at all frequencies with the most noticeable loss at the peak frequency. Comparing the wave spectral evolution of the control and vegetation reveals stronger wave dissipation occurs for the *S. alterniflora*. Wave energy is barely discernible by the end of the vegetation field.

Figure 42. Wave spectral transformation through coir control (left) and *S. alterniflora* (right) [l_{st}/h = 3.05, H_0 = 0.110 m, T_p = 1.5 sec].

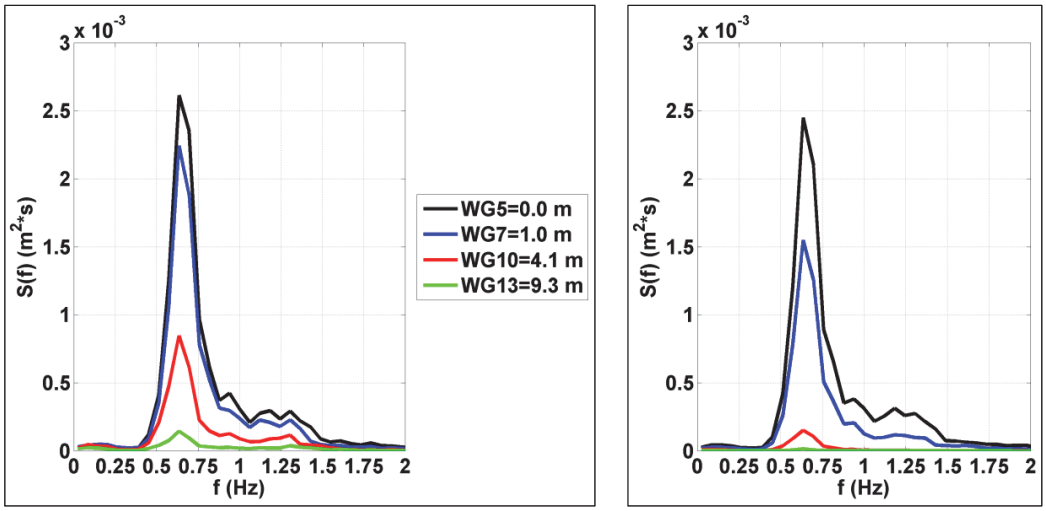

The background attenuation measured during the control tests is not small and should be removed in order to isolate the effect of the real vegetation on wave attention. The methodology of Augustin et al. (2009) was unsuccessful as the stage of dissipation between the control and vegetation tests was too great for linear comparison (i.e., the method does not take into account the rate of dissipation and the previous energy losses). Thus, wave decay was estimated using an exponential decay function modified to include the decay of two processes:

$$\frac{H}{H_0} = e^{-k_t \Delta x} = e^{-(k_c + k_v)\Delta x} \quad (4)$$

where:

H = local wave height (m)
H_o = incident wave height (m)
k_t = total decay coefficient (m^{-1})
k_c = decay coefficient for the coir control (m^{-1})
k_v = decay coefficient for the vegetation (m^{-1})
Δx = horizontal distance between gauges (m).

This equation assumes the total decay is given by the sum of the decay paths (dissipation due to the setup and vegetation, independently). The decay coefficients k_c and k_t were ascertained by fitting normalized wave heights of an unplanted coir test and the corresponding test with real vegetation to the decay model given by Equation 3. Figures of wave transformation over real *S. alterniflora* are given in Appendix B.

The exponential decay model captured the coir control and total wave attenuation very well, with R^2 exceeding 0.98 for all single- and double-peaked wave conditions. The vegetation decay coefficient (k_v) for *S. alterniflora* was estimated by subtracting k_c from k_t, and ranged from 0.073 to 0.213 m^{-1}. An example of measured coir and total wave decay as well as the estimated wave decay due to *S. alterniflora* is shown in Figure 43. For this wave condition, wave attenuation through *S. alterniflora* is estimated close to 80% along the length of the bed.

Figure 43. Measured wave decay fitted to exponential decay model and estimated wave decay due to *S. alterniflora* [l_{st}/h = 3.05, H_0 = 0.112 m, T_p = 1.75 sec].

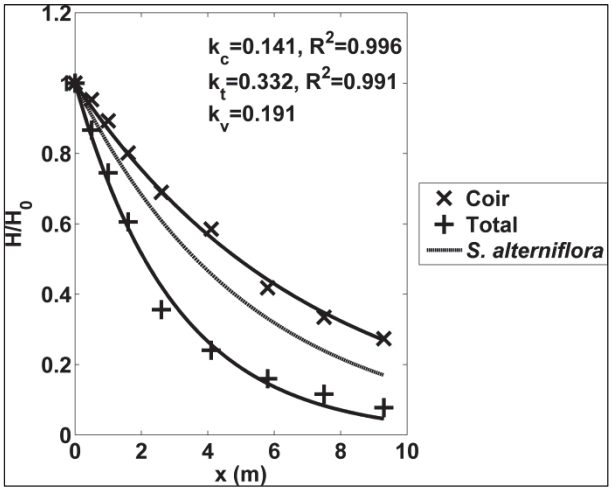

3.6.2 Single-peaked spectra

3.6.2.1 Presence of real vegetation

Measured wave attenuation for the unplanted coir mats and *S. alterniflora* is shown in Figure 44 for l_{st}/h = 3.05. A significant amount of wave attenuation, upwards of 75%, occurs through the unplanted coir control. Wave attenuation further increases at all wave gauges in the presence of real vegetation where approximately 90% of the wave energy was dissipated at x = 9.3 m.

Figure 44. Effect of *S. alterniflora* on wave attenuation.

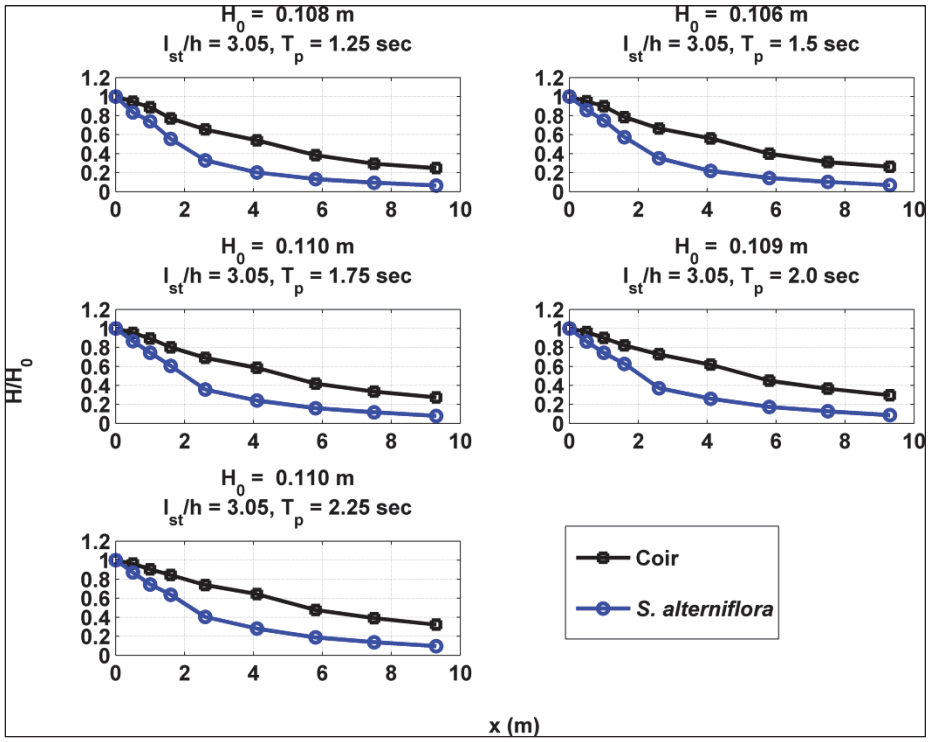

Interpreting the measured wave evolution curves is challenging as background losses are embedded in the measurements for *S. alterniflora* and contributed to the measured wave attenuation. Thus, the attenuation due to *S. alterniflora* will be represented in this study by the vegetation decay coefficient (k_v). Decay coefficients estimated for *S. alterniflora* are slightly greater than the decay coefficients for the unplanted coir control for all single-peaked wave conditions (Figure 45).

Figure 45. Decay coefficient for *S. alterniflora* (N = 162 stems/m²) versus unplanted coir control (N = 0 stems/m²).

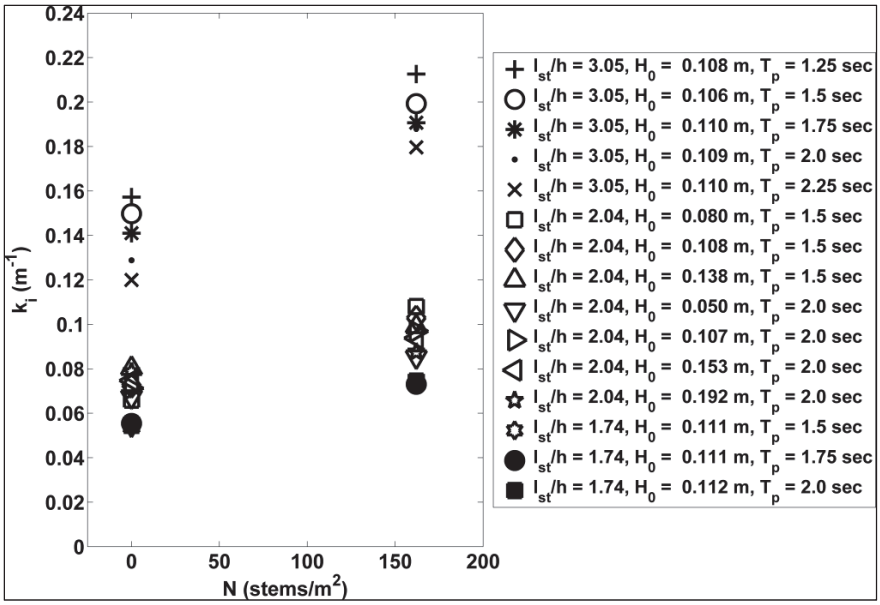

3.6.2.2 Vegetation submergence depth

The effect of vegetation submergence depth on total wave attenuation is shown in Figure 46 for the same incident wave condition (H_o = 0.109 m and T_p = 1.5 sec). Total wave attenuation decreased with smaller submergence ratios (i.e., deeper water depth). The total wave attenuation at the end of the bed was 93%, 78%, and 65% for l_{st}/h = 3.05, 2.04, and 1.74, respectively. The wave dissipation due to *S. alterniflora* followed this trend, as indicated by the increase in k_v with higher submergence ratio (Figure 46). Decay coefficients calibrated for the artificial vegetation followed a similar trend.

Figure 46. Effect of vegetation submergence ratio on wave decay (left) and decay coefficient (k_v) versus vegetation submergence ratio (right) [*S. alterniflora*].

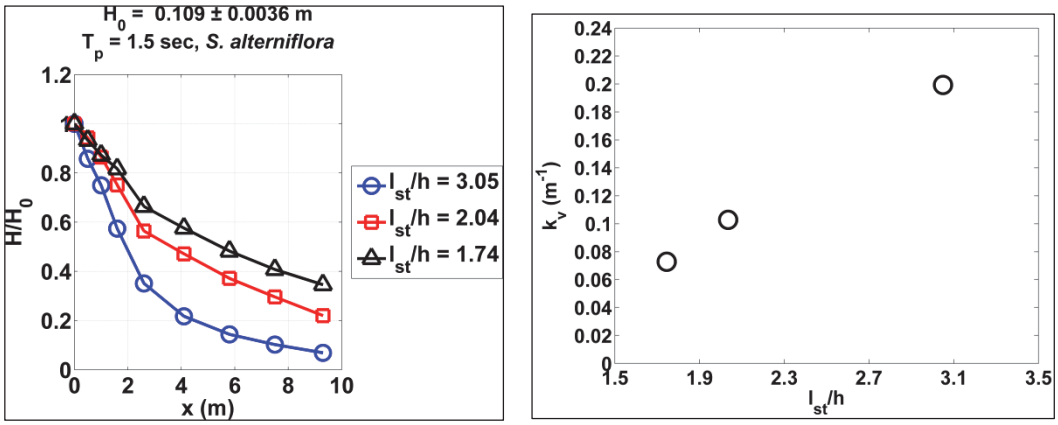

It was noted in Section 2.6.2.2 that wave attenuation decreases as water depth exceeds plant height, primarily because less of the water column is impeded, and more wave energy is able to transmit through the vegetation. This explanation makes sense for cases where the vegetation is either clearly emergent or submergent, which was true for the artificial test cases. However, modeled hydrodynamic conditions for *S. alterniflora* were all emergent, yet its attenuation capacity also decreased with deeper water depths. *S. alterniflora* is less effective at reducing wave energy as water depth increases, even while maintaining emergence, due to waves interacting with the thinner, more flexible leaves rather than the more substantial bottom portion of the plant.

3.6.2.3 Incident peak wave period

Figure 47 presents the effect of peak period on wave decay for tests at l_{st}/h = 3.05. Similar to the artificial vegetation, wave period had little effect on the total wave attenuation with x. A 3% increase in wave reduction is found between T_p = 2.25 and 1.25 sec at x = 9.3 m.

Figure 47. Effect of peak period on wave decay [S. *alterniflora*].

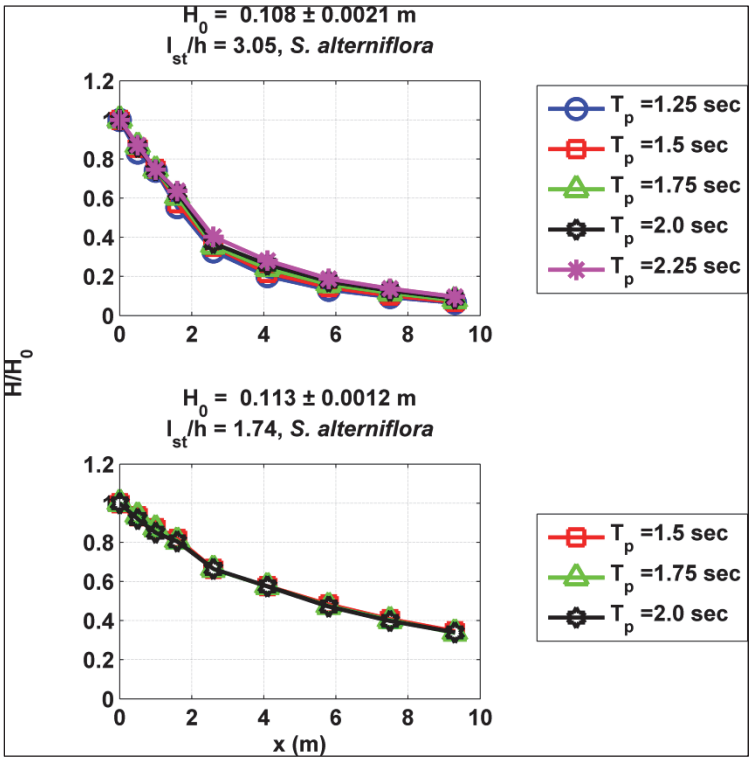

Decay coefficient (k_v) did not have a clear trend with respect to relative depth, analogous to the artificial tests (Figure 48). The vegetation decay

coefficient increased with h/L_p at l_{st}/h = 3.05 but remained nearly constant at l_{st}/h = 1.74. Interestingly, the decay coefficients for the artificial and real vegetation behaved similarly: Both increased as the waves approached deepwater classification at the lowest water level while remaining nearly constant at the highest water level. Again, a broader range of spectra is recommended in order to determine wave attenuation as function of peak period since results are based on the specifics of these experiments.

Figure 48. Decay coefficient (k_v) versus relative depth [*S. alterniflora*].

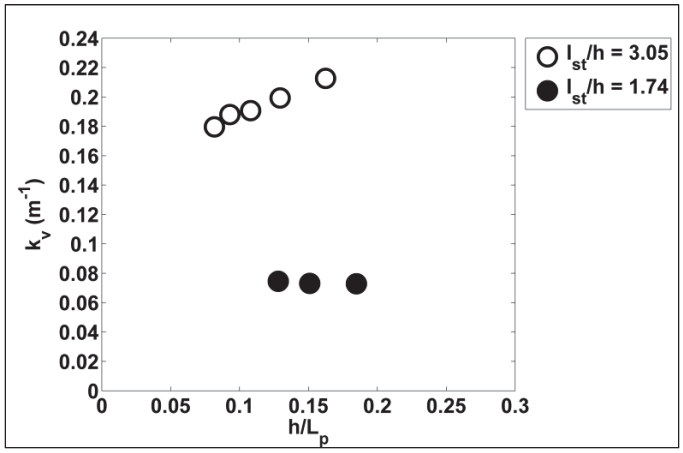

3.6.2.4 Incident wave height

Figure 49 presents the effect of incident wave height on total wave attenuation for l_{st}/h = 2.04. Total wave attenuation marginally increased with wave height for both T_p = 1.5 and 2.0 sec. Focusing on T_p = 2.0 sec, waves are reduced by 73% for H_o = 0.050 m. The amount of total attenuation increases slightly and then remains constant at 76%, 77%, and 76% for H_o = 0.108, 0.155, and 0.193 m, respectively. It is possible the change in wave dissipation due to wave height could not be discerned with the range available in the test facility, and it is recommended a broader range of wave types be tested in future experiments.

The decay coefficient for *S. alterniflora* decreased with larger wave heights for T_p = 1.5 sec and had no clear trend for T_p = 2.0 sec, unlike the artificial vegetation where k_i increased with larger wave height (Figure 50). This unexpected behavior in k_v is likely due to the nonlinearity of the dissipation process. Wave attenuation (at least to some extent) is a function of wave height and, thus, wave energy. The dissipation due to the coir bed and walls measured in the control will not be the same in the

presence of real vegetation since the available energy between the two systems is different (i.e., waves dissipated slower through the unplanted control than the *S. alterniflora*). As a result, the background dissipation and dissipation due to vegetation cannot be uncoupled fully assuming an exponential decay of two processes. It is recommended future studies of wave attenuation through real vegetation consider using a growth substrate with negligible attenuation properties.

Figure 49. Effect of incident wave height on wave decay [*S. alterniflora*].

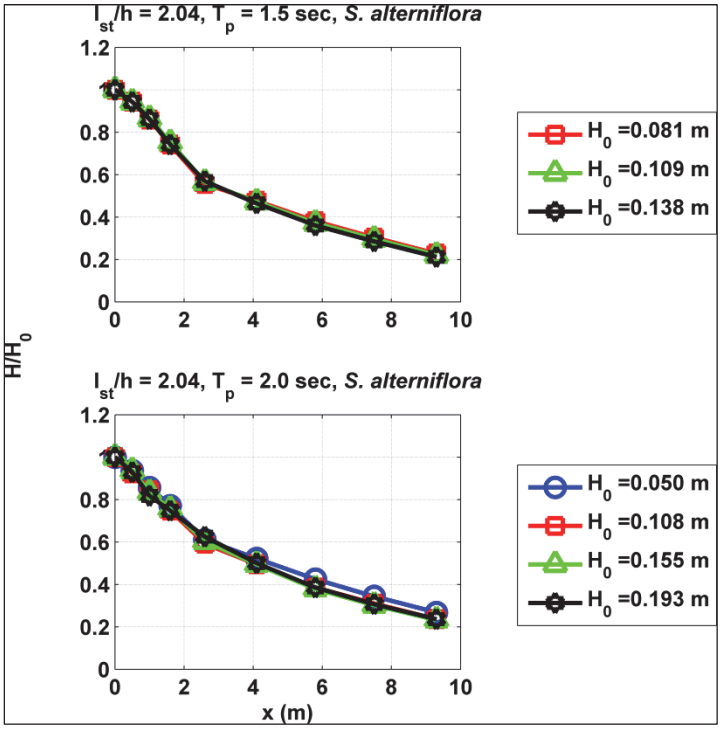

Figure 50. Decay coefficient (k_v) versus incident wave height (open symbols are T_p = 1.5 sec and closed symbols are T_p = 2.0 sec) [*S. alterniflora*].

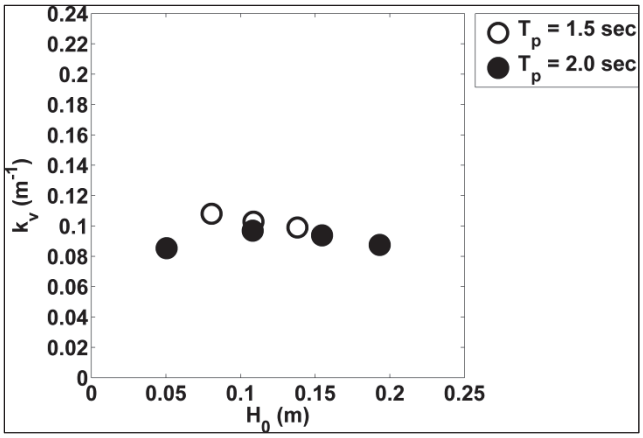

3.6.3 Comparing artificial and real vegetation

How well the artificial vegetation captured the wave evolution trend of real *S. alterniflora* is assessed by comparing the exponential decay coefficients. Figure 51 presents the decay coefficients for the three artificial vegetation arrays and *S. alterniflora* for all modeled wave conditions. *S. alterniflora* has greater decay coefficients than the artificial vegetation for all modeled wave conditions considering the same water depth, indicating the wave energy was more efficiently attenuated through real vegetation. The decay coefficients of real *S. alterniflora* are nearly twice those of the highest density artificial vegetation, although the average stem density was less than half (N = 162 versus 400 stems/m²).

Figure 51. Decay coefficients of artificial vegetation (N = 100, 200, and 400 stems/m²) versus real *S. alterniflora* (N = 162 stems/m²).

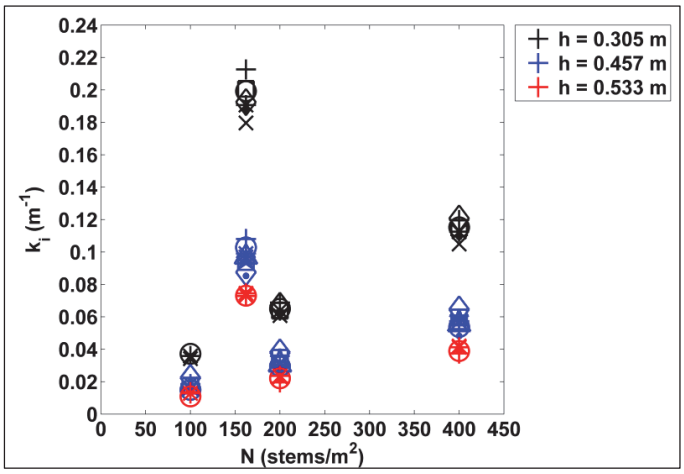

One of the reasons for the underestimation of the wave attenuation by the artificial vegetation is *S. alterniflora* has multiple long, tapering leaves on each stem. These leaves tended to lie over into the water column, forming a thick mat on the surface as seen in Figure 52. However, while leaves would impact the amount of wave attenuation, the relative contribution may be unrepresentative as the *droopiness* observed in the laboratory is not typical of *S. alterniflora*-dominant marshes. The containers were likely not deep enough for the plants to adequately support their own weight, an issue compounded by growing the plants in a greenhouse and preventing them from acclimating to environmental factors such as wind. Moreover, the plants were still young and may not be a scale representation of mature *S. alterniflora* stands.

Figure 52. *S. alterniflora* subjected to wave action.

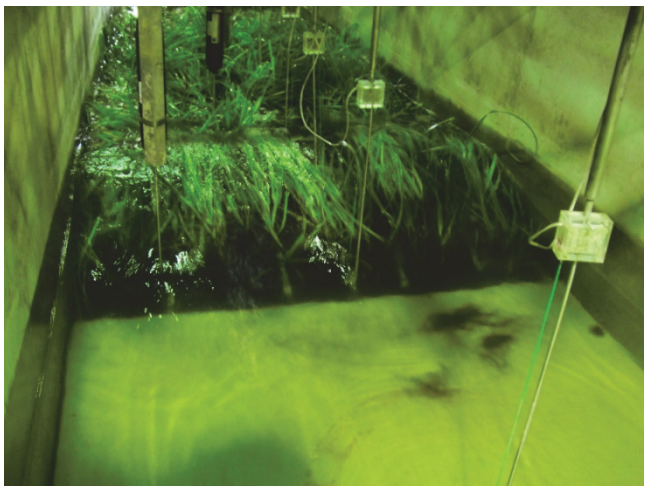

3.6.4 ADV results

3.6.4.1 Velocity reduction

Following the methodology used for the artificial vegetation in Section 2.7.4, the dissipation due to *S. alterniflora* can also be investigated by comparing velocity measurements. The change in the velocity magnitude for one wave condition (H_o = 0.11 m and T_p = 2.0 sec) at different submergence ratios is shown in Figure 53. As shown in the wave data, the unplanted coir matt reduced the wave energy by nearly 90% over the length of the test section. In the presence of real vegetation, the horizontal velocity magnitude was reduced by over 90% at x = 4.1 m and 99% at x = 9.3 m for l_{st}/h = 3.05. The *S. alterniflora* tests have considerable more dissipation than the artificial vegetation.

The real vegetation had nearly identical velocity reduction despite changes in peak wave period, in agreement with the wave attenuation analysis. A wave spectrum with T_p = 1.5 sec had a 98.8% reduction in horizontal velocity magnitude over the test section while T_p = 2.25 sec had a reduction of 98.5% at l_{st}/h = 3.05 (Figure 54). Figure 55 shows the change in velocity magnitude with different peak periods for l_{st}/h = 1.74. The total velocity reduction is the same for all periods tested (approximately 90%). Shorter waves were dissipated more through the unplanted control tests at larger submergence ratios.

Figure 53. Reduction in horizontal velocity with submergence ratio for T_p = 2.0 sec [*S. alterniflora*].

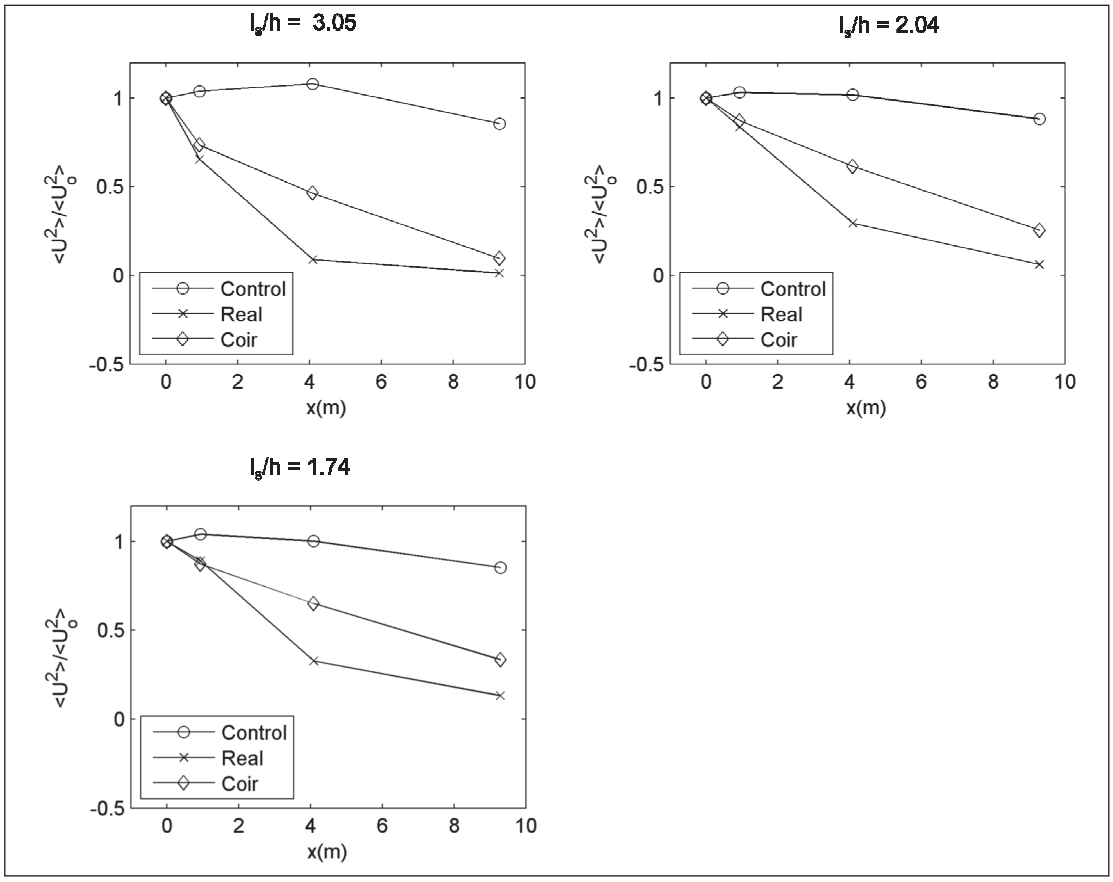

Figure 54. Reduction in velocity with varying peak period for l_{st}/h = 3.05 [*S. alterniflora*].

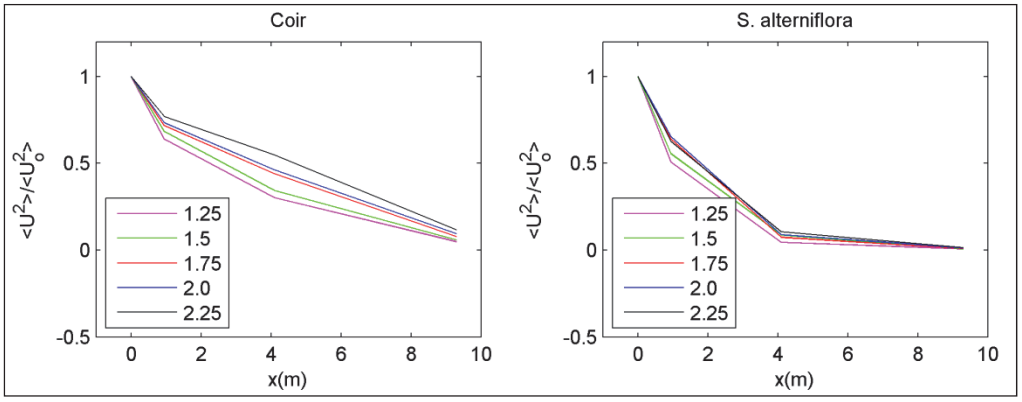

Figure 55. Reduction in velocity with varying peak period for l_{st}/h = 1.74. [*S. alterniflora].*

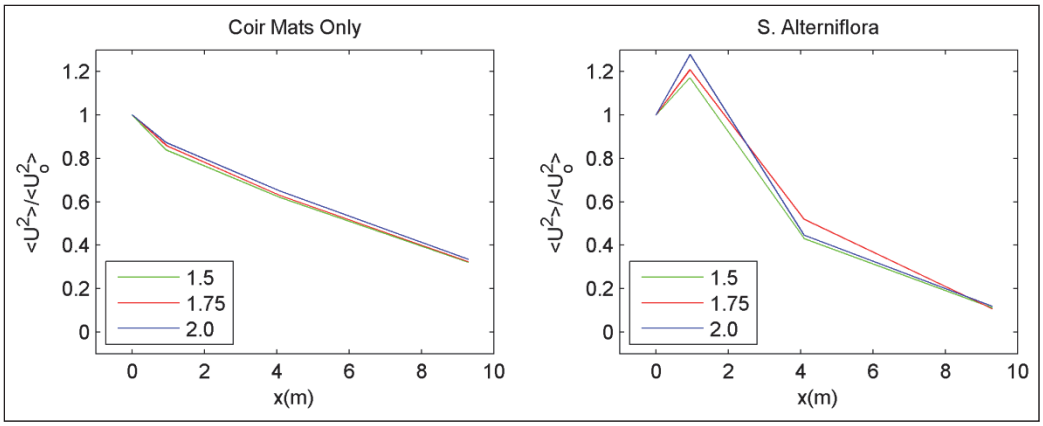

3.6.4.2 Turbulence generation

The effectiveness of vegetation to reduce wave energy is a combination of both the bed roughness associated with plant growth and the flow of water around the plants. This interaction is highly nonlinear, and decoupling the processes is difficult; however, the velocity spectra can offer some insights into these complicated processes.

The velocity spectra for T_p = 2.0 sec along the flume are given in Figure 56 for l_{st}/h = 3.05. The spectra are very similar in both the wave and turbulence region at x = 0.0 m. By x = 1.0 m there is considerably more energy in the turbulence portion associated with the real vegetation than the control tests. The wave energy (f < 2 Hz) in the coir bed and real vegetation has decreased significantly at x = 4.1 m compared to the plywood control of the artificial tests. Despite the smaller wave velocity, the turbulence portion of the velocity spectrum (f > 2 Hz) has similar magnitudes. By the final location, x = 9.3 m, the wave energy for the real vegetation is two orders of magnitude smaller than the plywood control. It is important to consider the location of the ADVs when analyzing these figures as the ADVs sampled in the water column, but the generation of turbulence by the coir mat would be near the bed. A similar pattern was seen for l_{st}/h = 2.04 and 1.74 (Figure 57 and Figure 58) where the real vegetation has much more turbulence generation, especially when considering the reduction in wave height.

Figure 56. Changes in velocity spectra (l_{st}/h = 3.05, H_0 = 0.110 m, T_p = 2.0 sec) [*S. alterniflora*].

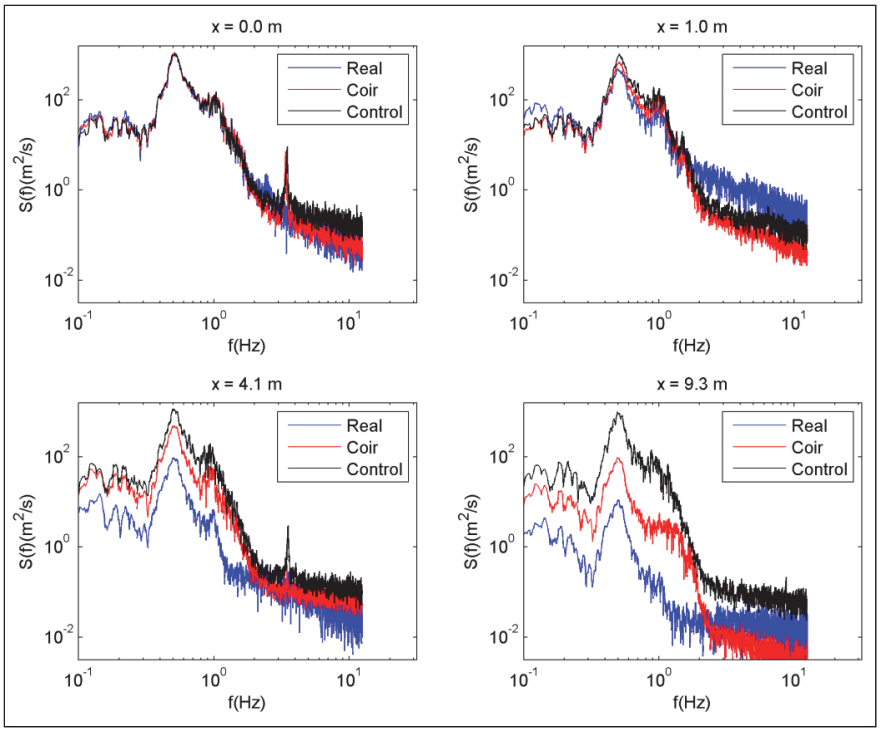

Figure 57. Changes in velocity spectra (l_{st}/h = 2.04, H_0 = 0.153 m, T_p = 2.0 sec) [*S. alterniflora*].

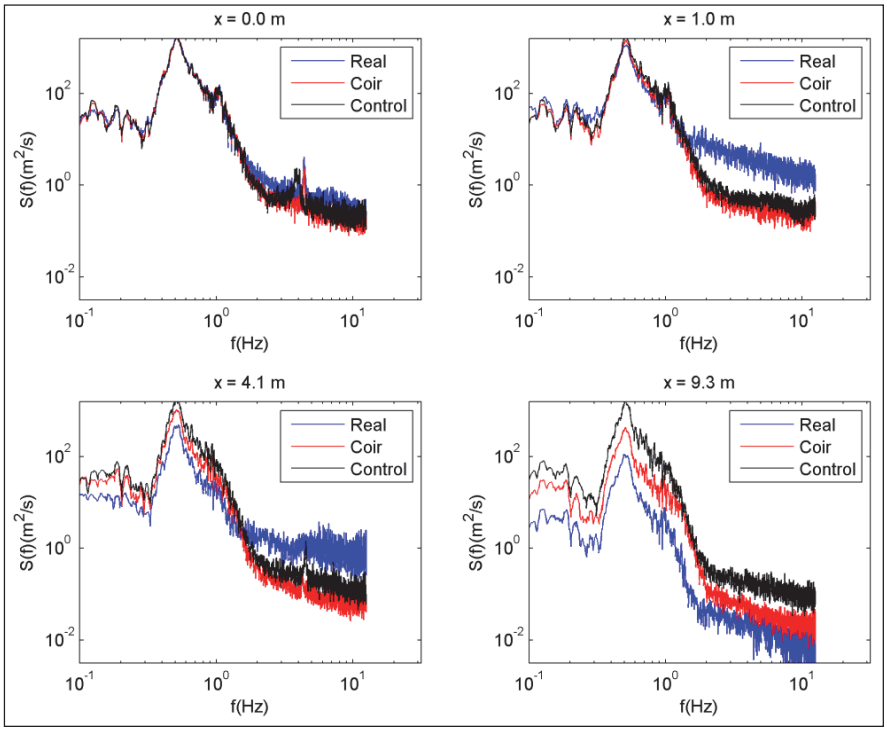

Figure 58. Changes in velocity spectra (l_{st}/h = 1.74, H_0 = 0.111 m, T_p = 2.0 sec [*S. alterniflora*].

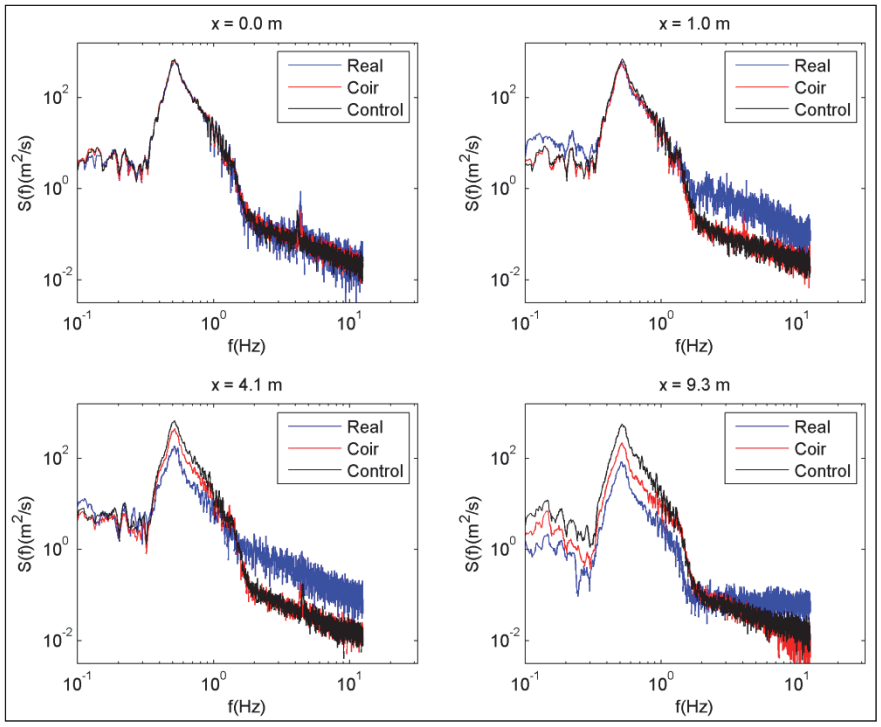

4 Summary

Wave attenuation characteristics of coastal plants are important to understanding their shore protection capabilities and application. In this study, data documenting the interactions of waves and vegetation were collected in a controlled laboratory environment. This chapter summarizes the results from the experiments and its importance to modeling wave-vegetation interactions.

4.1 Review of findings

The influence of plant density, water depth, incident peak period, and incident wave height on wave dissipation through artificial and real vegetation (*Spartina alterniflora*) was assessed by a parametric study. Both single- and double-peaked irregular wave spectra were modeled. The following conclusions can be drawn from this study:

- Both artificial and real vegetation were effective at reducing wave energy for all modeled single- and double-peaked wave conditions. An artificial vegetation bed reduced wave heights by as much as 60% while real vegetation reduced wave heights upwards of 80% over the same distance (x = 9.3 m).
- The exponential decay function proposed by Kobayashi et al. (1993) captured well the wave evolution through artificial and real vegetation.
- Wave attenuation occurred at all frequencies of the spectra with the most noticeable dissipation occurring at the spectral peak frequencies.
- Wave attenuation was most dependent on the stem density and vegetation submergence ratio, defined as ratio of average plant length to water depth. For the artificial vegetation, the greatest amount of wave attenuation occurred under emergent conditions. Wave attenuation decreased with smaller submergence ratios (i.e., at deeper water depths) for both the artificial and real vegetation. Also, wave transmission through different stem densities was a function of vegetation submergence depth. While wave attenuation increased with spatial stem density for all wave conditions, stem density was more influential in shallower waters.
- Wave attenuation was affected little by incident wave height and peak period. Wave attenuation through the artificial vegetation slightly increased with wave height for both modeled wave periods (T_p = 1.5

and 2.0 sec), while peak period appeared to have little effect on total dissipation through the artificial vegetation. A limited set of spectra was tested due to limitations of the laboratory facility, and more tests covering a wider range of wave types are necessary to determine the variation of wave dissipation as a function of incident wave height and spectral peak period.

- Two wave spectra were linearly superimposed to construct a double-peak spectrum. These two wave systems attenuated differently for emergent conditions where the high-frequency energy attenuated more than the low-frequency energy. The two wave systems decayed similarly for submerged vegetation.
- The wave attenuation due to real vegetation was never fully isolated due to the nonlinearity of the wave dissipation process, resulting in some counterintuitive results compared to those of the artificial vegetation tests. Future studies of wave attenuation through real vegetation should be completed using a growth media with negligible attenuation properties to resolve this issue.
- The wave attenuation through real vegetation was higher than all constructed artificial stem arrays. This is likely due to dissimilarities in mechanical properties and geometry, such as leaves.
- The change in velocity magnitude was controlled by stem density and submergence with no pattern identified with regard to wave height or period.
- The wave component of the velocity spectra was reduced equally across frequencies in the prescence of vegetation while turbulence increased for both artificial and real vegetation.

4.2 Implications of numerical modeling

The continuous collection of field and laboratory data on waves and vegetation allows for the calibration and refinement of existing models and the development of new models. The comprehensive dataset collected herein addresses the following topics fundamental to understanding wave and vegetated systems:

- irregular waves
- single- and double-peaked spectra
- varying hydrodynamic conditions including water depth, wave energy, and peak wave period
- artificial flexible vegetation of different densities
- real vegetation: *Spartina alterniflora*.

References

Anderson, M. E., J. M. Smith, and S. K. McKay. 2011. *Wave dissipation by vegetation*. ERDC/CHL CHETN-I-82. Vicksburg, MS: US Army Engineer Research and Development Center. http://chl.erdc.usace.army.mil/chetn.

American Society for Testing and Materials Standard D5323. 2011. Standard practice for determination of 2% secant modulus for polyethylene geomembranes [Online], ASTM International, West Conshohocken, PA. Available: http://www.astm.org[6 December 2012].

American Society for Testing and Materials Standard D3149. 2006. Standard specification for crosslinked polyolefin heat-shrinkable tubing for electrical insulation [Online], ASTM International, West Conshohocken, PA. Available: http://www.astm.org [6 December 2012].

Augustin, L. N., J. L. Irish, and P. Lynett. 2009. Laboratory and numerical studies of wave damping by emergent and near-emergent wetland vegetation. *Coastal Engineering* (56): 332-340.

Bradley, K. and C. Houser. 2009. Relative velocity of seagrass blades: Implications for wave attenuation in low-energy environment. *Journal of Geophysical Research* (114): F01004.

Cavallaro, L., C. L. Re, G. Paratore, A. Viviano, and E. Foti. 2010. Response of *Posidonia oceanica* to wave motion in shallow-waters : Preliminary experimental results. In *Proceedings of the 32nd International Conference on Coastal Engineering*, Shanghai, China, 1-10.

Chakrabarti, A., H. D. Smith, D. Cox, and D. A. Albert. 2011. Investigation of turbulent structures in emergent vegetation under wave forcing. In *Proceedings of Coastal Sediments 2011*, 2519-2532. Miami, FL.

Chatagnier, J. 2012. The biomechanics of salt marsh vegetation applied to wave and surge attenuation. MS thesis, Louisiana State University.

Cooper, N. J. 2005. Wave dissipation across intertidal surfaces in the Wash Tidal Inlet, Eastern England. *Journal of Coastal Research* 21 (1): 28-40.

Evangelinos, C. and G. E. Karniadakis. 1999. Dynamics and flow structures in the turbulent wake of rigid and flexible cylinders subject to vortex-induced vibrations. *Journal of Fluid Mechanics* (400): 91-124.

Feagin, R. A., J. L. Irish, I. Möller, A. M. Williams, R. J. Colón-Rivera, and M. E. Mousavi. 2011. Short communication: Engineering properties of wetland plants with application to wave attenuation. *Coastal Engineering* 58 (3): 251-255.

Fonseca, M. S. and J. A. Cahalan. 1992. A preliminary evaluation of wave attenuation by four species of seagrass. *Estuarine, Coastal and Shelf Science* (35): 565-576.

Goda, Y. and Y. Suzuki. 1976. Estimation of incident and reflected waves in random wave experiments. In *Proceedings of the 15th International Conference on Coastal Engineering*, 828-845. Honolulu, HI,

Hughes, S. A. 1993. *Physical Models and Laboratory Techniques in Coastal Engineering*. Singapore: World Scientific Publishing.

Kobayashi, N., A. W. Raichle, and T. Asano. 1993. Wave attenuation by vegetation. *Journal of Waterway, Port, Coastal, and Ocean Engineering* 119 (1): 30-48.

Knutson, P. L., R.A. Brochu, W. N. Seelig, and M. Inskeep. 1982. Wave damping in *Spartina alterniflora* marshes. *Wetlands* (2): 87–104.

Koch, E. W., L. P. Sanford, S. N. Chen, D. J. Shafer, and J. M. Smith. 2006. *Waves in seagrass systems: Review and technical recommendations*. TR-06-15. Vicksburg, MS : US Army Engineer Research and Development Center.

Koftis, T, P. Prinos, and V. Stratigaki. 2013. Wave damping over artificial *Posidonia oceanica* meadow: A large-scale experimental study. *Coastal Engineering* (73): 71-83.

Leonard, L. A. and D. J. Reed. 2002. Hydrodynamics and sediment transport through tidal marsh canopies. *Journal of Coastal Research*, SI (36): 459-469.

Lima, S. F., C. F. Neves, and N. M. L. Rosauro. 2006. Damping of gravity waves by fields of flexible vegetation. In *Proceedings of the 30th International Conference on Coastal Engineering*, 491-503. San Diego, CA,

Loder, N. M., J. L Irish, M. A. Cialone, and T. V. Wamsley. 2009. Sensitivity of hurricane surge to morphological parameters of coastal wetlands. *Estuarine, Coastal and Shelf Science* (84): 625-636.

Løvås, S. M. and A. Tørum. 2000. Effect of submerged vegetation upon wave damping and run-up on beaches: A case study of *Laminaria hyperborea*. In *Proceedings of the 27th International Conference on Coastal Engineering*, 851-864. Sydney, Australia.

Lowe, R. J., J. L. Falter, J. R. Koseff, S. G. Monismith, and M. J. Atkinson. 2007. Spectral wave flow attenuation within submerged canopies: Implications for wave energy dissipation. *Journal of Geophysical Research* (112): c05018.

Manca, E., I. Cáceres, J. Alsina, V. Stratigaki, I. Townend, and C. L. Amos. 2012. Wave energy and wave-induced flow reduction by full-scale model *Posidonia oceanica* seagrass. *Continental Shelf Research* (50-51): 100-116.

Markle, D. G. 1979. *Levee wave wash protection by trees*. Miscellaneous Paper No. HL-79-1. Vicksburg, MS: US Army Engineer Waterways Experiment Station.

Méndez, F. J., I. J. Losada, and M. A. Losada. 1999. Hydrodynamics induced by wind waves in a vegetation field. *Journal of Geophysical Research* 104 (C8): 18383-18396.

Nepf, H. M. 2012. Flow and transport in regions with aquatic vegetation. *Annual Review of Fluid Mechanics* (44): 123-142.

Neumeier, U. and P. Ciavola. 2004. Flow resistance and sedimentary processes in a *Spartina maritima* salt-marsh. *Journal of Coastal Research* 20(2): 435-447.

Nortek AS. 2011. http://www.nortek-as.com/

Pezeshki, S. R., H. S. Choi, and R. D. DeLaune. 1993. Population differentiation in *Spartina patens*: Water potential components and bulk modulus of elasticity. *Biologia Plantarum* 35(1): 43-51.

Salpeter, K. E., D. R. Millemann, M. F. Caputo, B. L. White, and B. W. Touchette. 2012. Delayed modifications in plant-water relations in the coastal marsh halophyte *Spartina patens* following sudden increases in soil salinity. *Botanic Martina* (55): 307-310.

Seelig, W. N., and J. P. Ahrens. 1981. *Estimation of wave reflection and energy dissipation coefficients for beaches, revetments, and breakwaters.* Technical Paper 81-1. Vicksburg, MS: US Army Engineer Waterways Experiment Station.

Serra, T., H. J. S. Fernando, and R. V. Rodríguez. 2004. Effects of emergent vegetation on lateral diffusion in wetlands. *Water Research* 38(1): 139-147.

Stoesser, T., S. J. Kim, and P. Diplas. 2010. Turbulent flow through idealized emergent vegetation. *Journal of Hydraulic Engineering* (136): 1003-1017.

Sorensen, R. M. 2006. *Basic Coastal Engineering, 3rd ed.* United States of America: Springer Science.

Touchette, B. W., K. L. Rhodes, G. A. Smith, and M. Poole. 2009a. Salt spray induces osmotic adjustment and tissue rigidity in smooth cordgrass, *Spartina alterniflora* (Loisel.). *Estuaries and Coasts* (32): 917-925.

Touchette, B. W., G. A. Smith, K. L. Rhodes, and M. Poole. 2009b. Tolerance and avoidance: Two contrasting physiological responses to salt stress in mature marsh halophytes *Juncus roemerianus* Scheele and *Spartina alterniflora* (Loisel). *Journal of Experimental Marine Biology and Ecology* (380): 106-112.

Tschirky, P., K. Hall, and D. Turcke. 2000. Wave attenuation by emergent wetland vegetation. In *Proceedings of the 27th International Conference on Coastal Engineering*, 865-877. Sydney, Australia.

US Department of Agriculture (USDA), Natural Resources Conservation Service (NRCS). 2012a. The PLANTS Database. http:/plants.usda.gov

US Department of Agriculture (USDA), Natural Resources Conservation Service (NRCS). 2012b. Plants Materials Program. http://plantmaterials.nrcs.usda.gov/lapmc/index.html

Wallace, S. and R. Cox. 2000. Effects of seagrass on nearshore current and wave dynamics. In *Proceedings of the 27th International Conference on Coastal Engineering,* 878-890. Sydney, Australia.

Wilson, C. A. M. E., T. Stoesser, P. D. Bates, and A. B. Pinzen. 2003. Open channel flow through different forms of submerged flexible vegetation. *Journal of Hydraulic Engineering* (129): 847-853.

Ysebaert, Y., S. L. Yang, L. Zhang, Q. He, T. J. Bouma, and P. M .J. Herman. 2011. Wave attenuation by two contrasting ecosystem engineering salt marsh macrophytes in the intertidal pioneer zone. *Wetlands* (31): 1043-1054.

Wamsley, T. V., M. A. Cialone, J. M Smith, B. A. Ebersole, and A. S. Grzegorzewski. 2009. Influence of landscape restoration and degradation on storm surge and waves in southern Louisiana. *Journal of Natural Hazards* 51(1): 207-224.

Wamsley, T. V., M. A. Cialone, J. M Smith, J. H Atkinson, and J. D. Rosati. 2010. The potential of wetlands in reducing storm surge. *Ocean Engineering (*37): 59-68.

Wu, W., Y. Ozeren, D. I. Wren, Q. Chen, G. Zhang, M. Holland, Y. Ding, S. N. Kuiry, M. Zhang, R. Jadhav, J. Chatagnier, Y. Chen, and L. Gordji. 2011. *Phase 1 Report for SERRI Project No. 80037: Investigation of surge and wave reduction by vegetation*. SERRI Report 80037-01. Oxford, MS: National Center for Computational Hydroscience and Engineering, University of Mississippi.

Yoon, H. D., D. Cox, D. Albert, N. Mori, H. Smith, and J. Zarnetske. 2011. Ecological modeling of emergent vegetation for sustaining wetlands in high wave energy coastal environments. In *Proceedings of Coastal Structures 2011,* C5-091.

Appendix A: Wave Transformation through Artificial Vegetation

The figures presented in this appendix show normalized zero-moment wave heights as a function of distance for the artificial vegetation experiments, where x = 0.0 at the beginning of the vegetation field (WG 5–13).

Single-peaked spectra

Figure A1. Wave transformation for h = 0.305 m, plywood control [single-peaked].

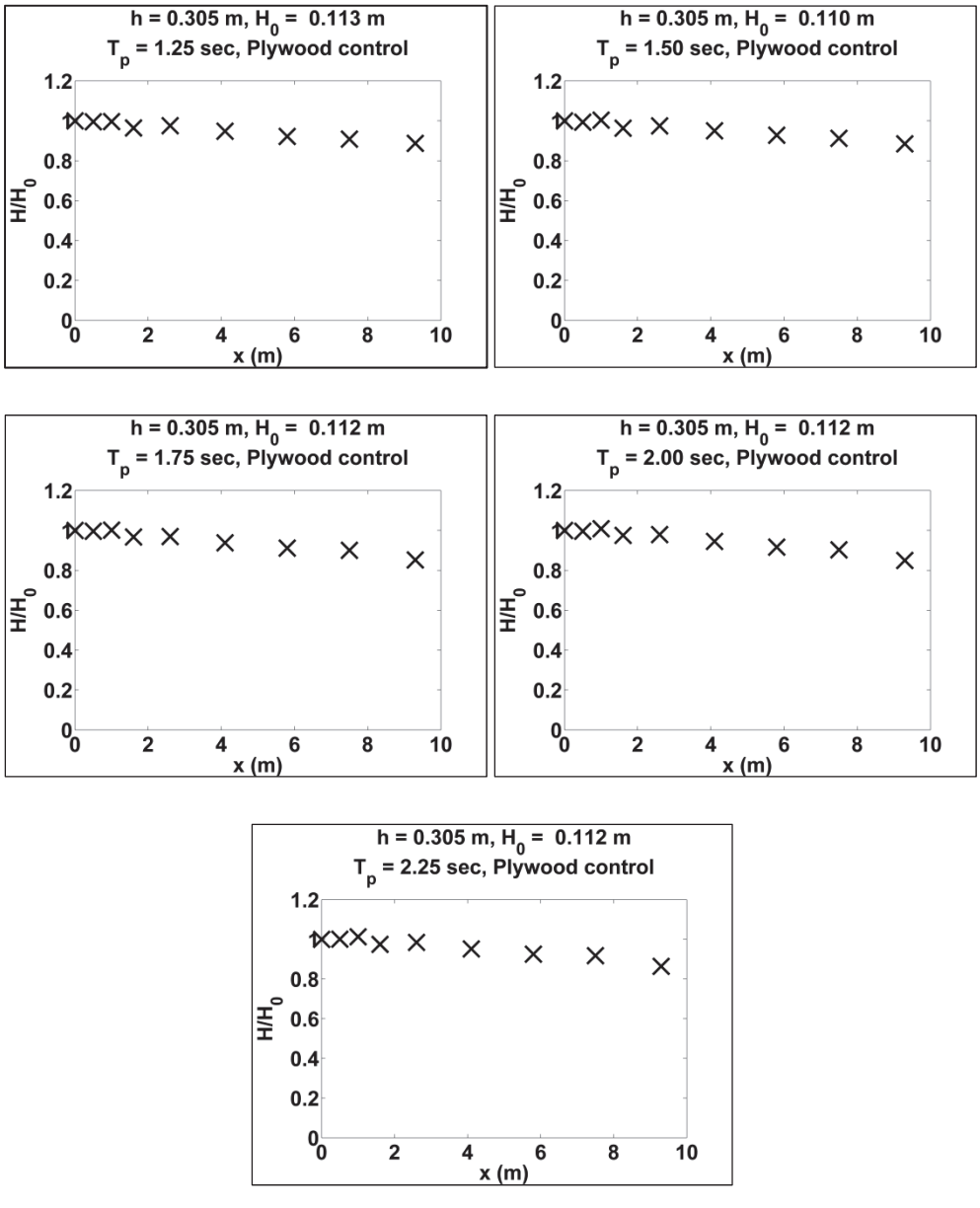

Figure A2. Wave transformation for *h* = 0.457 m, plywood control [single-peaked].

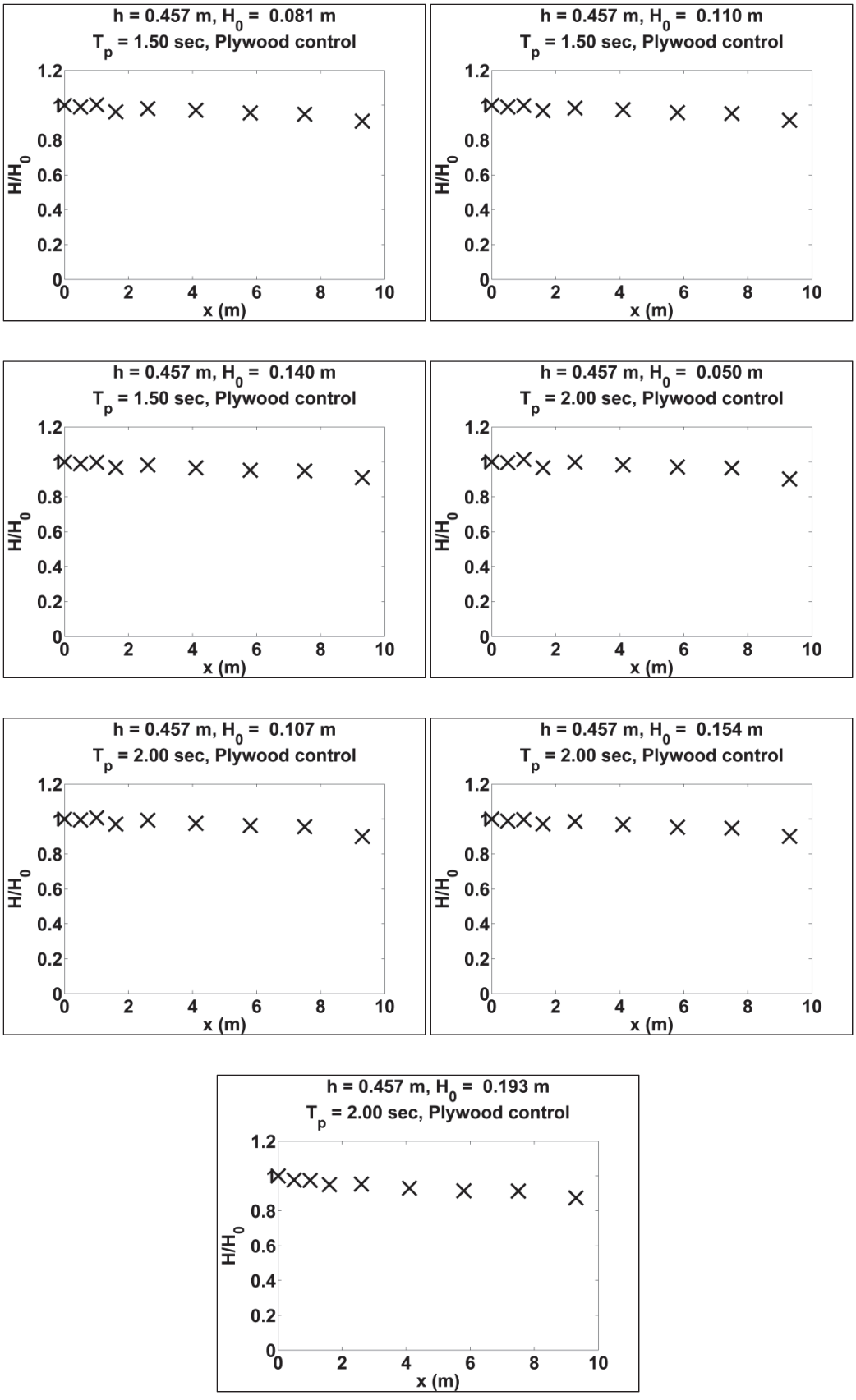

Figure A3. Wave transformation for h = 0.533 m, plywood control [single-peaked].

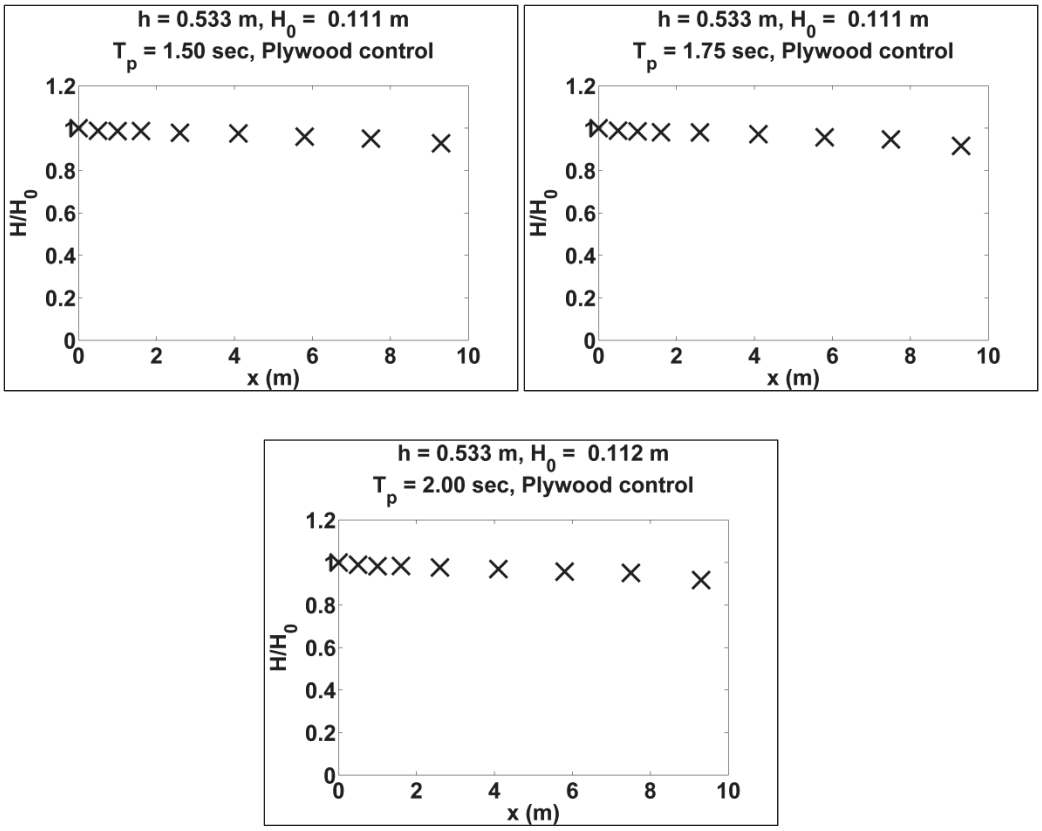

Figure A4. Wave transformation for h = 0.305 m, N = 100 stems/m² [single-peaked].

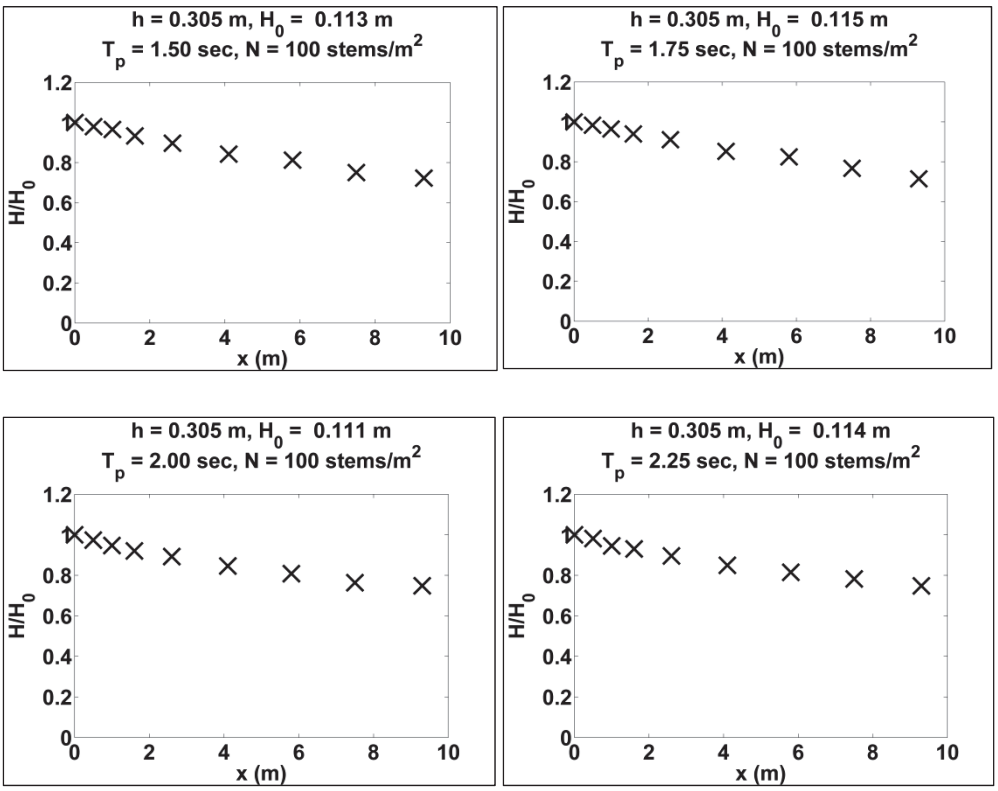

Figure A5. Wave transformation for h = 0.457 m, N = 100 stems/m² [single-peaked].

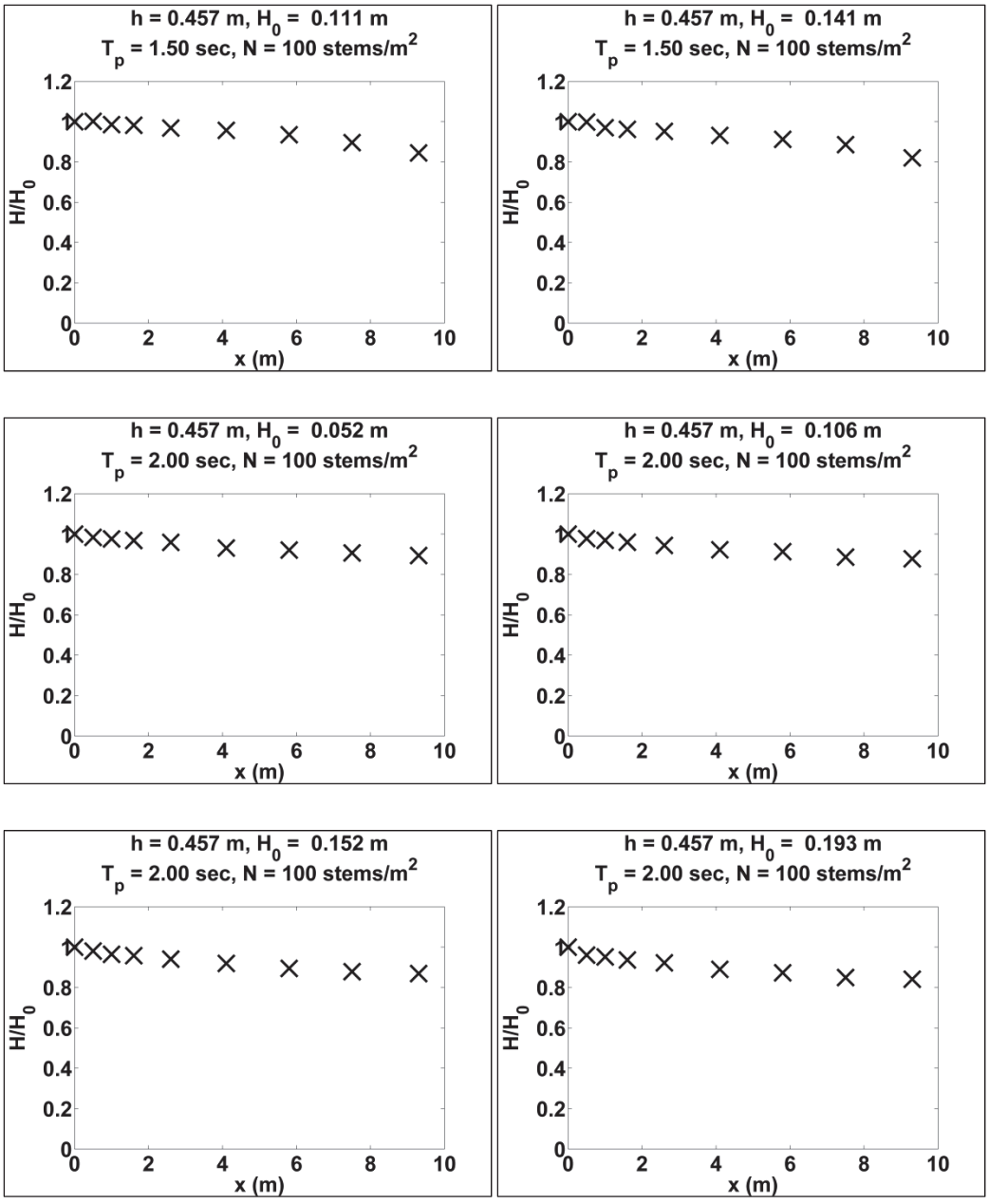

Figure A6. Wave transformation for h = 0.533 m, N = 100 stems/m² [single-peaked].

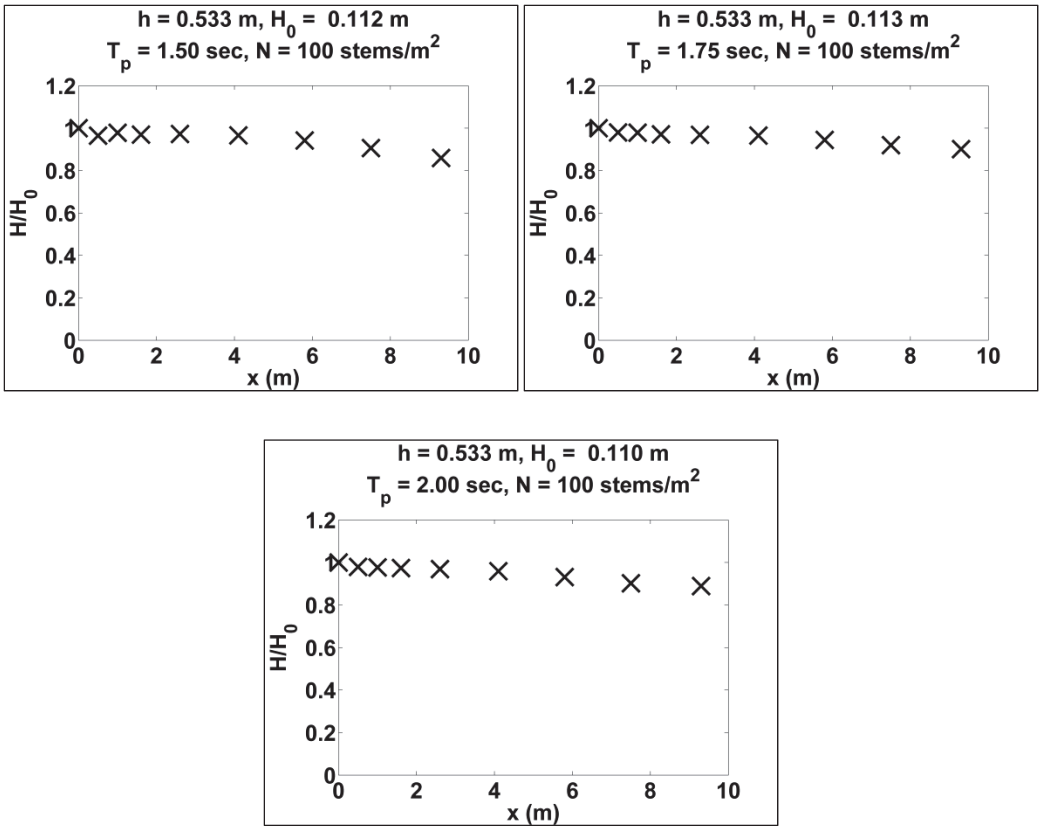

Figure A7. Wave transformation for h = 0.305 m, N = 200 stems/m² [single-peaked].

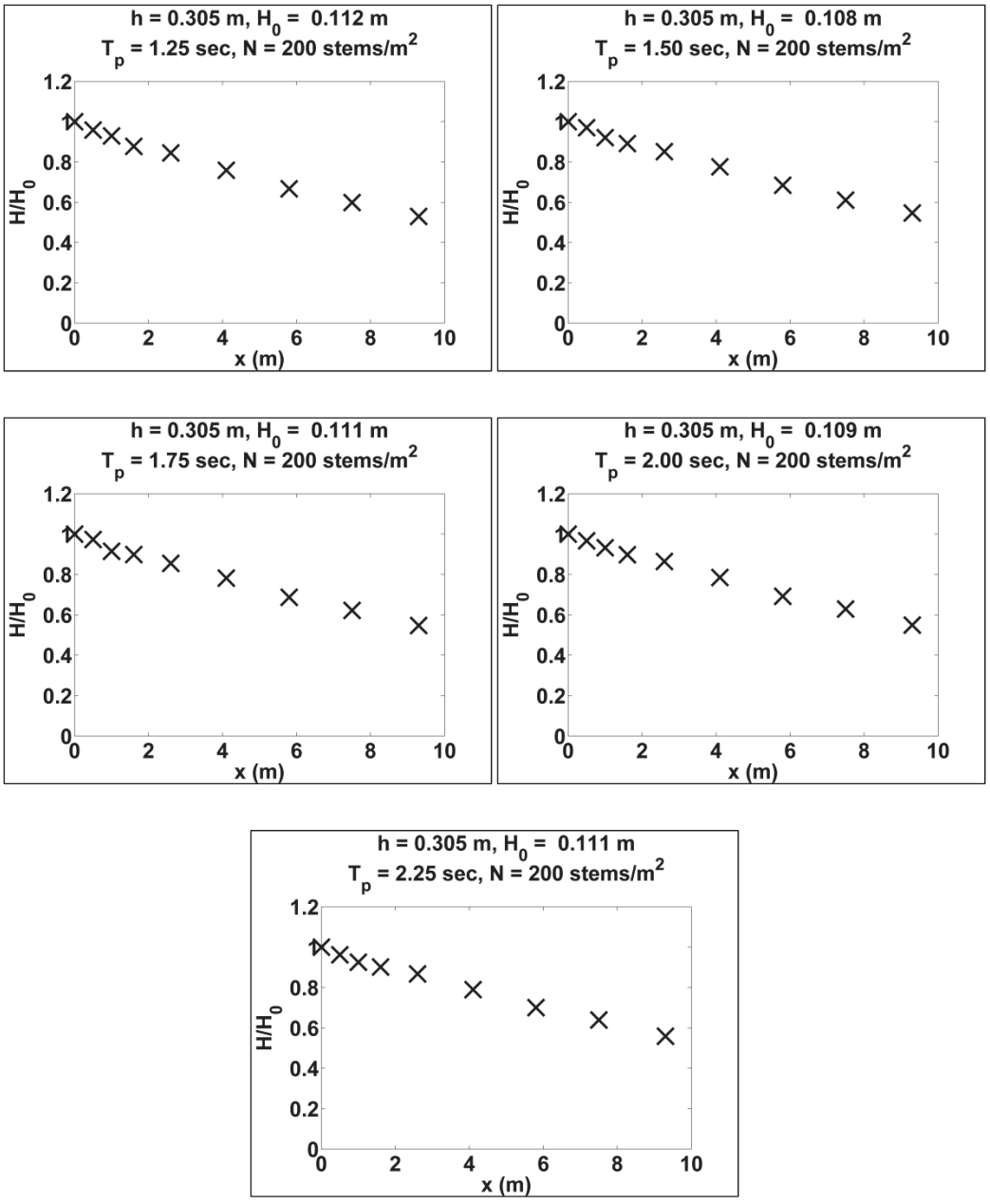

Figure A8. Wave transformation for h = 0.457 m, N = 200 stems/m² [single-peaked].

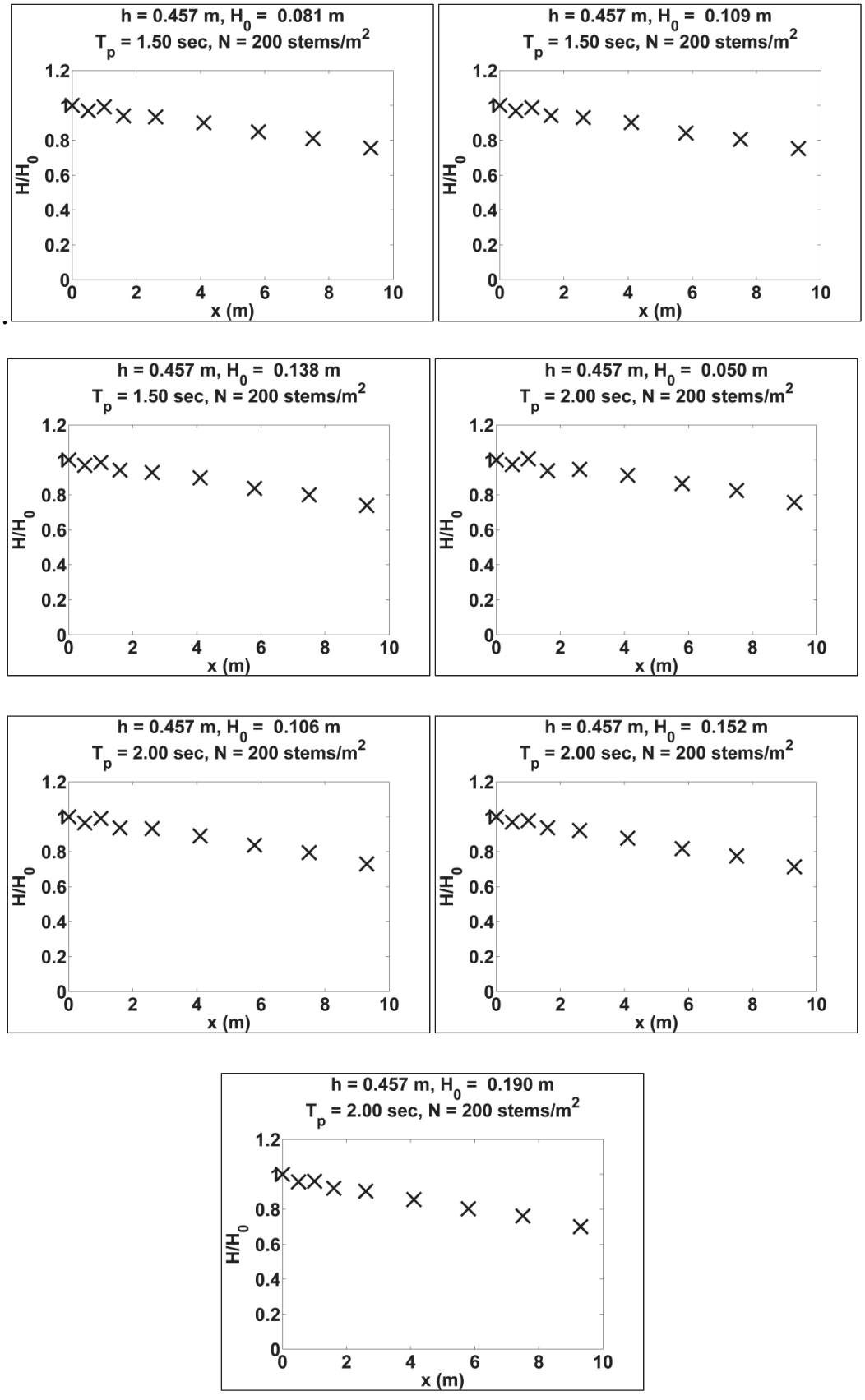

Figure A9. Wave transformation for h = 0.533 m, N = 200 stems/m² [single-peaked].

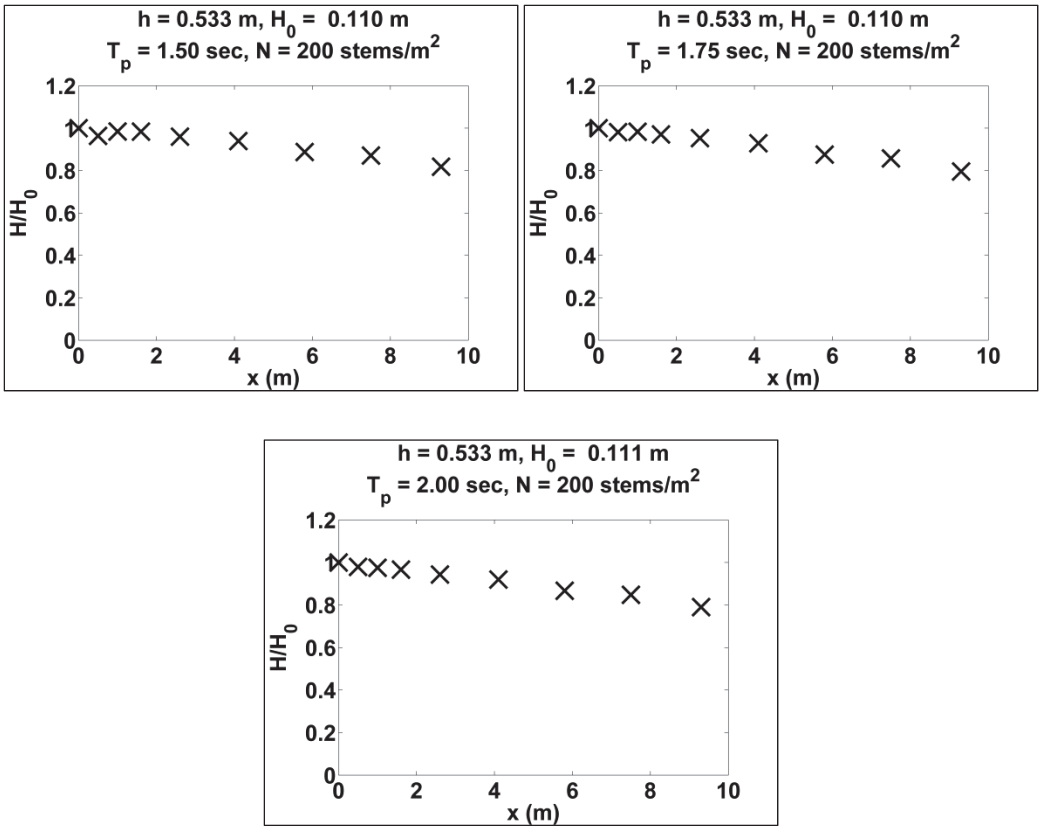

Figure A10. Wave transformation for h = 0.305 m, N = 400 stems/m² [single-peaked].

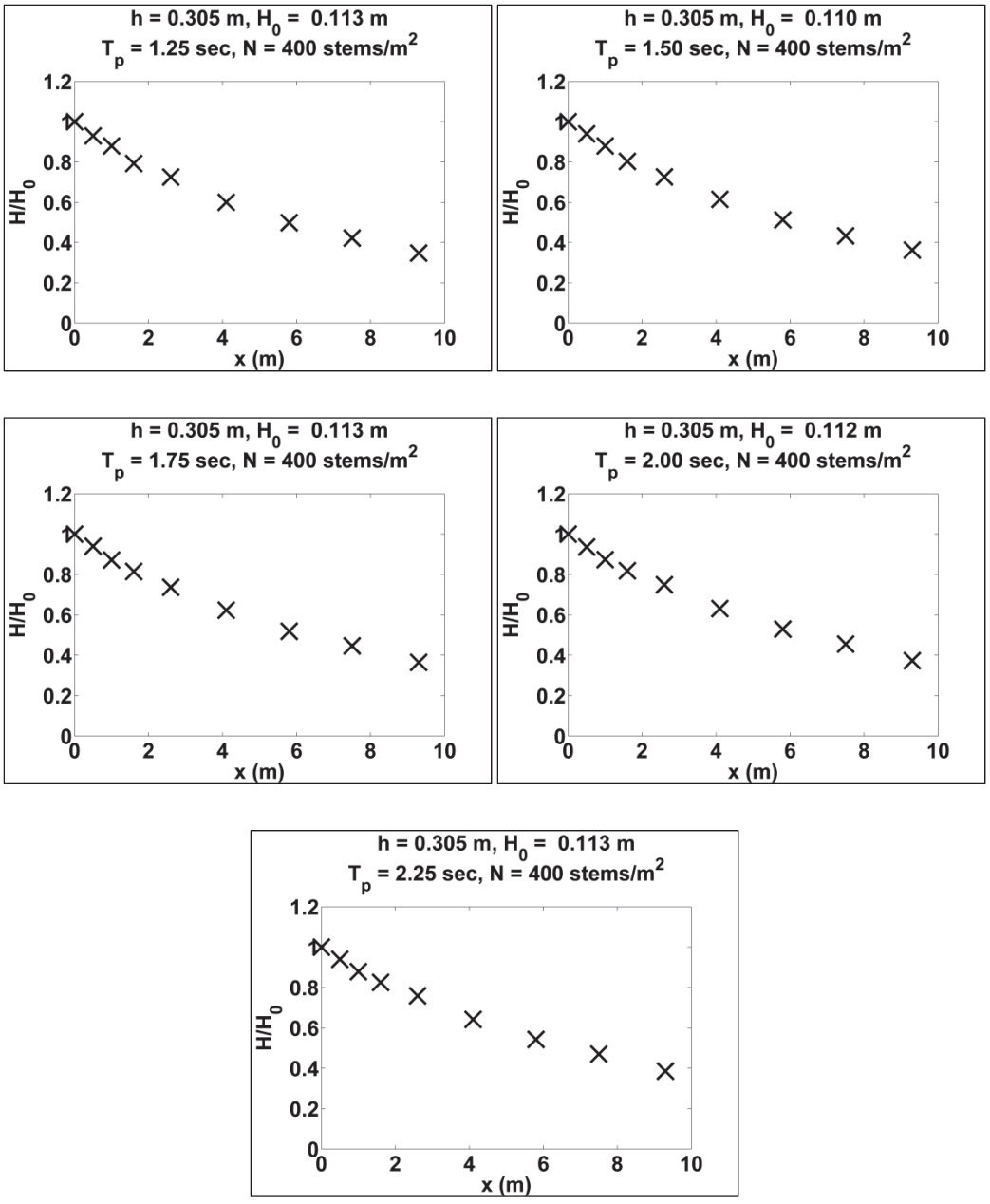

Figure A11. Wave transformation for h = 0.457 m, N = 400 stems/m² [single-peaked].

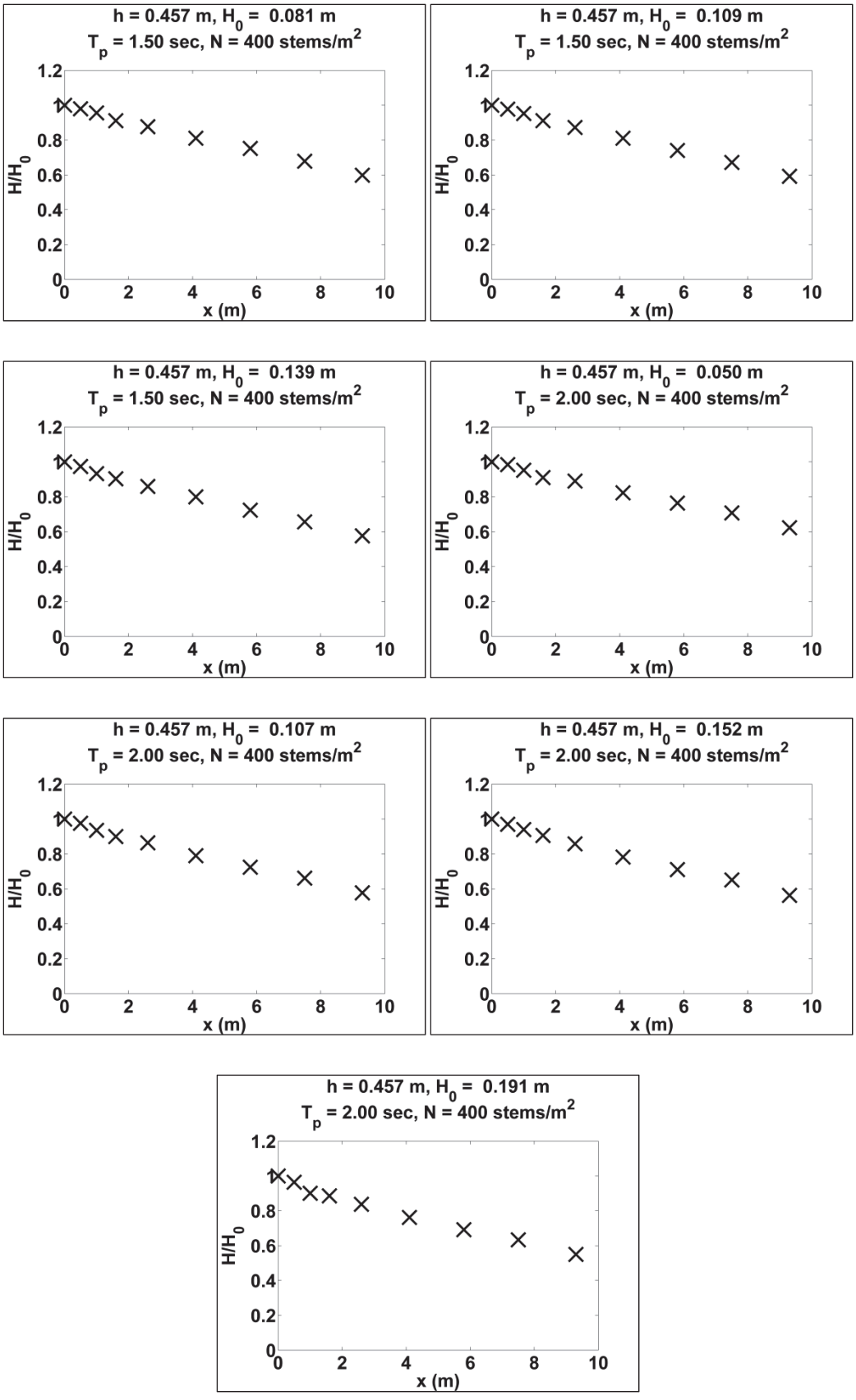

Figure A12. Wave transformation for h = 0.533 m, N = 400 stems/m^2 [single-peaked].

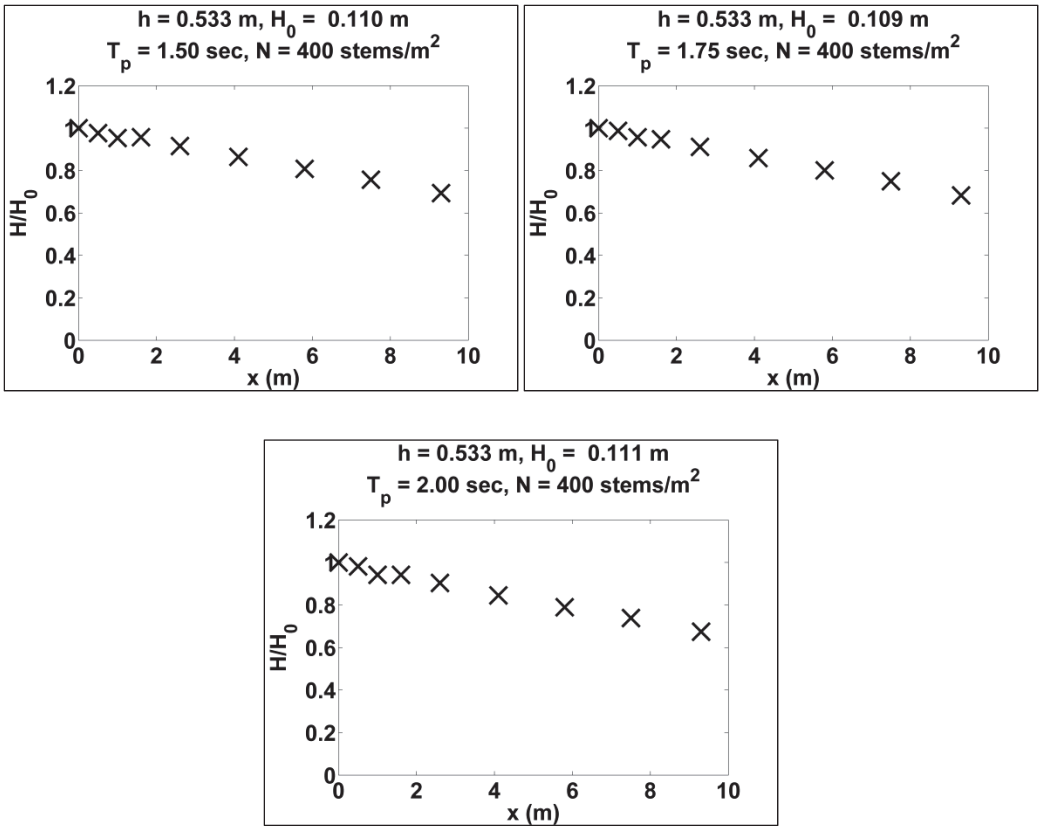

Double-peaked spectra

Figure A13. Wave transformation for *h* = 0.305 m, plywood control [double-peaked].

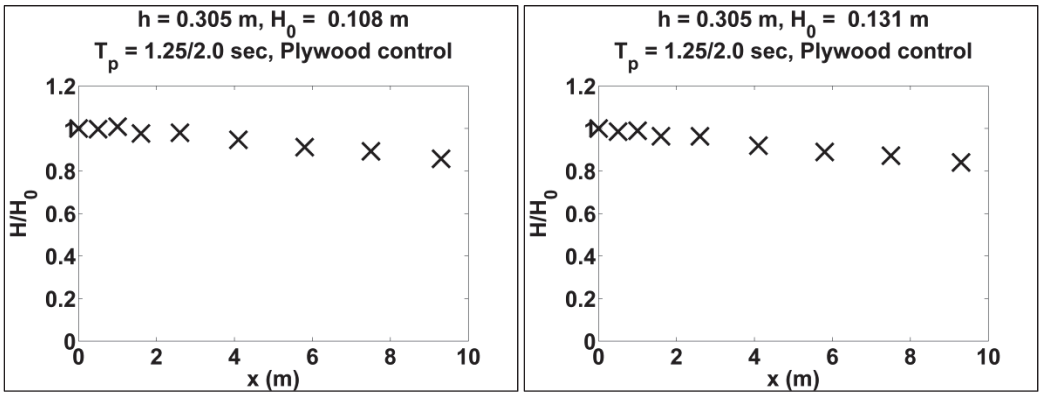

Figure A14. Wave transformation for *h* = 0.457 m, plywood control [double-peaked].

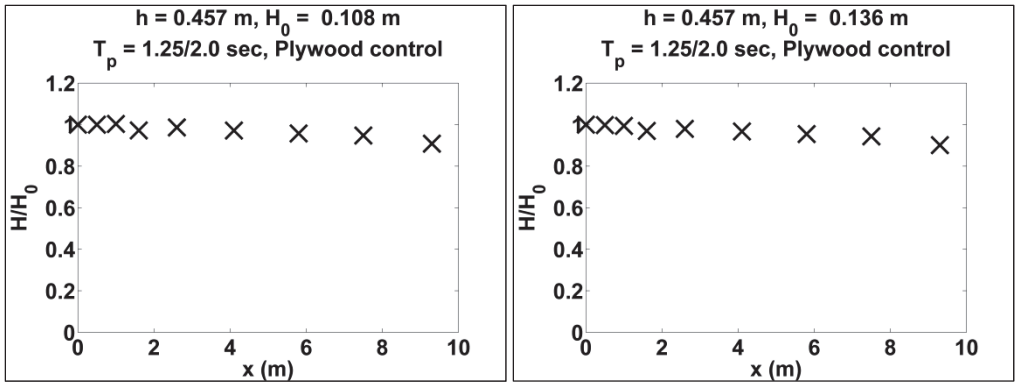

Figure A15. Wave transformation for *h* = 0.533 m, plywood control [double-peaked].

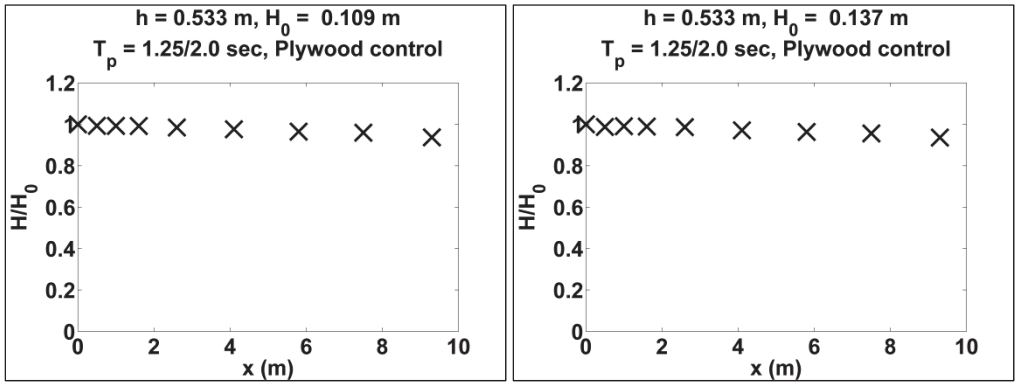

Figure A16. Wave transformation for h = 0.305 m, N = 200 stems/m² [double-peaked].

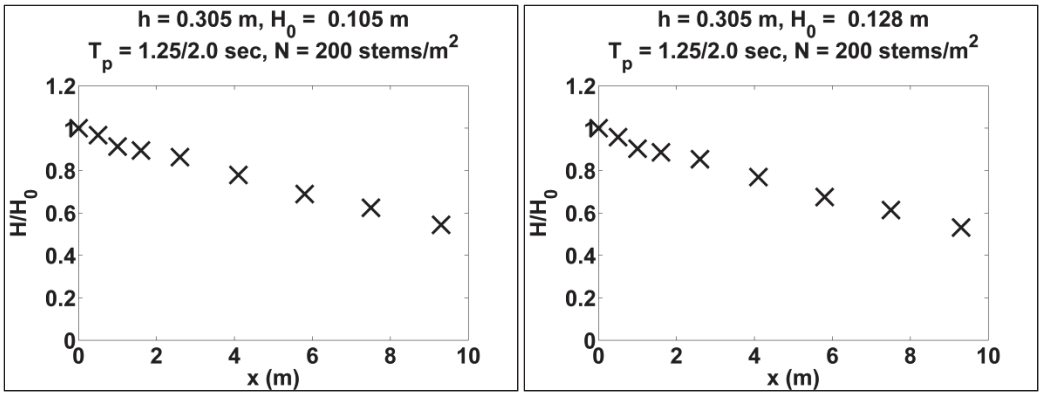

Figure A17. Wave transformation for h = 0.457 m, N = 200 stems/m² [double-peaked].

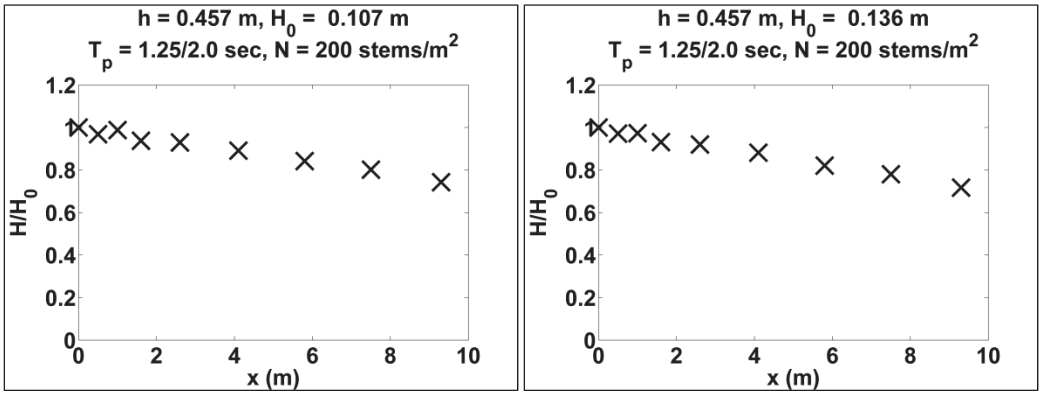

Figure A18. Wave transformation for h = 0.533 m, N = 200 stems/m² [double-peaked].

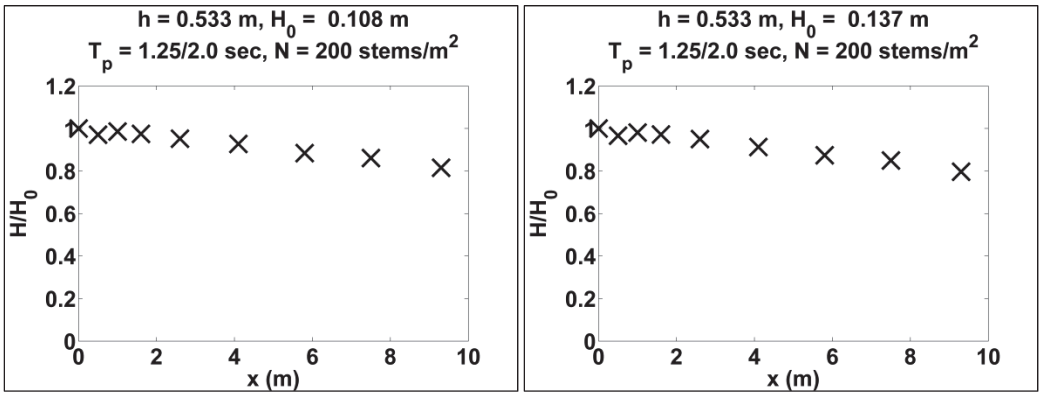

Figure A19. Wave transformation for h = 0.305 m, N = 400 stems/m² [double-peaked].

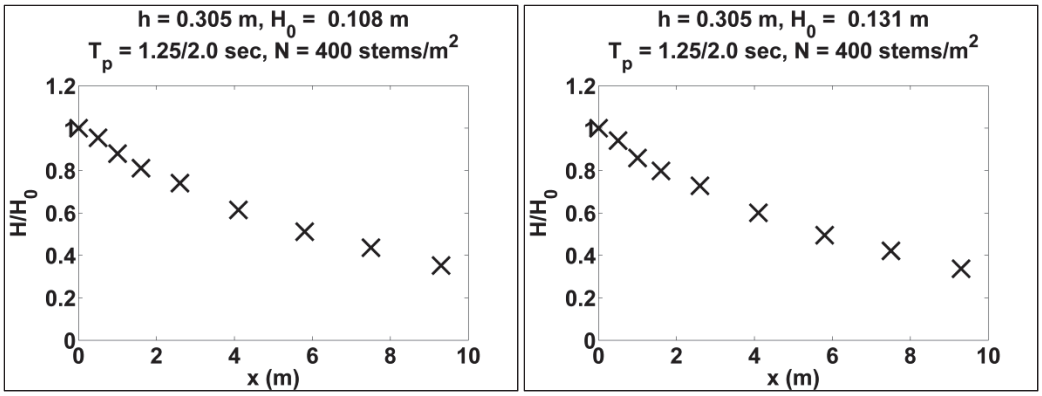

Figure A20. Wave transformation for h = 0.457 m, N = 400 stems/m² [double-peaked].

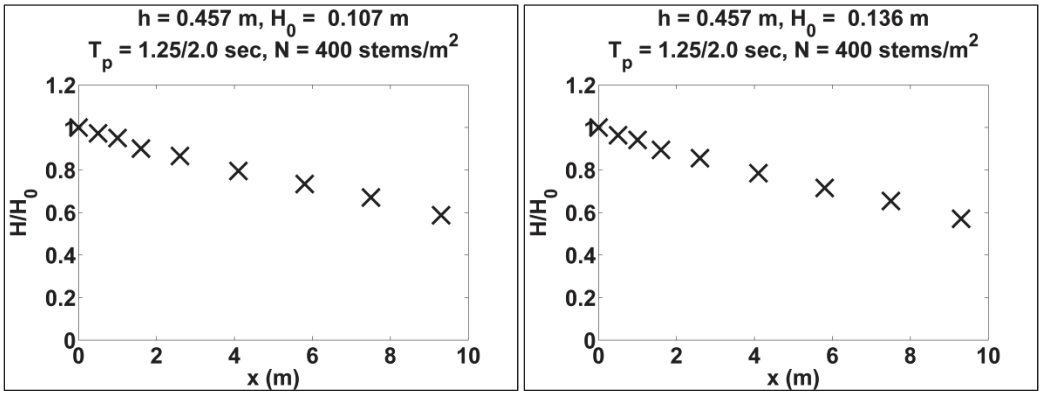

Figure A21. Wave transformation for h = 0.533 m, N = 400 stems/m² [double-peaked].

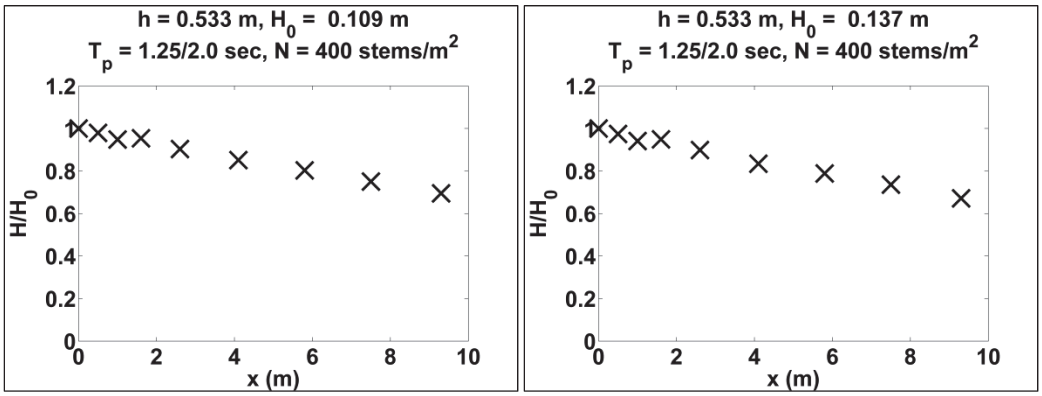

Appendix B: Wave Transformation through Real *Spartina alterniflora*

The figures presented in this appendix show normalized zero-moment wave heights as a function of distance for the real *S. alterniflora* experiments, where x = 0.0 at the beginning of the vegetation field (WG 5 – 13).

Single-peak spectra

Figure B1. Wave transformation for h = 0.305 m, coir control [single-peaked].

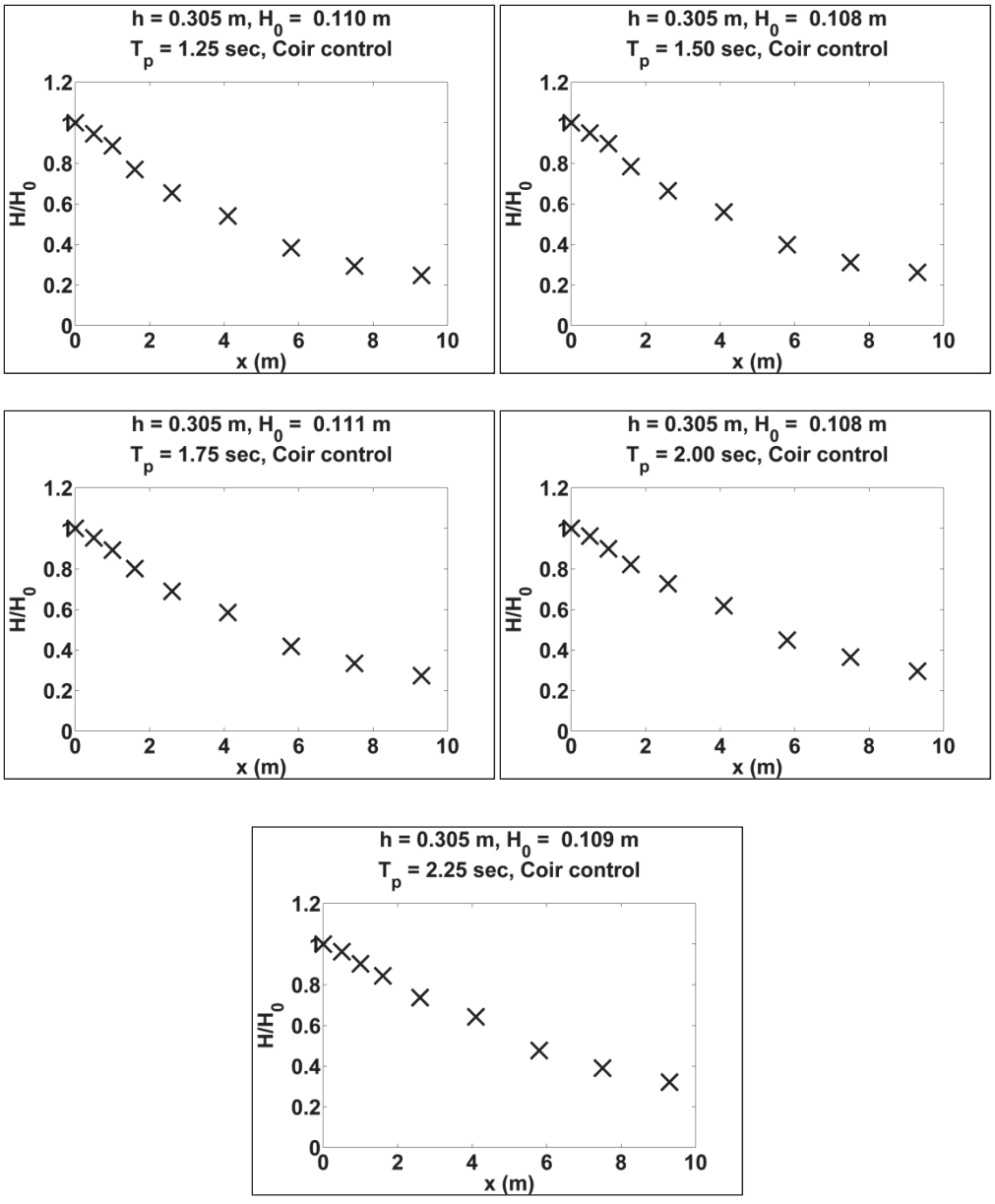

Figure B2. Wave transformation for *h* = 0.457 m, coir control [single-peaked].

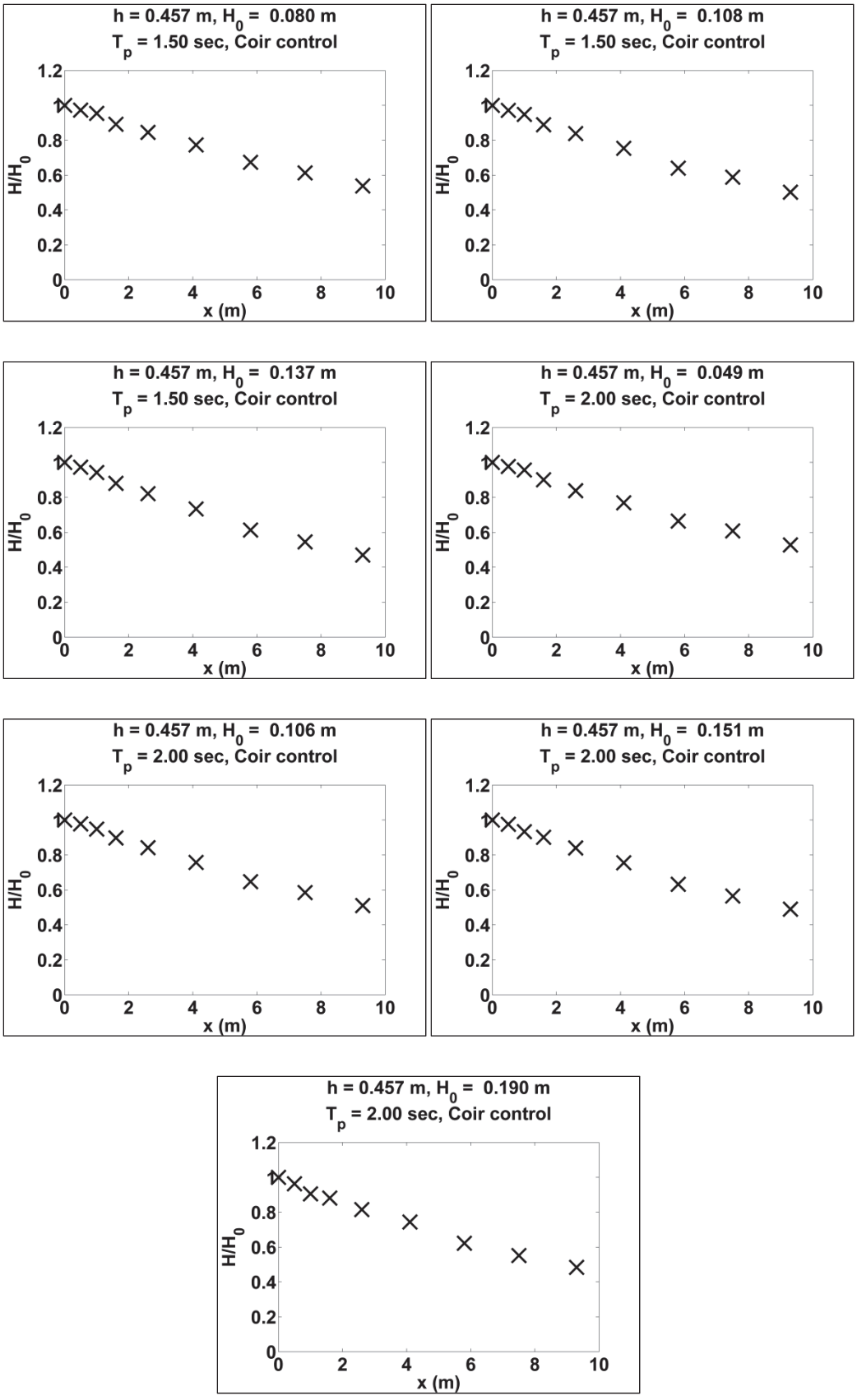

Figure B3. Wave transformation for *h* = 0.533 m, coir control [single-peaked].

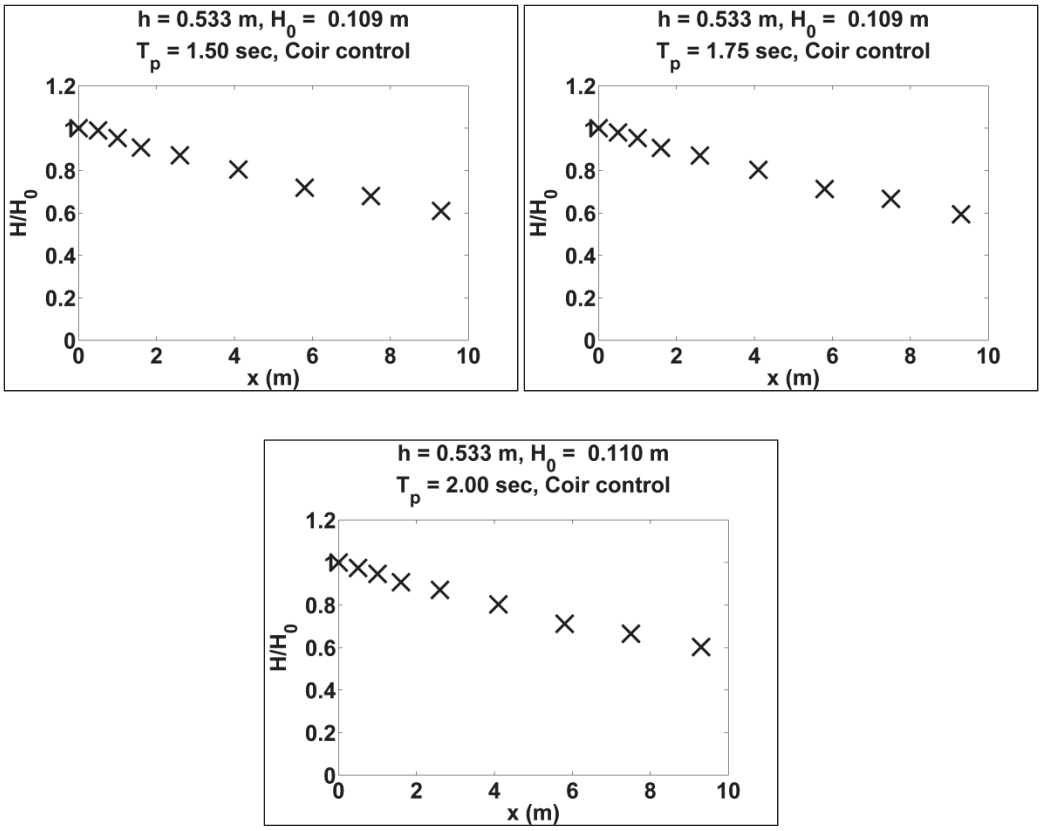

Figure B4. Wave transformation for *h* = 0.305 m, *S. alterniflora* [single-peaked].

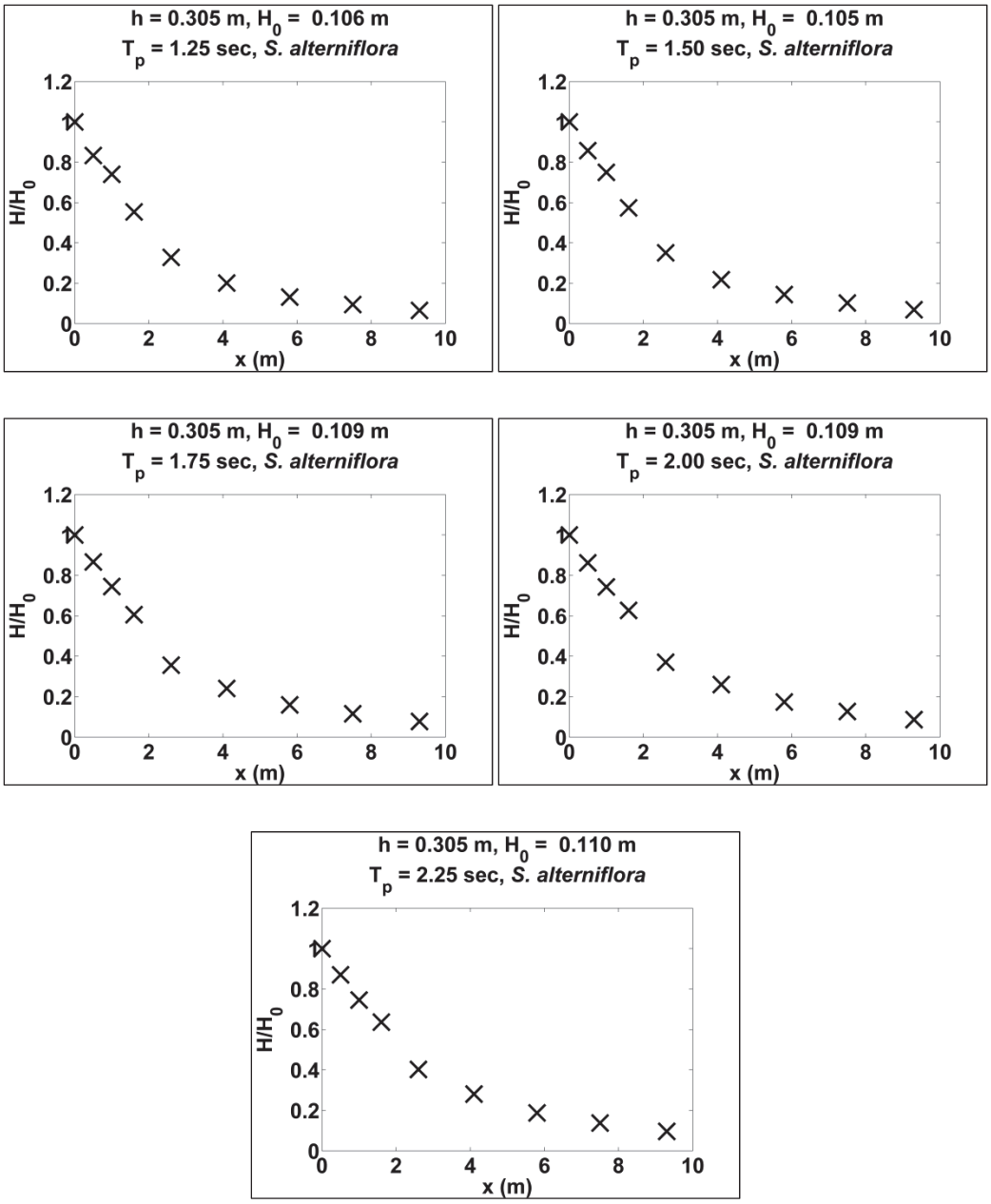

Figure B5. Wave transformation for *h* = 0.457 m, *S. alterniflora* [single-peaked].

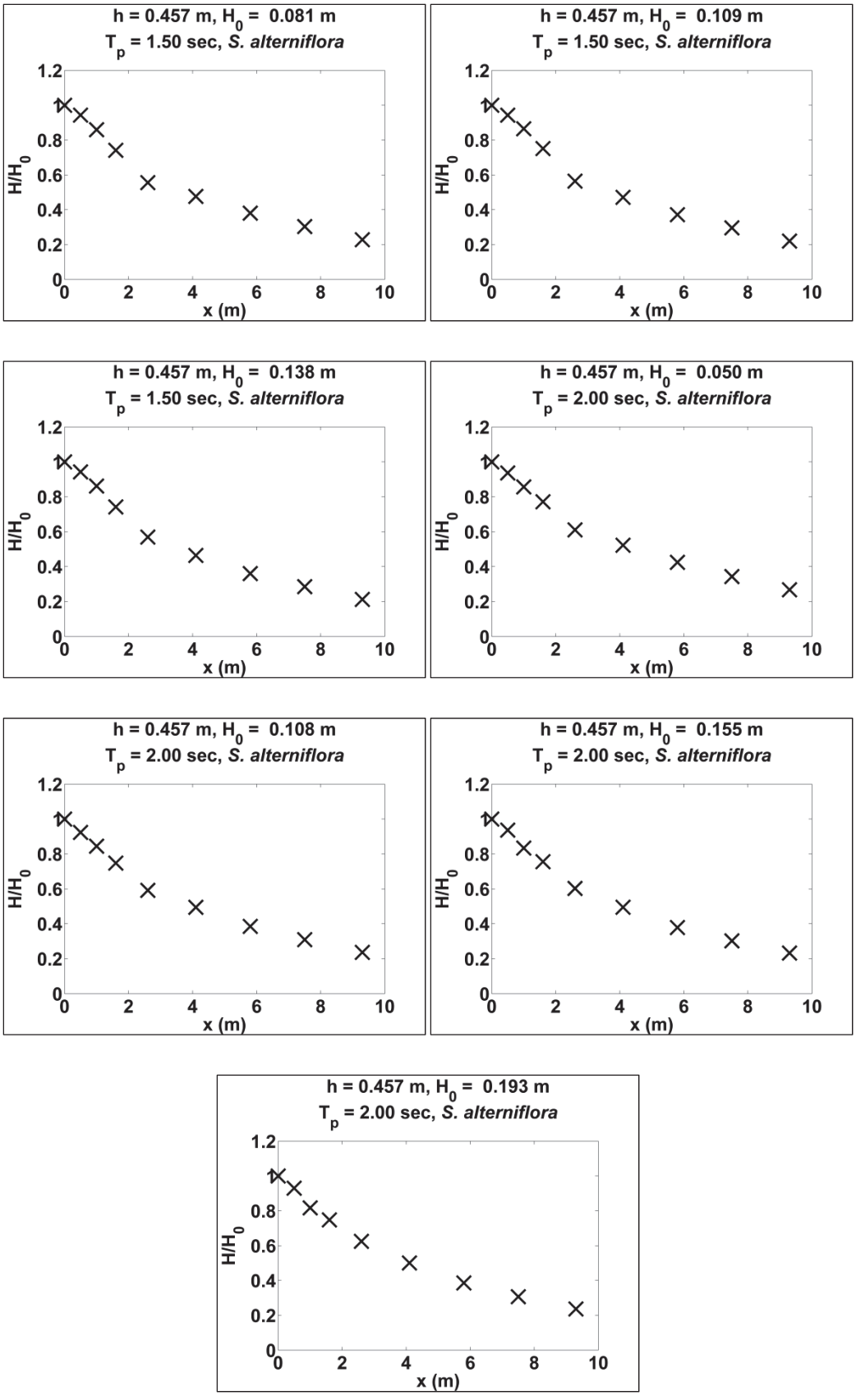

Figure B6. Wave transformation for *h* = 0.533 m, *S. alterniflora* [single-peaked].

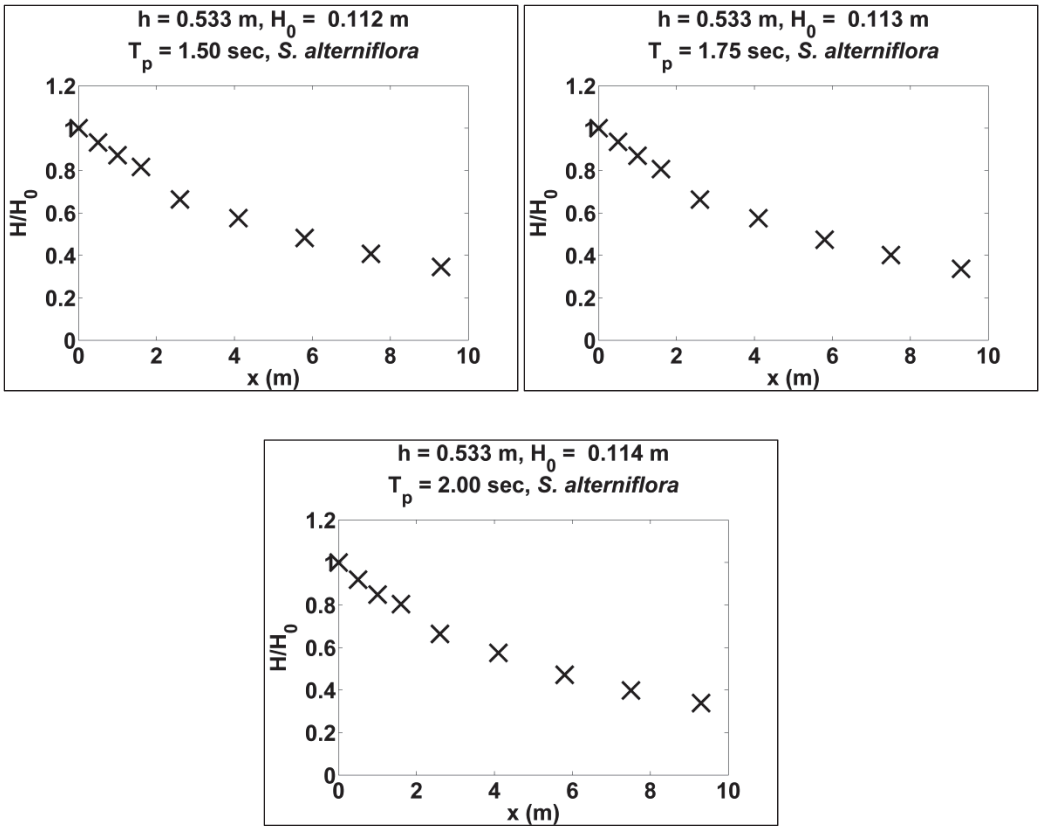

Double-peaked spectra

Figure B7. Wave transformation for *h* = 0.305 m, coir control [double-peaked].

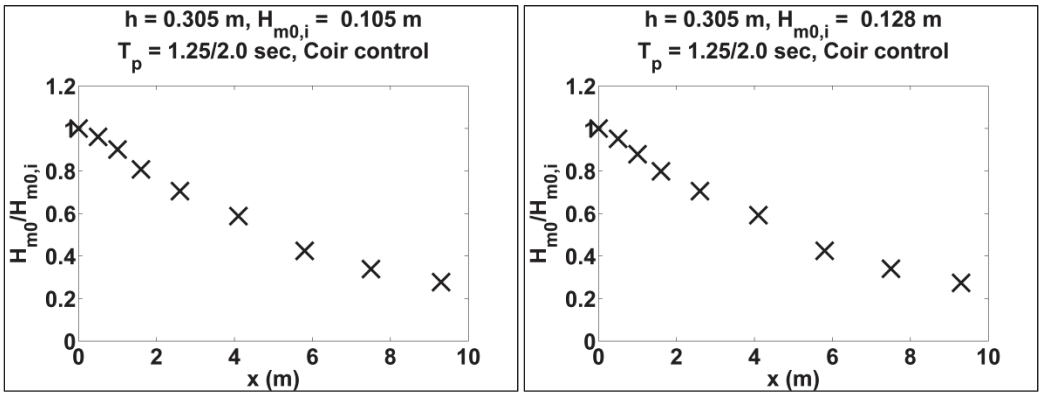

Figure B8. Wave transformation for *h* = 0.457 m, coir control [double-peaked].

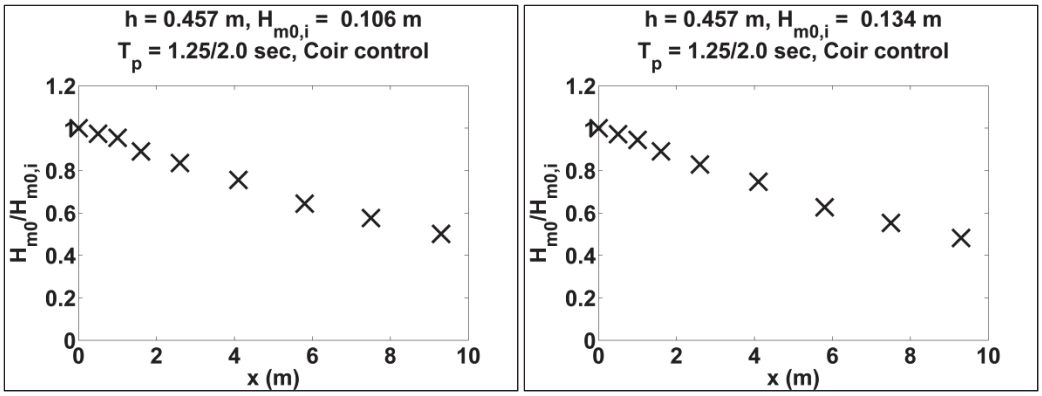

Figure B9. Wave transformation for *h* = 0.533 m, coir control [double-peaked].

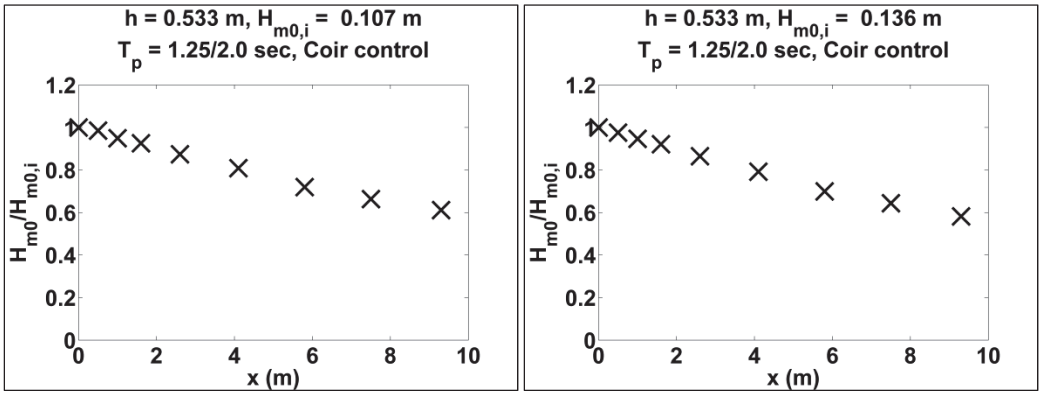

Figure B10. Wave transformation for *h* = 0.305 m, *S. alterniflora* [double-peaked].

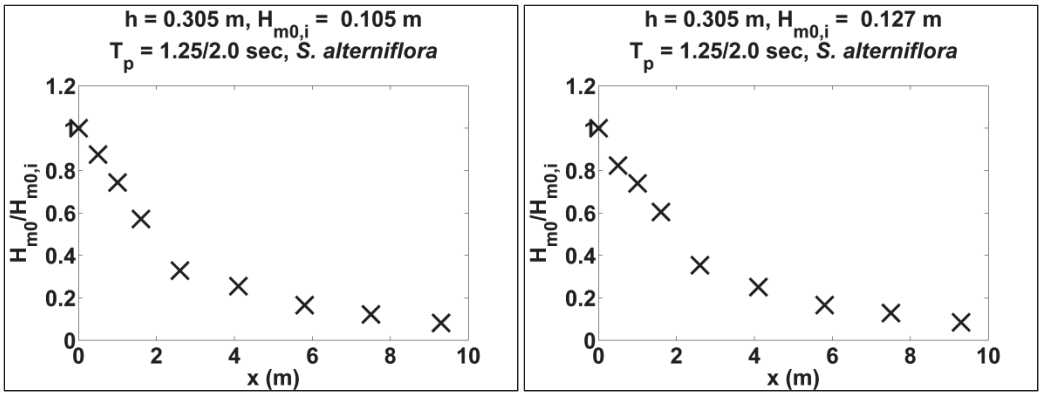

Figure B11. Wave transformation for *h* = 0.457 m, *S. alterniflora* [double-peaked].

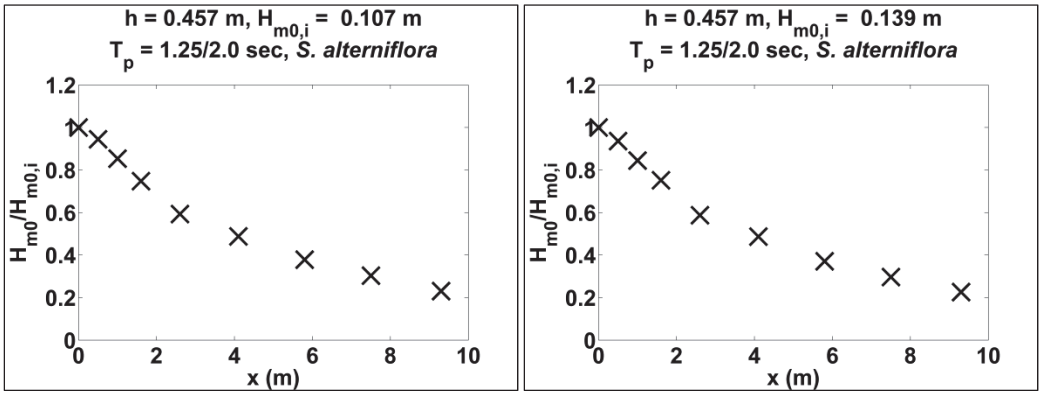

Figure B12. Wave transformation for *h* = 0.533 m, *S. alterniflora* [double-peaked].

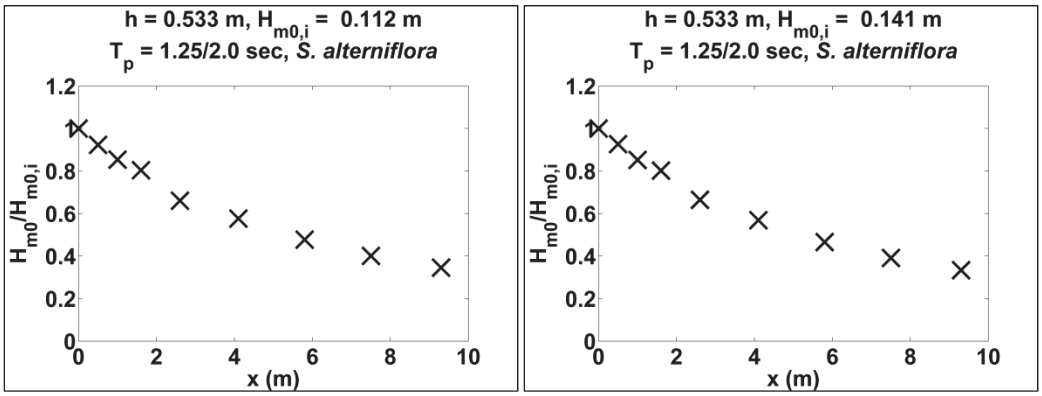

REPORT DOCUMENTATION PAGE

Form Approved
OMB No. 0704-0188

1. REPORT DATE *(DD-MM-YYYY)*	2. REPORT TYPE	3. DATES COVERED *(From - To)*
September 2013	Final report	

4. TITLE AND SUBTITLE

Laboratory Studies of Wave Attenuation through Artificial and Real Vegetation

5a. CONTRACT NUMBER

5b. GRANT NUMBER

5c. PROGRAM ELEMENT NUMBER

6. AUTHOR(S)

Mary E. Anderson, Jane McKee Smith, Duncan B. Bryant, and Robert G.W. McComas

5d. PROJECT NUMBER

5e. TASK NUMBER

5f. WORK UNIT NUMBER

7. PERFORMING ORGANIZATION NAME(S) AND ADDRESS(ES)

US Army Engineer Research and Development Center
Coastal and Hydraulics Laboratory
3909 Halls Ferry Road
Vicksburg, MS 39180-6199

8. PERFORMING ORGANIZATION REPORT NUMBER

ERDC TR-13-11

9. SPONSORING / MONITORING AGENCY NAME(S) AND ADDRESS(ES)

US Army Corps of Engineers
441 G. Street, NW
Washington, DC 20314-1000

10. SPONSOR/MONITOR'S ACRONYM(S)

11. SPONSOR/MONITOR'S REPORT NUMBER(S)

12. DISTRIBUTION / AVAILABILITY STATEMENT

Approved for public release; distribution is unlimited

13. SUPPLEMENTARY NOTES

A physical model study investigating the dissipation of wave energy by artificial and real *Spartina alterniflora* was performed in a large-scale two-dimensional flume. The purpose of the parametric study was to isolate the influence of a single plant or wave property on wave dissipation through vegetation by varying the parameter of interest while holding other parameters constant. The varied parameters included vegetation submergence depth, incident zero-moment wave height, incident peak wave period, and stem density. Measurements of the free surface and instantaneous velocity were collected for single- and double-peaked irregular wave spectra. The experiment setup and data collection methodology are described in detail.

Results from the artificial and real vegetation tests indicate vegetation submergence depth and stem density strongly influence wave attenuation, while the effects of incident wave height and peak period were small and unclear in comparison. An increase in stem density of the artificial vegetation resulted in a greater reduction in wave height for all modeled wave conditions. As water depth exceeded canopy height, the wave attenuation capacity of both the artificial and real vegetation decreased. Dissipation occurred at all frequencies of the spectra, with the most evident loss of energy at the peak frequencies; however, separating the double-peaked spectra into two wave spectra revealed a preferential dissipation of higher frequency wave energy compared to lower frequency wave energy through the artificial array.

The real vegetation was found to dissipate wave energy more efficiently than the artificial vegetation, which is likely due to the additional drag induced by the leaves.

15. SUBJECT TERMS

Wave dissipation
Physical modeling
Vegetation
Artificial vegetation
Spartina alterniflora
Wave flume

16. SECURITY CLASSIFICATION OF:			17. LIMITATION OF ABSTRACT	18. NUMBER OF PAGES	19a. NAME OF RESPONSIBLE PERSON
a. REPORT	b. ABSTRACT	c. THIS PAGE			19b. TELEPHONE NUMBER *(include area code)*
UNCLASSIFIED	UNCLASSIFIED	UNCLASSIFIED	UNCLASSIFIED	91	